1-1-1996

An object-oriented modeling approach to build data communication model

Wuqing Xu
University of Nevada, Las Vegas

INFORMATION TO USERS

This manuscript has been reproduced from the microfilm master. UMI films the text directly from the original or copy submitted. Thus, some thesis and dissertation copies are in typewriter face, while others may be from any type of computer printer.

The quality of this reproduction is dependent upon the quality of the copy submitted. Broken or indistinct print, colored or poor quality illustrations and photographs, print bleedthrough, substandard margins, and improper alignment can adversely affect reproduction.

In the unlikely event that the author did not send UMI a complete manuscript and there are missing pages, these will be noted. Also, if unauthorized copyright material had to be removed, a note will indicate the deletion.

Oversize materials (e.g., maps, drawings, charts) are reproduced by sectioning the original, beginning at the upper left-hand corner and continuing from left to right in equal sections with small overlaps. Each original is also photographed in one exposure and is included in reduced form at the back of the book.

Photographs included in the original manuscript have been reproduced xerographically in this copy. Higher quality 6" x 9" black and white photographic prints are available for any photographs or illustrations appearing in this copy for an additional charge. Contact UMI directly to order.

UMI

A Bell & Howell Information Company
300 North Zeeb Road, Ann Arbor MI 48106-1346 USA
313/761-4700   800/521-0600

EFFECT OF UNSATURATED ZONE SOIL MOISTURE CONTENT

ON VAPOR PHASE POLLUTANT PROPAGATION IN

CONTROLLED LABORATORY EXPERIMENTS

by

Joseph J. Squire

A thesis submitted in partial fulfillment
of the requirements for the degree

Master of Science

in

Geoscience

Department of Geoscience
University of Nevada, Las Vegas
August, 1996

UMI Number: 1381944

UMI
300 North Zeeb Road
Ann Arbor, MI 48103

The Thesis of Joseph J. Squire for the degree of Master of Science in Geoscience is approved.
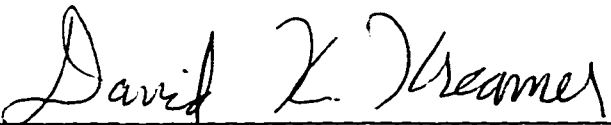
_____ $8\text{-}12\text{-}96$
Thesis Committee Chairperson, David K. Kreamer, Ph.D.   Date

_____ $8/12/96$
Examining Committee Member, Fred Bachhuber, Ph.D.   Date

_____ $8/15/96$
Examining Committee Member, Roger Jacobson, Ph.D.   Date
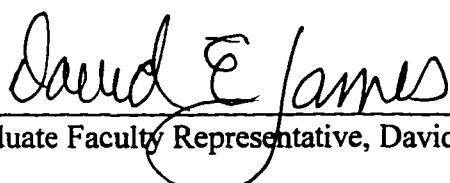
_____ $8/15/96$
Graduate Faculty Representative, David E. James, Ph.D.   Date

_____
Dean of Graduate College, Ronald Smith, Ph.D.   Date

University of Nevada, Las Vegas
August, 1996

Abstract

Experiments were conducted to assess and model the effects of unsaturated zone soil moisture content on vapor-phase pollutant propagation in a controlled setting. A two-dimensional sandtank was utilized for controlled vapor-phase experiments, with pollutant vapors of octane and diesel fuel introduced through a finely slotted source tube. Soil moisture content was varied from 0% to 10% by weight for octane experiments, and from 0% to 5% by weight for diesel fuel. The effects of introduced soil moisture on the transport of each pollutant vapor were observed via soil-gas sampling from access ports. Soil-gas samples were analyzed with FID gas chromatography to determine a gross hydrocarbon concentration for discrete time intervals and distances from the vapor source.

Analytical modeling methods based on Fickian diffusion, developed by Kreamer (1982), were used to estimate two primary diffusion parameters D_e, the effective diffusion coefficient, and A^*, the sorption corrected porosity. Estimations were carried out using a FORTRAN program with a non-linear subroutine. The estimated parameters were used to model concentration curves for each moisture content. The modeling indicated adverse effects on vapor propagation near 2% moisture content for octane and 2% moisture content for diesel fuel.

A trend observed for the octane vapor modeling illustrates the relationship of D_e, D_k, and A^* to the tortuosity factor. Tortuosity was observed to decrease as moisture content increased up to 5% by mass. As moisture content increase beyond 5% gravimetrically, tortuosity began to increase as the porosity became occluded by water molecules.

Table of Contents

List of Tables

List of Figures

Acknowledgments

I wish to express my sincere appreciation to Professor David Kreamer for his constant support, encouragement, understanding, guidance, perseverance, and patience with me in all phase of this thesis during the past few years. Thanks are due to Professors Fred Bachhuber, Jack Hess, Roger Jacobson, and David James for their support on my thesis committee and encouragement in the classroom.

Many true friends have helped me during all phases of this thesis and to them I extend a deep debt of gratitude. Vasanthakumar Rajagopalan was instrumental in helping with the laboratory set up. Rajkumar Rajagopalan came to the my rescue, when in the final phases of this thesis the computer program developed one bug after another. A special thanks to Tod Johnson, whom I have found to be invaluable in explaining the concepts of his work which are a key building block of this thesis. Jaishankar Sabapathi provided insight into almost every aspect of the experimental and thesis process from a Master student perspective. A particular thanks is due to Anitha Jaishankar, whose patient manner was imposed upon many times while I gained support from her husband, Jaishankar, a very special person and true friend.

To Evelyn, my wife and soulmate, and my children, Mattie, Joseph, and Charles, who supported, cared, encouraged, scolded, and loved me during the past few years that it took to complete this thesis. I am sure that it seemed that this thesis was like building a bridge across forever. Thank you. This thesis is dedicated to my wife, children, and

parents, Jackie and Joe Squire, who gave me the tools to persevere and achieve my dreams.

Chapter 1

Introduction

Early detection of leakage from liquid hydrocarbon storage tanks is critical to preventing wide-spread contamination of soil and groundwater. More than one-half of the United States population depends on groundwater as their potable water supply (Solley et al, 1988). Relatively small amounts of liquid hydrocarbon can result in the loss of these valuable groundwater resources for a period of several years and cost hundreds of thousand of dollars or more to remediate. The resultant contamination can cause public mistrust of groundwater supplies long after remediation has occurred, causing public water suppliers to expend additional resources to develop new and possibly costlier water supplies.

Early detection of leaks can to prevent disastrous results from occurring when a liquid hydrocarbon storage tank fails. Early detection of these leaks relies on the chemical and physical properties of the liquid hydrocarbon in storage and the porous media through which a leaked hydrocarbon travels as liquid or vapor. Typically, the detection system relies on the volatility of the liquid hydrocarbon, along with rapid transport of the gaseous phase to a detection system sensor. Gaseous transport can be up to 50 times faster than liquid hydrocarbon movement (McNerney, 1989). Placement of detection system vapor sensors is important when considering how a pollutant vapor is

1

likely to propagate from a hydrocarbon leak. Factors such as soil type, organic content, sorption capacity, stratigraphy, boundary conditions, and soil moisture content can affect pollutant vapor propagation (Johnson and Kreamer, 1994).

The purpose of this thesis was to evaluate the effects of soil moisture in the unsaturated zone on the propagation of volatile organic compounds (VOCs) in the gaseous phase. Specifically an important question is what moisture content impedes vapor diffusion at selected grain sizes. The approach was to vary moisture content in a two-dimensional sandtank model for a number of experimental trials. Effective diffusion coefficients were calculated and then used to mathematically model vapor migration in three dimensions The author's hypothesis is that low moisture contents can increase vapor propagation relative to dry soil conditions, however increasing soil moisture content will eventually impede vapor diffusion in the unsaturated zone.

The primary elements of this thesis include a study of the rates of vapor diffusion as a function of soil moisture content, analysis of data gathered in a two-dimensional physical model, and calculation of the effects of soil moisture on gaseous phase movement. Using the diffusion parameters measured with a two-dimensional physical model, a three-dimensional prediction of gaseous migration was made. Three-dimensional predictions would be applicable to a wide variety of environmental problems where gaseous build-ups occur.

Likewise, the monitoring techniques used in physical sandtank models are applicable to field investigations. Physical sandtank models are one way to create needed quantitative data, but it is necessary to accurately monitor vapor concentrations and

movement in the physical analogues. Methods to monitor the vapor movement in the unsaturated sandtank models have been demonstrated by Chaganti, (1990), and Johnson and Kreamer, (1994). The technique of choice is sampling small volumes of soil gas from ports located on the rear of the sandtank. The sandtank experiment's design allowed for this withdrawal. The vapor sampling ports were equipped with septa through which soil-gas samples could be withdrawn using gas-tight syringes (Chaganti, 1990). These experiments assessed the propagation of pollutant gases in unsaturated media conditions. This technique is time dependent because specific samples were collected at specific time intervals, hence sampling was non-continuous.

During the experimentation, withdrawn soil-gas samples were analyzed using an Hewlett-Packard model 5890 series gas chromatograph. The results of the soil-gas analyses were analytically modeled to determine the effects of soil moisture content on the propagation of pollutant vapor migration. Octane and diesel fuel were the experimental liquids used in this research.

The techniques using the gas chromatograph, gastight syringes, and septa covered sampling ports, provided the author with a method analogous to techniques commonly used in industry for field mapping of "real world" contaminant problems (Kerfoot, 1991). Using soil-gas technology, one can map the lateral extent of a volatile pollutant that may be in or overlying the groundwater.

Previous Work

Soil-gas migration has been described by a number of investigators; however, the described propagation does not typically include the effect of variable soil moisture

content commonly found in natural systems. Water content is the most common geologic barrier to the migration of VOCs in the unsaturated zone (Ballestero, 1991). The interpretation of soil-gas surveys, as related to vapor transport, is limited and qualitative due to the lack of adequate models and laboratory data with respect to soil moisture data and vapor diffusion (Silka, 1988). Chaganti (1990) suggested that the parameter of soil moisture content be varied as a continuation of his work in vapor transport modeling with air-blown dry soils. The need for additional study on the relationship between soil-gas propagation and soil moisture content is echoed by the lack of data and interpretation in other investigative works (Robbins, et al, 1990, Mendoza and McAlry, 1990).

Batterman et al (1995) described the relationship of soil humidity to hydrocarbon gas-phase transport. The relationship described was in terms of retardation coefficients for a given soil type and single hydrocarbon compound. An experimental chamber containing six grams of soil was connected directly to a gas chromatograph. The physical setup allowed for a known concentration of pollutant vapor to be passed through the soil column to a gas chromatograph where an analysis of the soil column pollutant vapor discharge was performed. This investigation focused on the sorptive competition between hydrocarbon and water vapors on soil surfaces. Although the physical method and subsequent analysis allowed retardation coefficients for pollutant hydrocarbon vapors to be determined for specific soil humidity or moisture contents, it did so in a single dimension. An effective diffusion parameter over two dimensions was not

determined and the small test chamber was sampled from a single point which exited directly to a gas chromatograph.

Beckett and Huntley (1994) stated that soil parameters control vapor flow in the subsurface. They also noted that knowledge of these parameters was necessary to design soil vapor extraction systems for cleanup of some hydrocarbon contaminated sites. A parameter discussed by these investigators is soil moisture. They noted that during the operation of soil vapor extraction systems, a decrease of capillary pressure occurs producing a corresponding increase in soil moisture content. This increasing soil moisture effect coupled with the knowledge of the soil moisture influence on pollutant vapor transport is not included in their subsequent analytical models. The Beckett and Huntley (1994) analytical models, based on Hantush-Jacob (1955) leaky flow analytic groundwater model, required additional study to determine the effect of stratigraphy and diffusion on soil vapor extraction systems, as the authors stated. Although their model allowed for determination of a pollutant vapor flux, it did not account for the effects of pollutant vapor diffusion or soil moisture content or the relationship between the two parameters.

Sepher and Samani (1993) developed and tested a three-dimensional finite-difference model intended for in situ remediation using vapor extraction wells. In their analytical model, they noted the distinct effect of soil moisture on the dynamics of pollutant vapor movement. The model developed accounted for the soil moisture effect by adjusting the soil air permeability and the air-filled porosity using a modified form of

equations developed by Brooks and Corey (1964). Effective saturation, S_e, was defined by Brooks and Corey (1964) as:

$$S_e = (\theta - \theta_r)/(\eta - \theta_r)$$

where θ is moisture content, θ_r is the residual soil moisture content, and η is the soil porosity. Brooks and Corey (1964) defined residual moisture content as the amount of moisture that can not be removed from a soil without increasing the capillary pressure (negative pressure). While this research is useful for modeling vapor extraction wells and potential vapor extraction effects on remediating subsurface pollutant vapors, it does not allow for the modeling of pollutant vapor migration. Also, the Sepher and Samani (1993) analytical model did not account for boundary conditions other than constant pressure boundaries.

Robbins, et al (1990) studied the effects of relative humidity in porous media on soil-gas movement in order to develop better field measuring instruments. In their study, they concluded that the use of soil-gas surveys for subsurface gasoline contamination delineation is influenced by the relative humidity of the soil air. Even though the emphasis of Robbins et al (1990) work was oriented toward the development of an instrumentation method correcting for humidity effects, quantitative data on the relation of vapor transport to soil moisture content (humidity) were not presented in their paper.

In another study investigating the relationship of soil moisture to hydrocarbon vapor movement, Mendoza and McAlary (1990) modeled vapor movement in a diffusion-dominated transport system. Their analytical model accounted for many factors related to diffusion transport. However, due to lack of quantitative data, an

assumption of "increased vapor retardation with increasing moisture content" (Mendoza and McAlary, 1990) was made. This again points out the need for quantitative information on the relationship between moisture content and gaseous diffusion.

Chiou and Shoup (1985) studied the effect of humidity in porous media on organic vapor soil sorption mechanisms and capacity. Their research demonstrated that increasing relative humidity in porous media caused a resultant decrease in organic vapor sorption on soils. They concluded that the water molecules strongly suppressed organic vapor sorption in preference to the sorption of water, especially for low-organic mineral soils. While Chiou and Shoup (1985) investigated the effects of soils moisture on organic vapor in porous media and developed analytical models useful in predicting vapor uptake (concentration) curves for a given organic vapor, their experimental apparatus was one dimensional and set up similar to that described above for Batterman et al (1995). Further, they did not account for boundary effects of their experimental apparatus.

Kreamer et al (1988) developed a technique to measure the tortuosity and sorption-affected porosity for gaseous diffusion of pollutant vapors in the unsaturated zone. To develop this technique, Kreamer et al (1988) physically set up a gaseous diffusion device in a field situation as a continuous point source to introduce a conservative tracer gas into an unsaturated soil zone. Soil-gas samples were drawn at discrete time intervals from observation wells spaced at several distinct distances from the continuous point source. The Kreamer et al (1988) analytical technique included governing equations for three-dimensional analytical models that can be used with the

appropriate data sets gathered from two-dimensional physical models similar to that described above. The analytical models of these researchers are based on analogies to heat flow equations (Carslaw and Jaeger, 1959) that solve two and three dimensional problems for continuous point sources. Further, this analytical model technique allows for data input of concentration values along with image sources and sinks from two-dimensional physical models. The output is a three-dimensional array of predicted concentrations that can be useful in setting up vapor detection systems. These detection systems can be vital in providing an early warning of leaks from hydrocarbon-containing underground storage tanks.

Based on work by Kreamer et al (1988), other researchers built sandtanks to collect the data necessary for calibration of a three-dimensional analytical model of gaseous phase pollutant propagation (Chaganti, 1990; Johnson and Kreamer, 1994). Unlike the previous work, these later researchers did not use field methods or a gaseous permeation source device. They employed physical sandtank models with a hydrocarbon liquid source that migrated through a dry porous media. Chaganti, 1990, and Johnson and Kreamer, 1994, accounted for the configuration of the spreading liquid source leak in their work.

Chapter 2

Theory

One-Dimensional, Transient-State Vapor Transport

In the unsaturated zone, vapor propagation can occur by several means, most importantly diffusion and advection (Chaganti, 1990). Additionally, vapor transport is influenced by partitioning into the liquid phase and sorbing onto the solid phase. Diffusion results from the motion of individual molecules subject to a concentration gradient, while advection is mass flux induced from a pressure gradient (Chaganti, 1990). Vapor diffusion can be the dominant propagation mode where pressure gradients in the gas phase are not large. In this case, random molecular motion results in a net transfer of mass from regions with high concentrations to regions of low concentrations.

Fick (1855) developed a quantitative analogy for diffusion from earlier work on heat flow by Fourier. Fick's second law, equation (2.1), describes the one-dimensional flow of one gas into another in which the change of concentration with respect to time can be determined.

$$\frac{\partial c}{\partial t} = D \frac{\partial^2 c}{\partial x^2} \qquad (2.1)$$

where,

c = concentration in of gas (g/cm^3)

9

t = time (sec)

D = general diffusion coefficient (cm^2/sec)

x = distance (cm)

Equation (2.1) neglects an advective term and assumes no variation in D with time, space, direction, or concentration (Chaganti, 1990).

Two-Dimensional, Transient-State Vapor Transport

Fick's second law can be modified to describe vapor diffusion in two dimensions in an unsaturated porous media by replacing the diffusion coefficient D with an effective diffusion coefficient D_e.

$$\frac{\partial c}{\partial t} = D_{ex} \frac{\partial^2 c}{\partial x^2} + D_{ey} \frac{\partial^2 c}{\partial y^2} \tag{2.2}$$

D_{ex} and D_{ey} are the effective diffusion coefficients in the x and y directions respectively. D_e can be described as (Kreamer et al, 1988):

$$D_e = \frac{\tau \theta_D D}{\theta_D + (\theta_D - \theta_T)\rho_w k_w + (1 - \theta_T)\rho_s k_s} \tag{2.3}$$

where,

τ = tortuosity factor accounting for the resistance to diffusion imposed by the structure of the porous media, dimensionless,

θ_D = drained or gas filled porosity, dimensionless,

θ_T = total porosity, dimensionless,

ρ_w = density of water, g/cm^3,

ρ_s = particle density of the granular material making up the solid matrix, g/cm^3,

k_w = liquid-gas partitioning coefficient, this describes the ratio of the concentration in the overlying gas phase under equilibrium conditions, [(mole/g of water)/(moles/cm^3 of gas)], (Chaganti, 1990), and

k_s = gas-liquid-solid distribution product describing the ratio of the moles of gas under consideration sorbed on the solid phase to the concentration of the gas in the soil atmosphere, [(moles/g solid)/(moles/cm^3 gas)]

It is assumed that the liquid phase is immobile, completely wets the solid phase, and has immediate equilibration with the gaseous phase with respect to dissolved and sorbed concentrations between the liquid and solid phases (Chaganti, 1990).

Considering the denominator of the right-hand side of equation (2.3) to be A^*, the sorption term (sorption-corrected porosity), and the numerator D_k, the effective diffusion coefficient neglecting sorption, then $D_e = D_k/A^*$ (Chaganti, 1990). If one assumes two-dimensional, radial outward diffusion in a homogeneous, isotropic media and neglecting advective transport, equation (2.2) reduces to:

$$\frac{\partial c}{\partial t} = \frac{D_k}{A^*}\left[\frac{\partial^2 c}{\partial r^2} + \frac{1}{r}\frac{\partial c}{\partial r}\right]$$ (2.4)

where,

$$D_{ex} = D_{ey} = D_e$$

r = the radial distance from the source, cm in cylindrical coordinates.

Analogy to Two-Dimensional Confined Groundwater Flow

An analogy can be drawn to the Theis equation (Theis, 1935) used in confined groundwater flow. Equation (2.5) describes groundwater flow in two-dimensions:

$$\frac{\partial h}{\partial t} = \frac{T}{S}\left[\frac{\partial^2 h}{\partial r^2} + \frac{1}{r}\frac{\partial h}{\partial r}\right] \tag{2.5}$$

where,

h = hydraulic head, m

T = transmissivity of the aquifer, m^2/day

S = storage coefficient of the aquifer

Comparing equations (2.4) and (2.5) shows that the sorptionless diffusion coefficient D_k is analogous to transmissivity T, and the sorption-corrected porosity A^* is analogous to the storage coefficient S (Chaganti, 1990). Theis obtained a solution to equation (2.5) as is shown in equation (2.6).

$$s = \frac{Q}{(4\pi T)}\, w(u) \tag{2.6}$$

where,

$$w(u) = \int_u^\infty \frac{e^{-u}}{u}\,du \quad \text{and} \quad u = \frac{r^2 S}{4Tt} \quad \text{(dimensionless)}$$

r = any point at a known radial distance, m.

s = drawdown at a distance r from the pump, m.

Q = rate of pumping, m^3/day

The ratio of the quantities T and S is called the aquifer diffusity (Chaganti, 1990). Substituting gaseous diffusion parameters in equation (2.6), the solution to equation (2.4) is:

$$c = \frac{q}{(4\pi D_k)} \, ei(u) \tag{2.7}$$

where,

$$ei(u) = \int_u^\infty \frac{e^{-u}}{u} \, du \quad \text{and} \quad u = \frac{r^2 A^\bullet}{4D_k t} \quad \text{(dimensionless)}$$

q = release rate of the vapors per length of the source, g/sec-cm.

Using the relation $D_k = D_e A^\bullet$, equation (2.7) can be re-written as:

$$c = \frac{q}{\left(4\pi D_e A^\bullet\right)} \, ei(u) \tag{2.8}$$

where,

$$u = \frac{r^2}{(4D_e t)}$$

Interpretation of the author's experiments is based on the above equations, specifically equation (2.8). Boundary effects in the sandtank experiments are dealt with a method analogous to conditions in groundwater hydrology. The method employs an analogy drawn from image well theory utilizing image sources or sinks, depending on the type of boundary (Chaganti, 1990 and Kreamer, 1991). The solution to equation (2.8) using image source and sink boundary conditions becomes:

$$c = \frac{q}{(4\pi D_e A^\bullet)} \sum_{i=1}^{n} \left[\pm ei(u_i)\right] \tag{2.9}$$

where,

$$u_i = \frac{r_i^2}{(4D_e t)}$$

n = number of sources or sinks.

r_i = the radial distance from the ith source or sink

The sign for ei is positive for sources and negative for sinks (Kreamer, 1991)

Three-Dimensional, Transient-State Vapor Transport

Application of the two-dimensional equations cannot be made to most real-world situations. A three-dimensional vapor transport equation that approximates real-world situations is given by Kreamer (1982) as:

$$c = \frac{Q_v}{(4\pi D_e A^{\cdot} r)} \, \text{erfc}\sqrt{u} \tag{2.10}$$

where,

erfc = the complimentary error function,

r   = radial distance (cm) in spherical coordinates

u   = as defined before excepting r changes from cylindrical to spherical coordinates and,

Q_v = rate of vapor mass production in g/s from a continuous point source.

All the other parameters are the same as previously described. The results of the author's research is applied to three-dimensional systems by Equation (2.10). Specifically, diffusion coefficients and sorption terms calculated from vapor concentration data in two-dimensional sandtank models, are used to predict vapor concentration distribution in time and space for three-dimensional field situations.

Chapter 3

Experimental Apparatus and Procedure

Sandtank Design

Vapor migration was simulated in a sandtank with the dimensions of 31.5 cm tall by 30 cm wide by 10 cm thick. Its base measures 20 cm wide by 60 cm long, which provided adequate stability during the experiment. Figure 3.1 illustrates the sandtank used in this study. The entire sandtank is constructed of clear Plexiglas® with a wall thickness of 0.645 cm. Each piece of Plexiglas® was grooved for a snug fit into its adjoining sides. Each groove was sealed with clear silicon caulking compound, which waterproofs the sandtank joints and binds the sandtank walls and floor together. This sandtank's advantages include that it is portable and can be moved by one person when filled with a nearly saturated porous media.

Another sandtank was used in initial experimentation. Similar aluminum and glass sandtanks were previously used in LNAPL experiments by other investigators (Sabapathi, 1993, and Rajagopalan, 1994). These sandtanks typically measured approximately 60 cm tall by 90 cm wide by 15 cm thick. This size of sandtank is moveable by lifting only when empty. The sandtank is constructed of aluminum, with a glass front panel for viewing purposes, allowing assessment of the uniformity of sand placement.

15
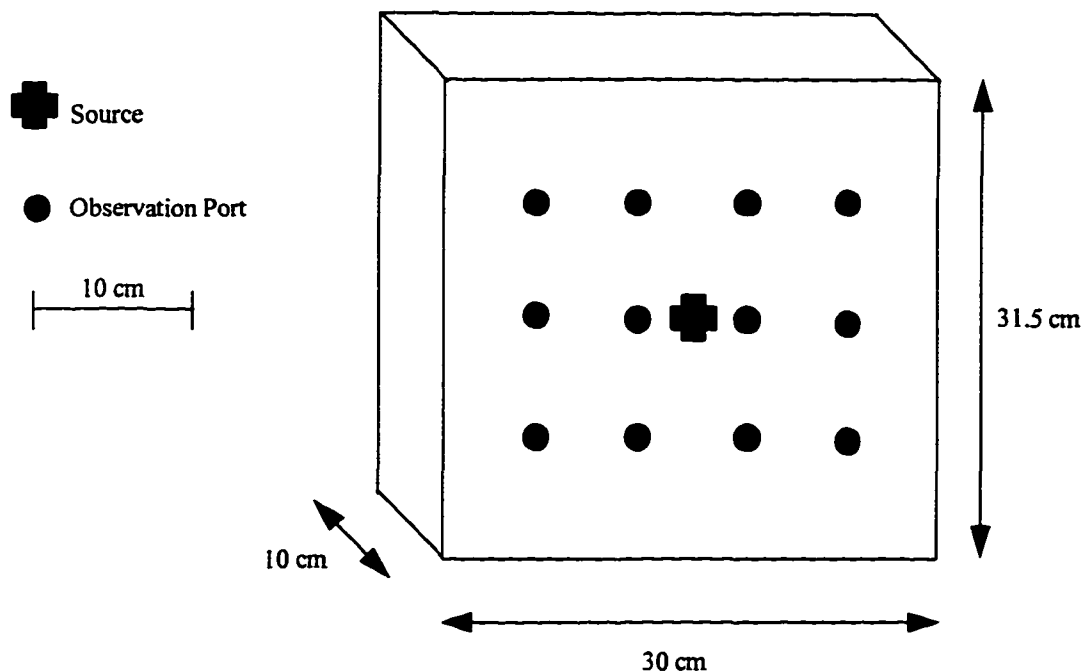
FIGURE 3.1 - SCHEMATIC OF SANDTANK WITHOUT BASE

The Plexiglas® sandtank was chosen over the glass and aluminum tank because experimental results indicated similar values for D_e without the added waste generation of the larger sandtank. It is noted that Plexiglas® and acrylics less hydrophilic than glass (Scheigg and McBride 1987). Had these experiments relied on liquid sources released into the sandtank, then experimental error could have been introduced due to the hydrocarbon preferentially wetting the sandtank walls and migrating along the wall-sand interface. Because these experiments relied on a vapor source, boundary condition effects can be modeled using an analogy to image-well theory, without the possible interference of preferential liquid hydrocarbon build-up at the boundary and assuming no vapor sorption on the sandtank walls.

Boundary effects were a consideration in deciding upon the dimensions of the sandtank. Schiegg and McBride (1987) demonstrated that the sandtank walls influence the movement of liquids due to localized increased porosity differences at the wall-sand interface. Chaganti, (1990) assumed this also applies to vapor movement. The wall presence computed to cause a porosity increase of up to 25% observable to a distance over four grain diameters away from a wall when using a sandtank system for liquid laboratory experiments (Schiegg and McBride, 1987). An analogy may be drawn from the liquid phase experiments. As the porosity increases along the boundary, vapor movement may be preferentially influenced. For example, if a vapor begins to collect along a boundary, if it has density greater than air vapor, it may move by gravity into the lower portions of the sandtank along the more porous boundary zone. This is analogous to the liquid experiments conducted by Chaganti (1990), Sabapthi (1993), Johnson and Kreamer (1994), and Rajagopalan (1994) in that experimental error is introduced by the increased porosity effect at the boundary.

The experimental error can be calculated by using an equation derived by Schiegg and McBride (1987) that consider the relationship of porosity, mean grain diameter, and the sandtank width:

$$(0.25)\,(8\phi)/\,W = \text{experimental error caused by the sandtank wall – sand} \quad (3.1)$$
$$\text{grain interface}$$

where,

ϕ = grain diameter (mm)

W = sandtank tank width

For the design sandtank width, a 25% increase in porosity occurs, affecting two walls of four grain diameters (ϕ) each, for a total of 8ϕ from the sandtank walls (Schiegg and McBride, 1987). Using equation (3.1) and the mean-grain diameter of 0.85 mm used in these experiments, an experimental error of less than 1.7% in moisture content or saturation over the 10 cm width (W) of the sandtank used in these experiments.

Backfill Material

The backfill material or "soil" used in each experimental trial consisted of commercially available kiln-dried white silica sand [Corona Industrial Sand Company (Cisco) Sieve 20]. The silica sand was packaged by the manufacturer in 45.5 kg bags. The packaging consisted of perforated paper layers which allowed for ambient air moisture movement and barometric pressure changes from the point of manufacture to the point of use. The moisture content of the dry silica sand was determined to average 0.11% by mass, by methods described in the Soil Moisture Section. Tables 3.1, 3.2, and 3.3 display the manufacturer's specifications for the sand used in this study.

Table 3.1 Typical Physical Specifications of Experimental Soil

Screen Sieve Number	Percent Passing	Direct Percent Retained
20	90.0	10.0
30	30.0	60.0
40	6.0	24.0
50	1.0	5.0
Pan		1.0

Table 3.2 General Properties of Experimental Soil

Properties	Normal Range
Specific Gravity	2.60 - 2.65
Hardness	6 to 7 on Moh Scale
Weight per Cubic Foot	90 lb - average
Acid Solubility	Less than 5%
Effective size	40 -50 sieve size
Uniformity Coefficient	1.65 - maximum
Grain Shape	Angular to Sub Angular
Moisture Content	Less than 0.10%
Porosity	40 - 45%

Table 3.3 Typical Chemical Properties of Experimental Soil

Element	Percent	Element	Percent
Silica Dioxide	93.13	Calcium Oxide	0.07
Aluminum Oxide	3.60	Barium Oxide	0.04
Iron Oxide	0.10	Magnesium Oxide	0.005
Titanium Oxide	0.11	Sodium Oxide	0.32
Chromic Oxide	0.001	Potassium Oxide	2.52

Loss on Ignition @ 1200° C = 0.1%

The silica sand had a low, solid phase organic carbon content of less than 0.1%, to minimize sorption losses of hydrocarbon vapors. The reported organic carbon content is based on the manufacturer's specifications of 0.1% loss on ignition at 1200° C and assuming the loss is attributable to carbon volatilization at high temperatures. Therefore, the most probable mechanisms of vapor hydrocarbon losses during a sandtank experiment could include: (1) volatilization from the top of the sandtank, (2) sorption

onto the silica particles; (3) partitioning into the soil moisture, (4) sorption on the sandtank sidewalls, and/or (5) degradation of the hydrocarbon. The porous media contained in the sandtank consisted of unsaturated backfield materials.

Soil Moisture

Consistent soil moisture was needed for each experiment and for duplication in subsequent trials. A method was developed in preliminary work to readily duplicate soil moisture content in experiments and subsequent trials. The method duplicated soil moisture content over a range of 0% to 10% soil moisture by mass, as describe in the following section.

The sandtank described above contained 14,000 gm of air-dry soil. Air-dry in this context means the ambient condition of the soil moisture as shipped from the manufacturer and found in the laboratory. In these experiments, the air-dry silica sand was found to contain 0.11% moisture by mass on average. This value was considered negligible in determining the initial soil moisture conditions.

With a mass of 14,000 gm of sand needed to fill the sandtank, calculation of the amount of water needed to obtain a given soil moisture condition by mass is straightforward. An 140 ml volume of water should be added to the silica sand to obtain the initial soil moisture conditions for each 1% of soil gravimetric moisture required for each experiment. Each 14,000 gram silica sand batch was split into two equal portions of 7,000 grams for ease of handling and better control of soil moisture mixing. Each split was then placed in a 7,545 ml new clean plastic bucket. The sand split, with a bulk density of 1.61 grams/ml, occupied about 4,350 ml of the bucket.

An identical amount of water was then added into each split by sprinkling a measured amount of water to obtain the desired soil moisture content. The buckets were sealed with a tight-fitting, water-proof, sealed plastic lid. The bucket with its contents was then vigorously shaken. After shaking the bucket was labeled with the date and soil moisture content. The sealed buckets of soil and known moisture content were placed in an area in the lab where they remained undisturbed for at least eight hours. The ambient temperature of the lab remained at 24° C throughout all of the experiments. This temperature facilitated the natural dispersion of the added water throughout each soil split. Prior to each experimental run, the splits were again vigorously shaken before opening the bucket. The lids were removed from two identical splits, these splits were then mixed into a 18,860 ml clean plastic bucket. From the larger bucket the wetted silica sand was placed into the sandtank. Soil moisture content determinations were made before each experimental trial.

Table 3.4 - Moisture Content Determinations

| Ex. Run | Mass A in grams | | Mass B in grams | | Moisture | | |
	Wet	Dry	Wet	Dry	A%	B%	Desired %
JSOC2	N/A	N/A	N/A	N/A	0.00%	0.00%	0.00%
JSOC6	71.253	70.462	68.785	68.122	1.12%	0.97%	1.00%
JSOC5	69.123	67.805	71.471	70.055	1.94%	2.02%	2.00%
JSOC14	71.269	67.834	69.585	66.305	5.06%	4.95%	5.00%
JSOC8	78.954	74.121	75.895	71.276	6.52%	6.48%	6.50%
JSOC9	64.287	59.865	65.884	61.311	7.39%	7.46%	7.50%
JSO10	62.784	57.825	68.293	62.948	8.58%	8.49%	8.50%
JSOC12	69.244	63.338	72.146	65.972	9.32%	9.36%	9.25%
JSOC11	68.127	61.981	61.279	55.752	9.92%	9.91%	10.00%
JSDI1	N/A	N/A	N/A	N/A	0.00%	0.00%	0.00%
JSDI2	74.235	72.743	64.187	62.959	2.01%	1.91%	2.00%
JSDI3	68.997	65.747	72.519	69.093	4.94%	4.96%	5.00%

Moisture determinations were made by obtaining two "soil" splits from each experimental run. The mass of each split was determined using an enclosed Mettler AC 100 balance. This balance has a range of 100 to 0.0001 g, with an accuracy of $\pm$ 0.0005 g. Mass readings are indicated on a LED display. The split was then placed into a drying oven for 24 hours at a temperature of 80° C. The split was removed from the oven, allowed to briefly cool, and weighed. The percent moisture content was then determined by Equation 3.2. The actual moisture content by mass was determined for each experimental run, see Table 3.4.

% moisture = (wet split mass - dry split mass)/(wet split mass)   (3.2)

After each experiment, the sandtank was emptied. No apparent moisture migration resulted with the exception of two experiments when moisture contents in excess of 9% by mass occurred. In these two experiments, nearing saturation, some gravity drainage toward the sandtank bottom appeared to occur over the duration of the experiment.

Soil Emplacement

The emplacement of the sand into the sandtank can have a profound effect on the experimental results. When using moist soil, it is possible to compress and compact the soil in a manner that could yield different results for different trials of the same soil moisture content.

For air-dry soil experiments, the soil was emplaced in a careful manner as to avoid layering. A predetermined mass of dry silica sand was measured into the plastic buckets. This ensured that the soil could be placed in one continuous pouring episode

into the sandtank. Once the soil was measured, it was methodically poured through a slotted cover placed over the entire width of the sandtank. The slots allowed the soil to be evenly distributed over the entire width of the sandtank at a steady flow rate. This method was found to produce a uniform soil column, without layering, similar to the vertical soil profiles of Sabapathi, 1993, and Rajagopalan, 1994.

For moist soil experiments, the openings in the slotted cover had a tendency to bridge with damp clinging particles. To avoid this problem, soil emplacement in these experiments merely consisted of pouring the moist soil directly into the sandtank. When the soil reached the sampling port intervals, the sandtank was gently moved from side to side to level the soil. This action prevented voids from developing below the sampling port tube, as had been observed in preliminary experiments. Hence, the sandtank was then filled in three successive lifts each approximately 10 cm in thickness. No layering was detected, a result similar to that reported by Sabapathi (1993). Because an exact amount of soil mass was added to a known volume in the sandtank, settlement could be measured. Compaction after filling was relatively consistent and was approximately 2% of the volume. This did not appear to have a detrimental effect on the experimental outcome.

Vapor Delivery

Since the sandtank is a finite-width, two dimensional model, a line source perpendicular to the front wall was used as a source. This is similar to the work of Johnson and Kreamer (1994), Chaganti (1990), Sabapthi (1993), and Rajagopalan (1994). The leak source had an internal volume of 0.37 ml. The source device was

constructed of a finely-slotted, stainless tube filled with a liquid hydrocarbon. The source tube extended through the sandtank wall. Like the sampling ports, the source tube was silicon-caulked into place to prevent leakage or air-flow. Inside the sandtank, the source tube was slotted over a 7 cm length (Figure 3.2). The 24 slots were 0.23 mm in width and extended through one-half of the source tube's 1.0 mm diameter. The slotted area was centrally located within the sandtank.
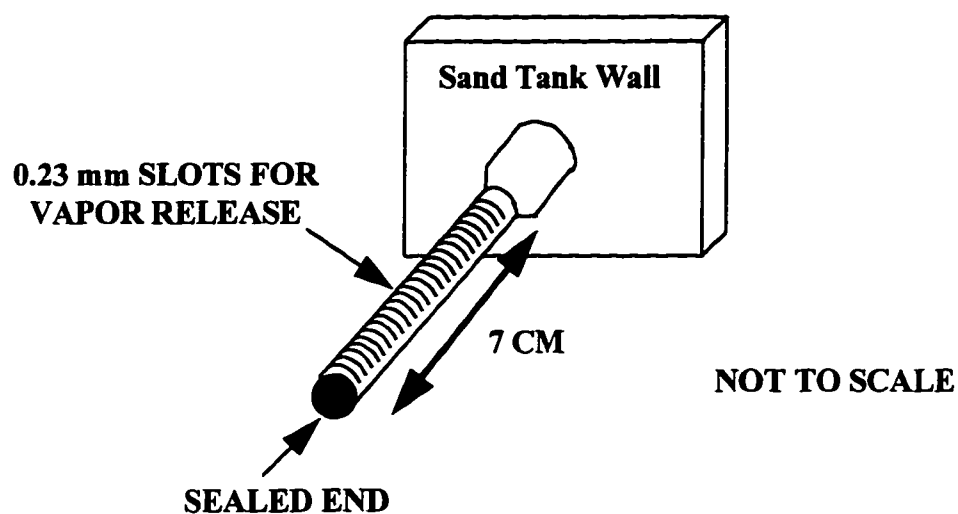
Figure 3.2 - Source Tube

The source tube was filled from outside of the sandtank via a septa. The hydrocarbon was injected with a graduated syringe through the septa located on the exterior end on the source tube. During source tube calibration tests, an even flow from all slots of liquid was clearly observed when the source tube was purposely overfilled. The source tube was inspected for obstruction, such as very fine sand particles, prior to each experimental run.

The advantage of a vapor only source device for these experiments was the ability to control the flow rate of the hydrocarbon vapor into the sandtank without the possible

interference and randomness in source configuration from an irregularly distributed liquid. Reproducibility can be a problem with a liquid leak source because of random "fingering" effects during the downward migration of the liquid hydrocarbons (Johnson, 1992). By reducing or eliminating liquid hydrocarbon in the experimental runs, error may be reduced.

Source Hydrocarbon and Calibration

Octane was chosen as one experimental hydrocarbon because of it represented a single molecule type that would simplify the experimental runs due its uniform physical behavior. Diesel fuel was chosen as the other experimental fuel, so that a comparison could be made between a complex mixture of molecules and a single compound source. Further comparison can also be made to the previous work of Johnson (1992) and Chaganti (1990), who both used diesel fuel in similar experiments and analyses.

The source tube was calibrated for both octane (Figure 3.3) and diesel fuel (Figure 3.4), using the following steps. The source tube was removed from the sandtank during the calibration trials. A 0.37 ml sample of the liquid hydrocarbon was drawn into a clear

Figure 3.3 - Octane Calibration
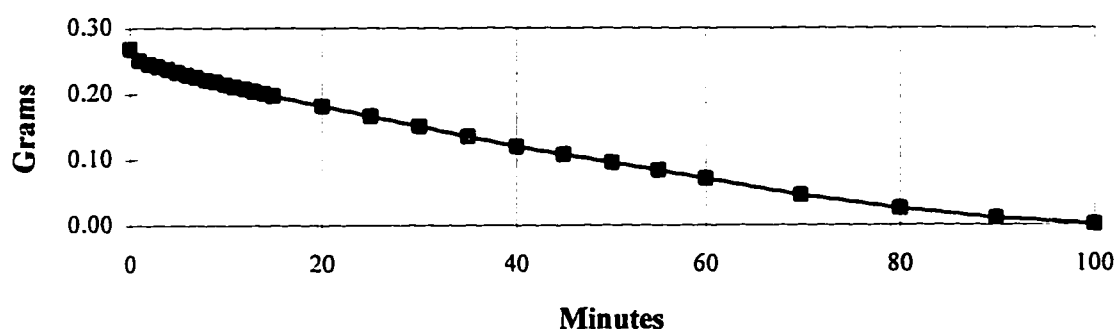
glass graduated syringe. The sample was then injected through the source tube septa covering the injection port. The source tube which contained the hydrocarbon liquid was placed on a Mettler AC 100, the same balance as previously described. Mass readings were then recorded and plotted for discrete times as the octane and diesel fuel volatilized.

Figure 3.4 - Diesel Fuel Calibration
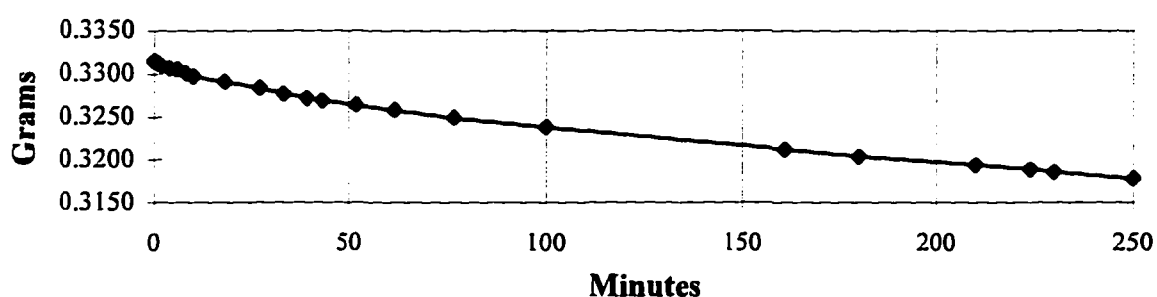
Both Figures illustrate that the source discharged evenly in a linear fashion over time, except for the earliest time of diesel fuel volatilization. During early volatilization, diesel fuel is likely to have its most volatile compounds leave the source tube rapidly, relative to the bulk of the diesel fuel liquid. This was evident during the diesel fuel calibration as the mass loss rate decreased in the first few minutes of the calibration test. The mass loss rate stabilized in about six minutes, as seen in Figure 3.4. The volatilization rate for the octane was found to be 9.79 ug/s/cm of source length. The average volatilization rate for diesel fuel was found to be 0.542 ug/s/cm of source length.

General properties of the octane, as provided by the supplier, used in these experiments are found in Table 3.5. The octane for these experiments was supplied by Aldrich Chemical Company, Milwaukee, Wisconsin. The supplier reported a 99+% purity for the octane.

Table 3.5 - Octane General Properties

Formula	$CH_3(CH_2)_6CH_3$
Molecular Weight	114.23
Boiling Point	125°C to 127°C
Melting Point	-57°C
Density	0.73 g/cc

The general properties of the diesel fuel sample, as provided by the supplier Atlantic Richfield, used in these experiments are found in Table 3.6. The diesel fuel was supplied, as a courtesy, by Nevada Power Company, Las Vegas, Nevada, from their bulk

Table 3.6 - Diesel Fuel General Properties

API Gravity	30.0 to 42.0	Viscosity @ 37.7°C	1.9 to 4.1 centistokes
Specific Gravity	0.83 to 0.87	Sulfur, wt %	0.05%
Flash Point	58°C (minimum)	Color, Saybolt	2.5
Pour Point		Carbon Residue on 10% Bottoms	0.35
-Summer	-12°C (maximum)		
-Winter	-17°C (maximum)	Water and Sediment	0.05%

diesel fuel storage tanks. The diesel fuel sample was obtained two days before the experimental runs. This was done to reduce diesel fuel degradation once in the laboratory, however, this does not account for diesel fuel degradation that may have occurred while in the Nevada Power Company bulk fuel storage tanks. The diesel fuel sample was stored in 40 ml VOA vials with Teflon septa. The Teflon septa facilitated withdrawal of the diesel fuel from the VOA vial without removing the lid of the vial.

This procedure was followed so that the most volatile diesel fuel molecules would not be allowed to volatilize from the surface of an open vial, thus changing the composition of the diesel fuel.

Sampling Ports

The propagation of the vapor phase from the point source leak was monitored from sample ports located on the sampling side of the sandtank (Figure 3.5). Septa for soil gas withdrawal via syringes were mounted on the sampling side of the sandtank.
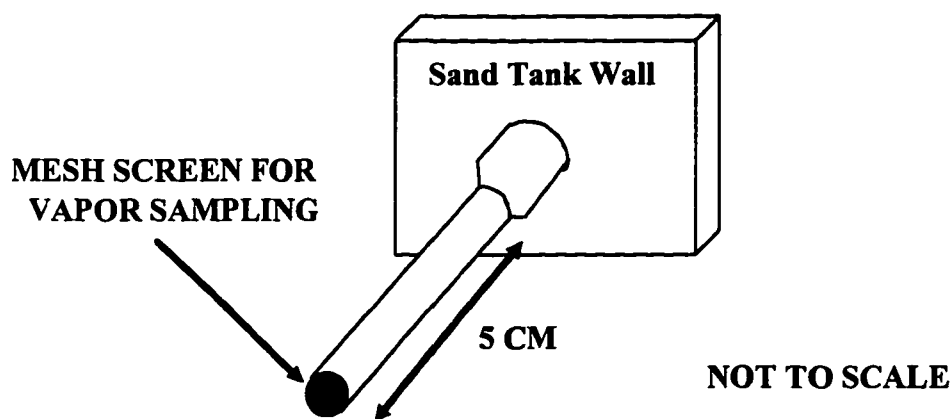
Figure 3.5 - Vapor Sampling Port

Soil gas samples were withdrawn to determine total petroleum hydrocarbon concentrations. A total of 12 individually labeled sampling ports were symmetrically placed around the hydrocarbon source (Figure 3.6).
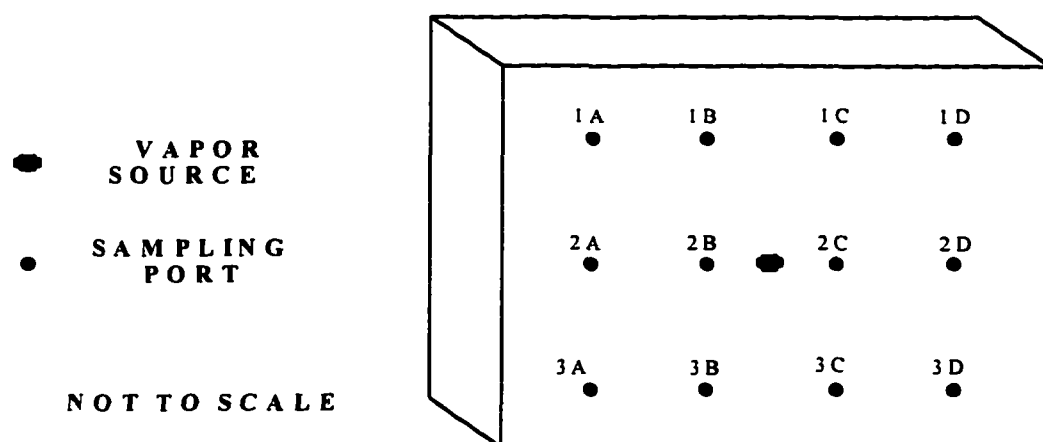
Figure 3.6 - Vapor Sampling Port Identification Labels

Reproducibility was determined by the use of multiple experimental trials and by the ability to predict the empirical outcome using the modeled analytical solution of the each experimental trial for a given set of initial conditions. The 12 samples withdrawn during each discrete time sampling interval were analyzed using a Hewlett-Packard 5890 Series II gas chromatograph. GASTIGHT syringes from Hamilton Company of Reno, Nevada, were used in all experimental runs. Initially, 2 ul syringes were used, however, vapor concentrations below the detection limits of the gas chromatograph were frequently encountered at this sample size. During the experimental runs used to collect the data for this thesis, 10 ul GASTIGHT syringes were used for vapor withdrawal from the sandtank and injection into the gas chromatograph. The 10 ul sample size was found to be adequate for the sample detection and gas chromatograph resolution. The porosity of the air-dry soil was determined to be 39.2% based on the bulk density of 1.61 g/cm^3 and a grain density of 2.65 g/cm^3, then approximately 3708 ml of soil-gas existed in the sandtank. With 3708 ml of available soil-gas, a 10 ul sample drawn with the

GASTIGHT syringe would account for about 0.00027% of the available soil-gas volume for air-dry soils in these experiments. For experiments containing up to 10% water by mass, a corresponding soil-gas volume of approximately 2308 ml would result. With 2308 ml of available soil-gas, a 10 ul sample drawn with the GASTIGHT syringe would account for about 0.00043% of the available soil-gas volume for soils in these experiments containing 10% moisture content by mass.

The Hewlett Packard Series 5890 gas chromatograph was equipped with a flame ionization detector (FID). The gas chromatograph column was a 30 m long, 0.54 I.D., capillary column with a film thickness of 1.2 mm (Alltech Associates, catalog no. 955130). Table 3.7 illustrates the gases and pressure settings used to operate the gas chromatograph.

Table 3.7 - Gases Used in the Gas Chromatograph

Gas	Pressure
Hydrogen	40 psi
Compressed Air	60 psi
Helium	40 psi
Nitrogen	30 psi

The gas chromatograph oven temperature was set at 260° C. The inlet and detector were maintained at 275° C. These temperatures facilitated rapid, consistent analysis of injected samples. An appropriate time interval was allowed to pass between subsequent sample injection to allow the gas chromatograph column to be purged of the

previous sample. This protocol allowed for analyses to be conducted one after another. For octane, the gas chromatograph yielded a distinct peak and integrated area corresponding to concentration for each sample analysis using this technique. Calibration samples were also injected prior to each experimental run.

The same technique was used for diesel fuel vapor trials. However, it does not allow for the development of a typical gas chromatograph plot or curve one would expect for a typical diesel fuel analysis. A single peak and integrated area are produced, like that of the octane analyses. This single measure of total hydrocarbons was necessitated by the number of samples collected during the discrete sampling time intervals. A gas chromatograph analysis of diesel fuel that resolved individual hydrocarbons would take approximately 30 minutes per sample, rather than the two minutes required of the technique, described above for total hydrocarbons. Johnson and Kreamer (1994) and Chaganti (1990) used a similar technique to measure total diesel fuel hydrocarbons in their experiments. Additionally, this method of total hydrocarbon analysis has been used in a number of field investigations for diesel fuel investigation (Block and Bishop, 1990).

The data generated by the gas chromatograph was analyzed using the HP 3365 ChemStation Series II software on a computer tied directly to the gas chromatograph. The software allowed for the integration of the peaks produced from each sample analysis. The integrated area then was converted to a concentration when compared to a known calibration area. The integrated data was imported from the HP ChemStation software into a Microsoft Excel spreadsheet program. The spreadsheet program facilitated further analysis of the data, described in Chapter 4.

Chapter 4

Results and Discussion

A total of 33 experimental runs were conducted for this thesis. Of these experimental runs, 21 physical models were needed to develop techniques and quality assurance described in Chapter 3. These early experiments were compared with later experimental runs, with reproducible results. Twelve of the later experimental runs were chosen for analysis. These experimental runs, nine for octane vapor and three for diesel-fuel vapor, were chosen because they represented data sets that span soil moisture contents from air-dry to near saturation for the physical experiments with the least amount of observed experimental failure. Failure typically was produced by leakage from septa or syringes with worn teflon seals, giving non-representative concentrations.

The results of the physical experiments are analytically modeled using equations derived by Kreamer (1988). The analytical model estimates values for the effective diffusion coefficient, D_e, and sorption corrected porosity, A^*. Once the D_e and A^* parameters are calculated using the empirical data from the physical model, a three-dimensional model can be calculated for a given gravimetric moisture content. These calculations are in the sections that follow.

32

Vapor Phase Migration

Because the vapor sources were confined to the volatilization of the hydrocarbon from the source tube, the experiment is greatly simplified. It is observed that no liquid hydrocarbon leakage occurred from the source tube during the calibration trials and the same is assumed to be true during the sandtank experiments. When removing the sand from the sandtank, after each experimental run, no evidence was found that suggested liquid hydrocarbon leakage. If liquid hydrocarbon leakage had occurred, the experimental runs would be complicated by factors described by Johnson and Kreamer (1994) and Chaganti (1990). These factors could include vapor propagation from random "fingers" of liquid hydrocarbon moving in the sandtank at unknown rates and directions. Eliminating this type of random liquid hydrocarbon movement and subsequent vapor propagation allows analytical modeling of soil moisture effects on the propagation of pollutant vapor from a two-dimensional line source.

The distance between the vapor source and an observation point (sampling port) must be known to use Equation 2.8. Further, the boundary conditions of the sandtank model were included in analysis conducted, as shown in Equation 2.9. Image well theory (Freeze, et al, 1979) was used to determine the radial distance to three image sources and one image sink as they relate to the observation point and the actual vapor source.

The analytical mathematical model developed from the image sources, image sink, actual vapor source, and observation point is identical to that of Kreamer et al (1988), Chaganti (1990) and Johnson and Kreamer (1994). Figure 4.1 illustrates the

general spatial relationship of the image sources, image sink, vapor source, and observation port to each other.

VAPOR SOURCE

OBSERVATION PORT

IMAGE SOURCE

IMAGE SINK
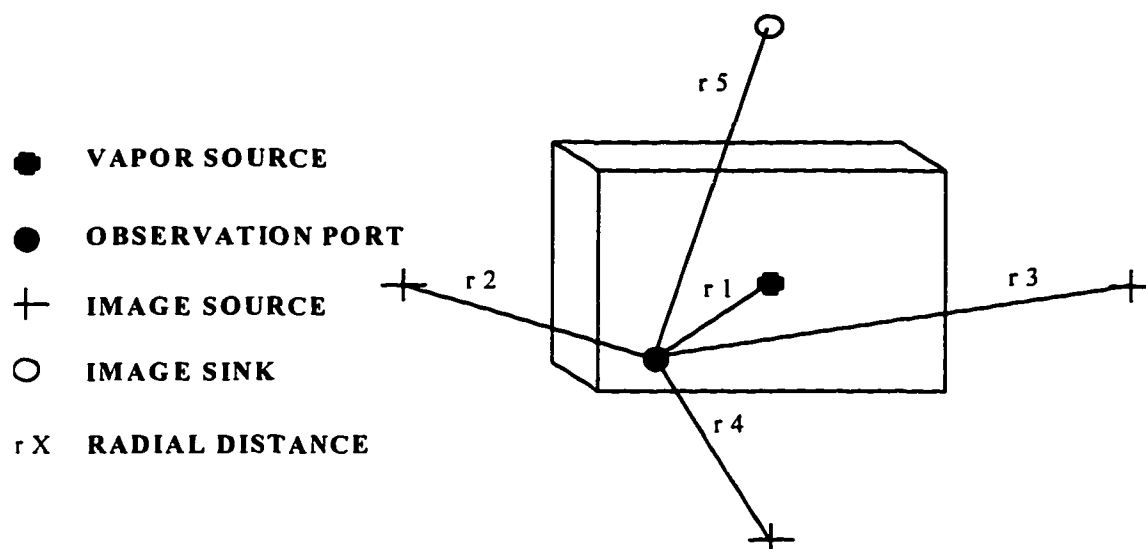
r X **RADIAL DISTANCE**

**Figure 4.1 - Image Sources and Sink, Vapor Source, and Observation Port
General Spacial Relationship with Radial Distance Designations**

An infinite number of image sources and sinks can be added to an analytical model with parallel boundaries (Kreamer, 1982). Additional image sources and sinks represent the reflections of images about parallel boundaries of the sandtank used in this research. For this research, one set of image sources and sinks was used in each analytical model, three image sources below and beside the model and one image sink above. A second set of images was analytically modeled and found to make less than 2% difference for the observed vapor concentrations versus the analytically modeled concentrations.

Vapor Data Analysis

Data collected from the gas chromatograph vapor analyses were values expressed in integration units by the HP 3365 ChemStation software residing in a computer attached directly to the gas chromatograph. The HP ChemStation allows for the transfer of data to other software packages. For this study the data was transferred into Microsoft's Excel spreadsheet software.

Once the data were input into the Excel spreadsheet, they were converted from integration units to concentrations of parts per million (ppm) by several computational steps. Based on the calibration source, the conversion process proceeded as follows.

Firstly, the integration units were translated to ppm units by mass. Secondly, a conversion factor for ppm units by volume (ppmv) was developed based on the Ideal Gas Law, using a method illustrated in Flagan and Seinfeld (1988). This conversion process proceeded as shown below in Equation 4.1. The average molecular weight for diesel-fuel is obtained from Sabapathi (1993). This represents a calculated molecular weight average of three diesel-fuel samples analyzed by Core Laboratories of Long Beach, California.

Assuming the constants below (Weast, 1983):

$P = 1.0133 * 10^5$ Pa

$T = 298°K$ (room temperature was 24°C)

$R = 8.314$ joule per gram-mol^{-1} degree^{-1}

Molecular weight of octane $= 114.23$ g/mole

Molecular weight* of diesel-fuel $= 173.3$ g/mole

$$ppmv = \left(\frac{SMIug}{40ml}\right) \times \left(\frac{RT \times 10^6}{MW \times P}\right) \qquad (4.1)$$

where,

SMI = calibration sample liquid mass in ug injected into 40 ml sealed vial

MW = Molecular Weight of hydrocarbon

With the conversion factor, a spreadsheet was set up in Microsoft Excel to convert the integrated area into a ppmv value. The ppmv value was combined with its corresponding sampling time interval and radial distances from the source to the observation points and image wells. The data sets were saved as Text files (.TXT) for further analytical modeling.

Estimating Parameters

The analytical model estimated parameter values in of Equations 2.8 and 2.9; D_e, the effective diffusion coefficient, and A^*, the sorption parameter. The source flowrate, q, was determined by methods described previously in Chapter 3.

The method of solution and the descriptions that follow are based on the previous work of Johnson (1992) and Chaganti (1990). The solution method uses a FORTRAN program, found in Appendix A, written with Microsoft's FORTRAN PowerStation software (Microsoft, 1994). The program incorporates and accesses an IMSL subroutine called RNLIN (Visual Numerics, 1994). RNLIN uses a nonlinear, inverse, exponential regression model and an effective modified Levenberg-Marquardt finite difference algorithm as a means to estimate parameters. RNLIN calculated values of the parameters

described in Equation 2.8 and 2.9, (Johnson, 1992). RNLIN modifies initial guesses of D_e and A^* until several convergence criteria are met as described in the RNLIN subroutine user "help notes" (Visual Numerics, 1994). The described solution is an inverse mathematical problem where the observed values of the dependent variable are used to estimate parameters in the governing equations. A similar inverse mathematical solution occurs in groundwater hydrology when estimating storativity and transmissivity from analysis of observed pump test data (Johnson and Kreamer, 1994).

The mass balance of the hydrocarbon vapor release should ideally be checked in the physical model (Johnson 1992). Unfortunately, several factors preclude this from occurring. The mass of the hydrocarbon vapor is known from the amount injected into the source tube, and it is assumed that no free hydrocarbon liquid enters the sandtank. However, it is not known how much or how fast the hydrocarbon vapor sorbs onto the soil particle or into the moisture introduced into the experiment (Johnson and Kreamer, 1994).

Johnson (1992) points out there are at least two potential pitfalls to be considered in using numerical models; (1) non-uniqueness, and (2) instability. Initial non-unique solution estimates are a common problem in nonlinear estimation models (Johnson and Kreamer, 1994). Non-uniqueness did not appear to be a problem in this thesis research, because the results computed from analytical models consistently converged to the same values, even though a wide range of initial guesses were input to the FORTRAN program.

A wide range of possible data input values can be contribute to the second pitfall, which is numerical instability. Input variation over a five order magnitude range, and the equations in which the terms are used can lead to instability. For example, the u-term of both Equations 2.8 and 2.9 is evaluated by the Well Function, an inverse exponential function. The FORTRAN program (analytical model) utilized for this research returns a zero value for the Well Function, if the u-term is more than 10. Despite the seemingly narrow range of magnitude between the u-term and Well Function, additional analysis indicated that the Well Function varied by two orders of magnitude as the u-term ranges from 10^{-5} to 10^{-10} (Johnson, 1992). The result of this instability means that for small values of the u-term, the program did not return a converge to any solution, instead it reported one of two instability errors: (1) storage overflow or (2) a maximum step error in the program. The storage overflow error means that no convergence had occurred prior to exceeding the limits of program storage. Program storage in this study is known to ability to cary out 20,000 iterations, although the absolute maximum is not known. The second instability error-type resulted from the maximum number of steps in one direction being completed, thus an asymptote reported in the RNLIN subroutine. Scaling factors are one way to achieve model stability during solution convergence. A scaling factor of 100 was used in the analytical model to achieve stability in this research. Johnson (1992) notes that neither error indicates that the analytical solutions are non-unique or incorrect; rather, the limits of the computer routines have been reached.

Experiments with Dry Soil

Using the analytical techniques described above, two data sets were evaluated to determine the gaseous diffusion parameters D_e and A^* in a dry media. One data set was from an experimental run using octane as the hydrocarbon vapor source and no added moisture. The other data set was from an experimental run using diesel-fuel and no added moisture. Both of these experiments were conducted in a manner similar to Johnson and Kreamer (1994) and Chaganti (1990).

The data from each experiment were evaluated by using image well theory to simulate boundary conditions in Equation 2.9. The input for the models, including image distances, are found in Appendix B. Graphs of analytical model results, comparing observed concentration values and estimated concentration values for each experimental run, are found in Appendix C. The estimated concentration values are derived from the analytical model described in the Estimating Parameters section of this chapter, above, and using the measured source flowrates (q) of 68.4 ug/s for octane vapor and 3.8 ug/s for diesel fuel vapor.

These graphs, found in Appendix C, visually illustrate the correlation of observed concentration value versus the analytically modeled estimated concentration value. The sandtank observation points were symmetrical pairs. Hence, there was one estimated concentration for each of those pairs at each discrete time interval which was compared to both observed values. The identical symmetric estimated concentration values therefore overlay each other in a manner that appears to indicate that only one estimated concentration value was calculated for several observed concentration values. In fact,

each observed concentration value has a corresponding estimated concentration value derived from the analytical, mathematical model. The observed concentrations for the experiments are listed in Appendix B.

Experiments with Wet Soil

Using the analytical techniques described above, ten experiments were evaluated to determine the gaseous diffusion parameters D_e and A^* in wet soils. Eight data sets were from experimental runs using octane as the hydrocarbon vapor source and added moisture ranging from 1% to 10% by mass. The other two data sets were from experimental runs using diesel-fuel and added water content of 2% and 5% by mass. All of these experiments were conducted in a manner similar to Johnson and Kreamer (1994) and Chaganti (1990).

The data from each experiment with wet soil were evaluated by using image well theory to simulate boundary conditions in Equation 2.9 in a manner described above in for experiments with dry soil. The input for the models including image distances are found in Appendix B. Graphs of model results comparing observed concentration values and estimated concentration values for each experimental run are found in Appendix C. The estimated concentration values are derived from the analytical model described in the Estimating Parameters section of this chapter, above.

Octane Experiments

Data from each physical model included: (1) radial distances between the observation points and the leak source, (2) radial distances between the observation points and the

images (sources and sinks), (3) sampling time intervals, and (4) observed vapor concentrations. All of these data were included in each analytical- (mathematical) model run. The results of the octane analytical model runs are summarized in Table 4.1. The r-correlation factor is also illustrated for each data set corresponding to moisture content by mass. The r-correlation indicates how well the observed concentration values correspond to the estimated concentration values of the analytical model, using estimated values of D_e and A^*. A r-correlation value of 1.00 would indicate the best possible fit between the observed data set and the estimated data set based on the estimated values of D_e and A^*.

Table 4.1 - Analytical Modeling Results from Octane Experiments					
Experimental Run	Moisture % by Mass	D_e cm²/sec	D_k cm²/sec	A^* dimensionless	r-Correlation
JSOC13	0.00%	0.186	0.422	2.27	0.866
JSOC6	1.00%	0.214	0.417	1.95	0.855
JSOC5	2.00%	0.412	0.314	0.762	0.914
JSOC14	5.00%	0.167	0.339	0.203	0.821
JSOC8	6.50%	0.121	0.050	0.416	0.836
JSOC9	7.50%	0.049	0.054	1.106	0.808
JSO10	8.50%	0.184	0.109	0.595	0.778
JSOC12	9.25%	0.041	0.030	0.736	0.575
JSOC11	10.00%	0.135	0.297	2.201	0.709

Combining the data sets was accomplished by arranging the data sets to include data from only ports 1A, 1D, 2A, and 2D. Image source and sink radial distances, actual source distance, sampling time interval, and observed vapor concentration were included in the individual-port mathematical analyses. Therefore, only data from ports furthest

from the source were included in the individual port analyses. Table 4.2 illustrates individual port results for each experiment run.

Table 4.2 - Analytical Modeling Results from Octane Experiments Using Individual Ports - 1A/1D/2A/2D

Experimental Run	Moisture % by Mass	D_e cm^2/sec	D_k cm^2/sec	A^* dimensionless	r- Correlation
JSOC2	0.00%	0.151	0.344	2.28	0.881
JSOC6	1.00%	0.333	0.492	1.48	0.834
JSOC5	2.00%	0.816	0.439	0.539	0.999
JSOC14	5.00%	0.165	0.032	0.194	0.918
JSOC8	6.50%	0.224	0.075	0.334	0.815
JSOC9	7.50%	0.125	0.103	0.820	0.738
JSO10	8.50%	0.139	0.104	0.746	0.866
JSOC12	9.25%	0.151	1.072	7.10	0.779
JSOC11	10.00%	0.075	0.218	2.91	0.777

The variation in the values for D_e and A^* between analytical models summarized in Tables 4.1 and 4.2, could be caused by one or more factors. The factors may include experimental error and gas chromatograph analysis error. Another factor is possible efficient sorption of the gaseous pollutant closer to the line source relative to less efficient sorption occurring at a greater distance from the line source. Potential error sources in the models are discussed later in this chapter.

Diesel Fuel Experiments

Diesel fuel experiments were conducted to evaluate the effect of moisture content on a more complex set of hydrocarbons. Three moisture contents were chosen for the physical modeling runs. The first, 0% moisture, was selected because values of D_e and

A* could be compared to that of previous work completed by Johnson and Kreamer (1994) and Chaganti (1990). The other moisture content values were chosen because, in early work with octane, it was found that moisture contents between 2% and 5% by mass began to profoundly effect the propagation of hydrocarbon vapor. There was a marked increase in the observed concentration during the octane physical modeling as the water content approached 5% by mass. With a water content of 6.5% by mass the observed concentrations were less than that for 5% water content for the same time interval during the octane physical modeling.

The results of the diesel-fuel model runs are illustrated in Table 4.3. These were modeled using similarly gathered data sets as that for the octane physical experiments. The r-correlation factor is also illustrated for each data set corresponding to moisture content by mass.

Table 4.3 - Analytical Modeling Results from Diesel Fuel Experiments

Experimental Run	Moisture % by Mass	D_e cm^2/sec	D_k cm^2/sec	A* dimensionless	r-Correlation
JSDI1	0.00%	1.878	0.0017	0.092	0.896
JSDI2	2.00%	1.567	0.0015	0.098	0.931
JSDI3	5.00%	0.706	0.0011	0.161	0.902

Trends of D_e, D_k, and A*

With the data from Tables 4.1 and 4.3, D_e, D_k, and A* were graphed on a double Y-axis graph to evaluate the trends of both parameters relative to moisture content by mass (Figures 4.2 and 4.3). Octane D_e and D_k values (Figure 4.2) ranged from 0.0409 to

0.410 cm^2/sec and 0.030 to 0.422 cm^2/sec, respectively, over the distribution of moisture contents analyzed.

Figure 4.2 - Comparision of Octane D_e, D_k and A^* Parameters relative to Moisture Content
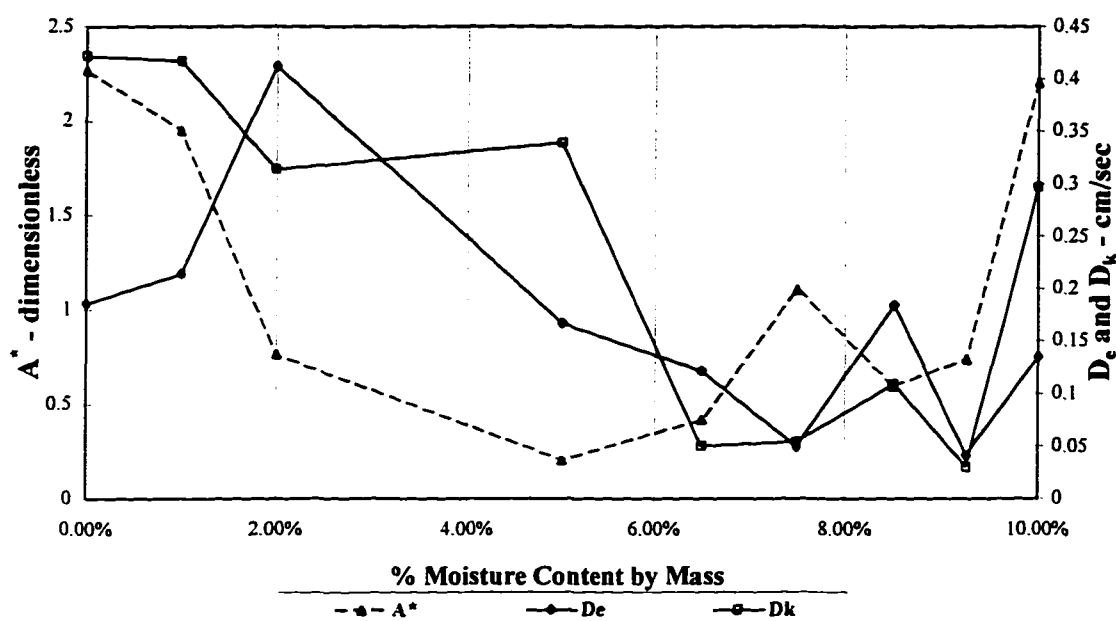
The D_e values for 0% and 1% are interesting to compare, because it appears that the difference in moisture content of 1% by mass caused no significant difference of D_e. The gas chromatograph empirical data from the sandtank model concurs with this observation. Measured concentrations were within one to two ppmv for any given port and discrete time interval for moisture contents of 0% and 1% by mass. When 2% moisture content was added to the sandtank, observed concentrations increased relative to 0% and 1% moisture content. Above 2% moisture content, the D_e values decrease, in general, while A^* continued to decrease up to 5% gravimetric moisture content. After 5%

moisture content, the A^* values, in general, rise with increasing moisture content. The graph presented in Figure 4.2 illustrates calculated D_e and A^* values.

Figure 4.3 - Comparision of Diesel Fuel D_e, D_k, and A^* Parameters relative to Moisture Content
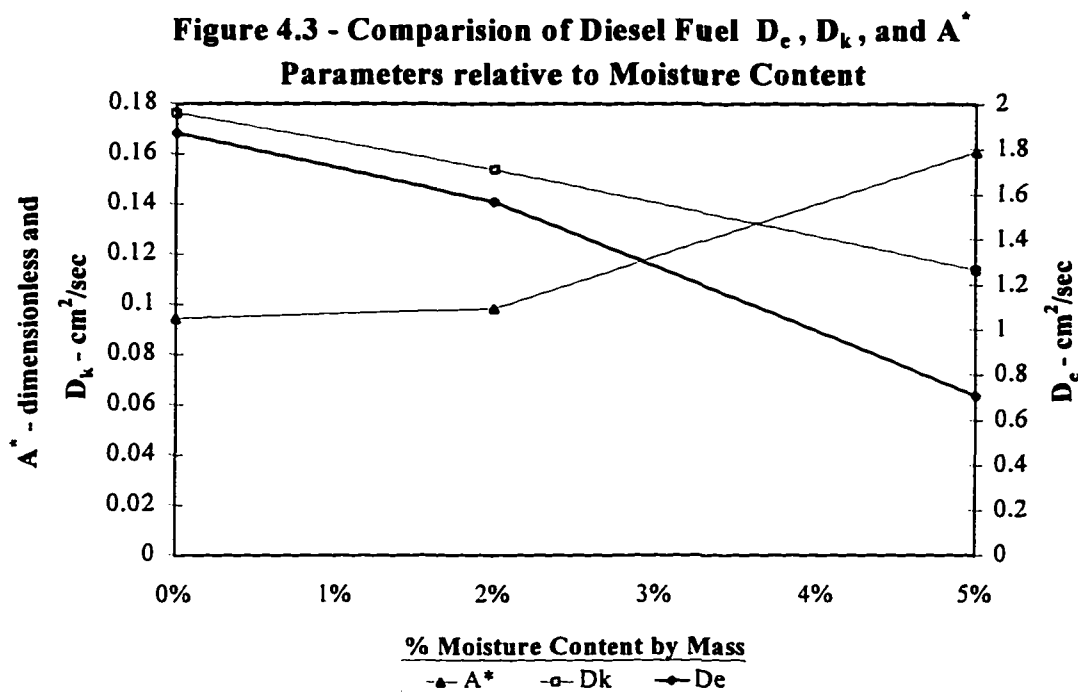
Diesel fuel vapor D_e values (Figure 4.3) were found to range from 0.706 to 1.878 cm^2/sec over the distribution of moisture contents analyzed. Based on the data, it appears that the added moisture decreased D_e. The values of A^* range from 0.645 to 1.130 (dimensionless). The values of A^* track D_e values. When the D_e values decrease, the A^* value increase.

Moisture content effected the octane vapor diffusion adversely after or near 5% moisture content by mass. Diesel-fuel vapor , was affected in the same way as the octane, however, the moisture content was more than 2% and less than 5% when diffusion was impacted.

Tortuosity

Moisture content is an impedance to gaseous diffusion that contributes to tortuosity in natural systems. However, moisture content is not the only impedance. Tortuosity is affected by pore size distribution, pore geometry, and the nature of the pore interconnections (Kreamer et al, 1988).

The results from the analytical modeling allowed for the tortuosity of the system to be calculated for each moisture content. From Equation 2.3

$$D_e = \frac{D_k}{A^*} = \frac{\tau \theta_D D}{\theta_D + (\theta_D - \theta_T)p_w k_w + (1 - \theta_T)p_s k_s}$$

On the right side of Equation 2.3, the denominator of is A^*, while the numerator is D_k, the effective diffusion coefficient not corrected for sorption. The drained porosity, θ_D, was calculated for each moisture content as shown in Table 4.4. The general diffusion coefficient, D, can be calculated by a method developed by Jarvis and Lugg (1968) for single compound liquids, like octane. Their method is described by Lyman et al, (1990). Using the Jarvis and Lugg (1968) method, the general diffusion coefficient of octane vapor into air was calculated to be 0.0658 cm^2/s. A deviation of ±5% between calculated values versus measured values is typical (Jarvis and Lugg, 1968). The calculated tortuosity factor, τ, is shown for octane vapor experiments, from this thesis, in Table 4.4.

Table 4.4 - Tortuosity Calculations from Octane Vapor

Analytical Modeling Results of the Outer Ports

Experimental Run	Moisture % by Mass	θ_D	D_e cm²/sec	$A^{\bullet}$ dimensionless	D cm²/sec	τ
JSOC2	0.00%	0.415	0.151	1.598	0.0658	8.836
JSOC6	1.00%	0.400	0.333	1.037	0.0658	13.12
JSOC5	2.00%	0.384	0.816	0.377	0.0658	12.18
JSOC14	5.00%	0.337	0.165	0.136	0.0658	1.01
JSOC8	6.50%	0.314	0.224	0.234	0.0658	2.54
JSOC9	7.50%	0.298	0.125	0.574	0.0658	3.66
JSO10	8.50%	0.283	0.139	0.522	0.0658	3.90
JSOC12	9.25%	0.271	0.151	5.029	0.0658	42.59
JSOC11	10.00%	0.260	0.075	2.042	0.0658	8.95

Lyman et al, (1990) also described equations from Hamaker (1972) that can be used to calculate the general diffusion coefficient when the molecular weight of each two compounds is known and one of the general diffusion coefficients is known. The average molecular weight of diesel fuel was previously discussed in this chapter. Using the Hamaker (1972) method, the general diffusion coefficient of diesel fuel vapor into air was calculated to be 0.0534 cm²/s. The drained porosity, θ_D, was calculated for each moisture content as shown in Table 4.5, along with the calculated tortuosity factor, τ.

Table 4.5 - Tortuosity Calculations from Diesel Fuel Vapor

Analytical Modeling Results

Experimental Run	Moisture % by Mass	θ_D	D_e cm²/sec	$A^{\bullet}$ dimensionless	D cm²/sec	τ
JSDI1	0.00%	0.415	1.878	0.092	0.0534	7.80
JSDI2	2.00%	0.384	1.567	0.098	0.0534	7.49
JSDI3	5.00%	0.337	0.706	0.161	0.0534	6.28

Tortuosity factors, for each moisture content, from octane and diesel fuel vapor

analytical models are plotted in Figure 4.4.

**Figure 4.4 - Tortuosity Factors of Octane and Diesel Fuel
Vapors for Various Moisture Contents**
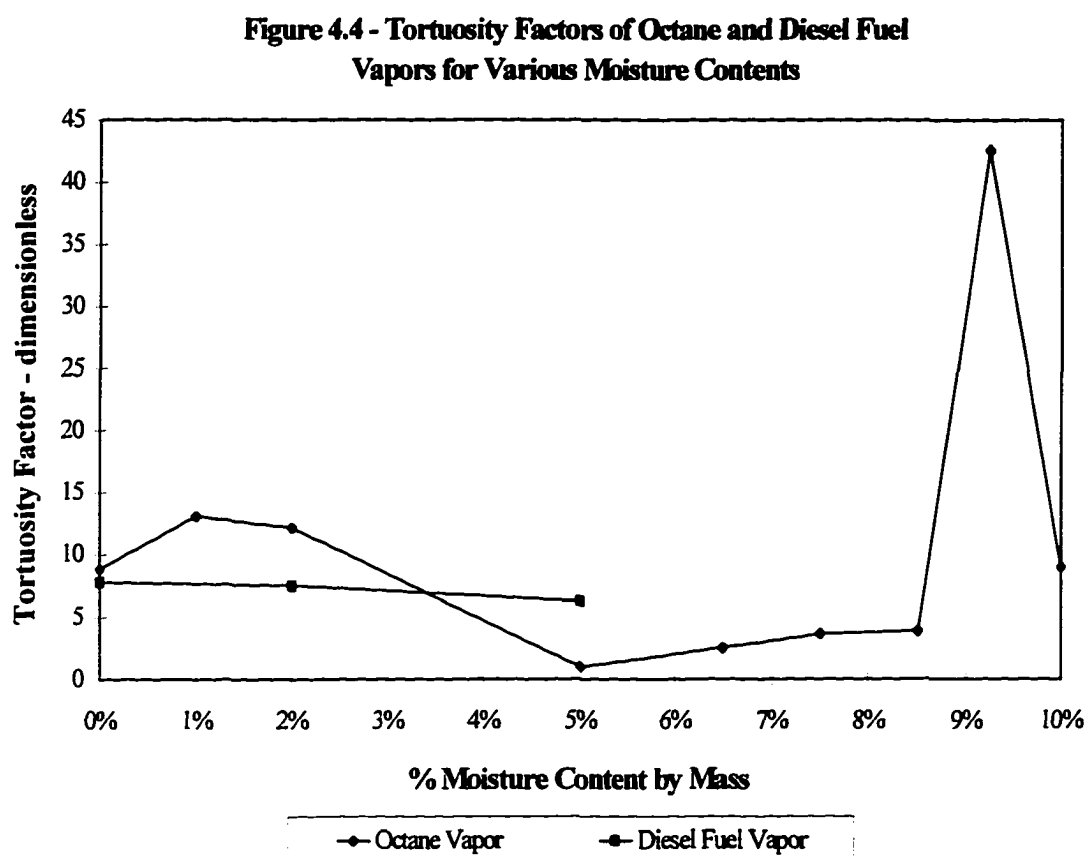
Results indicate that with higher moisture contents the available pathways for

vapor propagation were either: (1) being occluded to the point of blockage so diffusion is

decreased with time, space and increasing moisture content, (2) being effected by

sorption which had been occurring up to 6.5%, but not a dominant factor until this

moisture content was reached, or (3) being effected by a combination these or some other

unknown factor.

Three-Dimensional Modeling

The estimated values of D_c, D_k, and A^*, for each moisture content (see Tables 4.1 and 4.3) were used in the three-dimensional analytical model described in Equation 2.10 to predict vapor concentrations for octane and diesel-fuel, respectively. It is important to note that this analytical model only accounts for diffusion of a vapor from a stationary source like that used in the experiments described earlier. Therefore, the physical system characteristics matched the model requirements.

The calculated gaseous octane concentrations for gravimetric moisture contents ranging from 0% to 5% are plotted in Figure 4.5. The octane results for moisture contents from 5% to 10% are plotted in Figure 4.6. The 30-day diesel-fuel three-dimensional modeling results are compared to the respective 0%, 2% and 5% 30-day octane modeling results in Figure 4.7. These results assume that the soil would be similar to that used in the sandtank model to predict the three-dimensional spreading of vapor. Likewise, the gravimetric moisture contents would have to be similar and homogenous throughout the soil.

The estimated D_c and A^* values chosen for the three-dimensional models were those computed from the two-dimensional analytical mathematical predictions that used the entire data set in the modeling analysis. The source flowrate, Q_v, was assumed to be 10 g/s in the calculations needed to develop the vapor concentration curves. A Microsoft Excel® spreadsheet was used to calculate the resulting vapor concentrations at a variety of distances ranging from 1 cm to 1000 cm for three different discrete times, 1 day, 7 days, and 30 days. The vapor concentration curves for each moisture content by mass

and fuel type are included in Appendix D. These vapor concentration curves are graphs of 1-day, 7-day, and 30- day analytical models for each moisture content by mass.

Figure 4.5 shows that, with increasing moisture content by mass, the predicted octane vapor concentrations increase up to 2% moisture content. Above 2% moisture content, the predicted octane vapor concentrations decrease. These predictions generally agree with the physical model results. However, the value of r-correlation decreases, indicating increased uncertainty. As previously mentioned, the modeled values for 0% and 1% gravimetric moisture contents are very similar.

An increase in concentration occurs in the three-dimensional, analytical model as noted in Figure 4.6 for gravimetric moisture contents ranging from 5% to 6.5%. As noted previously, caution is required interpreting results for 6.5% and higher moisture contents because of low r-correlation values and moisture movement to the bottom of the sandtank. Vapor concentrations decrease after 6.5% moisture content, in general neglecting the vapor concentration from 9.25% moisture content which has a low r-correlation value.

Figure 4.5 - Octane Vapor 30-day Concentration Curves
for 0% to 5% Moisture Contents by Mass
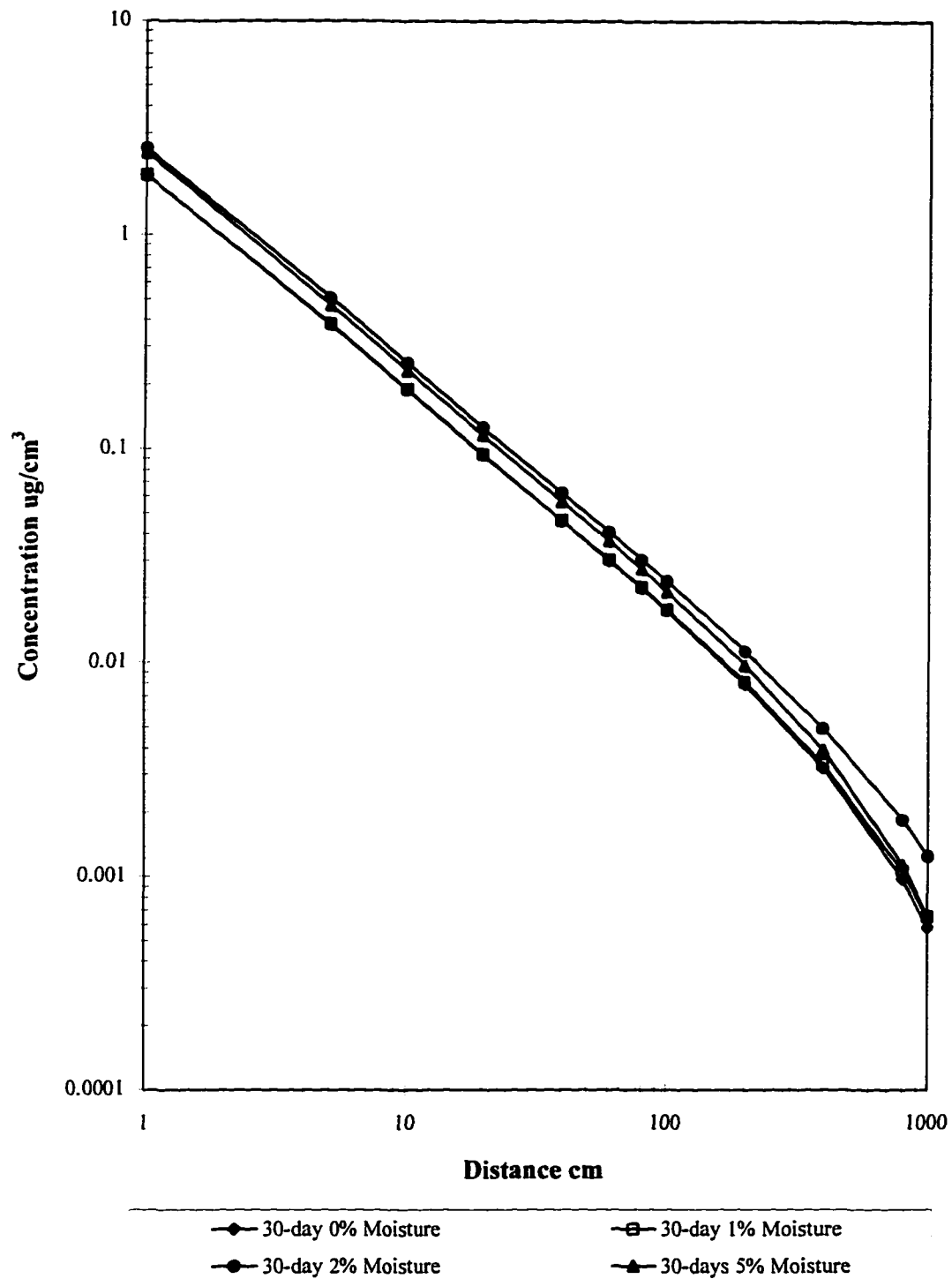
**Figure 4.6- Octane 30-day Concentration Curves
for 5% to 10% Moisture Contents by Mass**
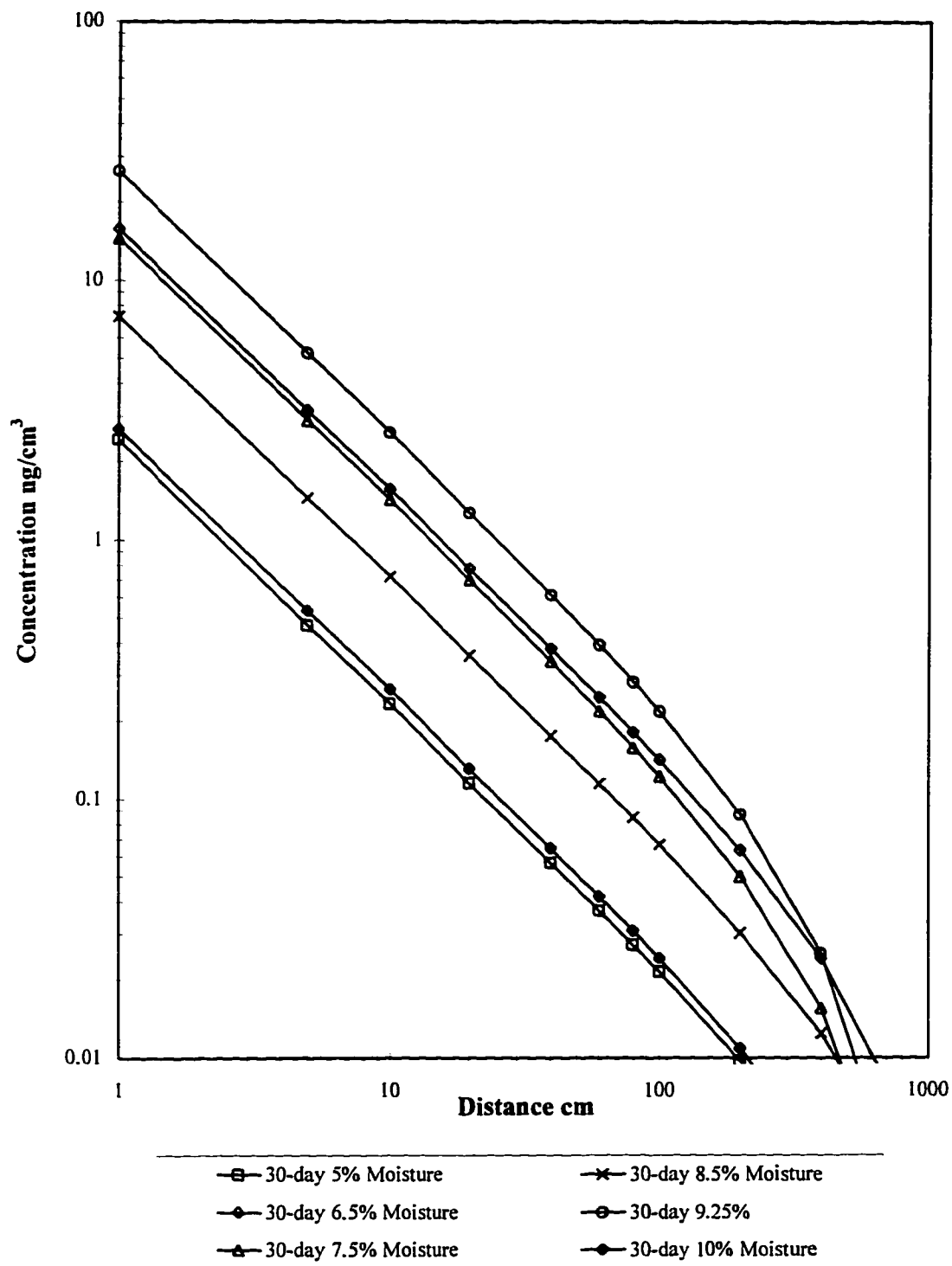
For the vapor concentration curves corresponding to 7.5% and 9.25% gravimetric moisture content, there appears to be a factor from the physical experiment that has influenced the calculated data sets. These two curves have a distinctly different shape relative to the other curves in the graph (Figure 4.6). The observed increased curvature seems to be related to their respective D_e values that are a factor of three to four times lower than those obtained at other moisture contents (Tables 4.1 and 4.2). Whereas it seems likely that this may be the result of physical experimental error, the cause of this phenomena should be examined in subsequent investigations, as discussed in Chapter 5.

Octane vapor analytical three-dimensional modeling results for moisture content of 0%, 2%, and 5% by mass were compared to diesel-fuel vapor, analytical three-dimensional modeling results for the same moisture contents. Figure 4.7 illustrates predicted 30-day vapor-concentration curves modeled for octane and diesel-fuel.

The diesel-fuel curves are similar to those of octane except for the magnitude of the vapor concentration. The concentration differences are expected because of the lower physical experiment source flowrate related to the lower volatility of diesel-fuel vapor compounds relative to octane vapor. The diesel-fuel vapor concentration curves are also very close to each other, graphically and numerically. As a result, in field conditions, predicted diesel vapor transport mat not appear to vary significantly with soil moisture content below 5%.

Figure 4.7 - Octane vs. Diesel Fuel 30-day Vapor Concentration Curves for Moisture Contents 0%, 2% and 5% by Mass
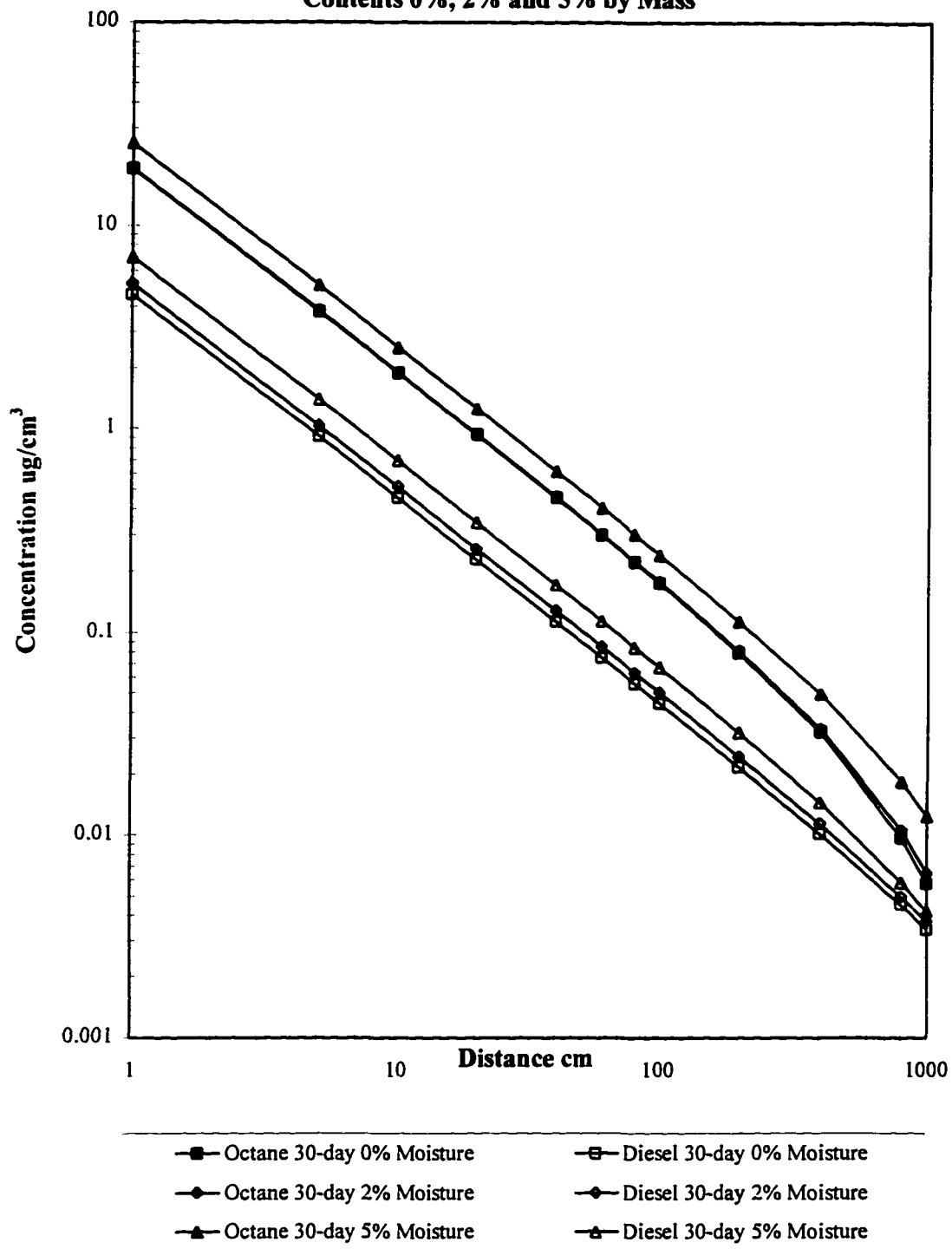
Limitations of the Model

The physical model was carefully constructed to maximize the information collected similar to that of Chaganti (1990), Sabapathi (1993), Rajagopalan (1994), and Johnson and Kreamer (1994), all of whom used similar physical models and each of whom discuss the errors associated with sandtank physical modeling. In order to allow mathematical modeling using Equations 2.8 and 2.9, the physical model was constructed to simulate vapor flow in only two dimensions. To further simplify the model, only silica sand from one manufacturer with a low organic content was used for each experimental run. The number of phases which the hydrocarbon vapor could occupy varied, and was complicated by moisture content.

Many previous investigators have suggested that increased soil moisture content will increase the velocity and concentration of pollutant vapors (Robbins et al, 1990, Mendoza and McAlary, 1990). This result was observed in octane experiments conducted in this thesis at moisture contents of 2% to 8%. The shape of the curve describing dependence of D_e and moisture is not currently accounted for in existing models.

Another simplifying factor was the placement of the soil. In all experimental runs the soil was implaced, to the extent possible, without layering. Previous work by Johnson (1992) has demonstrated that the orientation of soil layers impacts the propagation of pollutant vapor. Efforts were made in the experimentation presented in this thesis to minimize layering. Consequently, the physical model was limited, but designed to acquire information needed for the mathematical model.

The mathematical model was constructed to use data obtained from the physical model. The physical model was two-dimensional and allowed for information to be acquired from each sandtank experiment. The information was collected from discrete, time-dependent observation points.

For diesel-fuel experiments, the composition of the vapor is likely to change with time and space as the more volatile molecules evolve from the source tube in early time, with the less volatile molecules following at a later time.

The mathematical model considers only diffusion, assuming constant vapor consistency. Advection in the sandtank was excepted to be minimal over the duration of the experiment. Gaseous advection in the vadose zone can be triggered by barometric pumping, groundwater table fluctuations, and gravity convection of dense gases.

The mathematical model is also limited by the inverse method of solution for this type of mathematical problem. Inverse methods allow for estimation of governing parameters when the results of the system are known. Usually, the more data points or observations that are collected, the greater the likelihood that a stable, unique solution may be found. The experiments conducted for this thesis have a limited number of observations. This allows that some of the inverse mathematical solutions predicted in the work herein could be non-unique.

A number of steps were followed to reduce error in the physical and mathematical models. Nevertheless, error introduced by sampling and analytical technique can easily be introduced in any experiment by the operator. Gas chromatographs can produce error when not properly functioning or maintained due to

sensitive optics, proper gas flow, and good quality septa. The gas-tight syringes used for each experiment were carefully handled as to avoid contamination from liquid sources. Additionally, high purity gases were used for all gas chromatograph analyses. The gas chromatograph septa was changed with regular frequency to avoid the physical and thermal breakdown that can occur with numerous sample injections and prolonged gas chromatograph heating cycles.

Four image sources and sink calculations were included in the analytical model for each observation point (Figure 4.1). Previous investigators suggest image sources and sinks do not significantly impact the diffusion parameters (Johnson and Kreamer, 1994 and Chaganti, 1990). Analysis of a second set image sources and sinks was conducted in this thesis beyond the three image sources and one image sink for each observation point and found to have a less than 2% impact on the observed versus the estimated vapor concentration results. This relatively low percentage impact appears to concur with the previous investigators. No additional investigation was therefore made beyond a second set of image sources and sinks

The combination of the errors discussed above did cause a range of final parameter estimates for a given moisture content when modeling port-by-port. However, multiple experiments with identical moisture contents by mass yielded similar physical data. The results are similar to the previous work of Johnson and Kreamer (1994) and Chaganti (1990) in how they were derived.

Chapter 5

Conclusions and Recommendations

Conclusions

In the experiments conducted for this thesis, soil moisture content by mass was varied to simulate a variety of moisture conditions that affected vapor diffusion rates from different two vapor pollutants, octane and diesel fuel. Experimental results showed that soil moisture content influenced propagation of hydrocarbon vapors from a source. The effects of each soil moisture condition were mathematically modeled.

The physical sandtank model allowed adequate introduction of a vapor only source and subsequent monitoring of vapor concentrations from observation points. Analytical modeling predictions based on the two-dimensional physical model vapor concentrations established that analytical modeling is reproducible for moist soil. Physically observed vapor concentrations correlate well with the estimated vapor concentrations predicted in the mathematical model.

Moisture content, up to 2% by mass, had profound effects on octane vapor propagation in that it increased vapor concentration with a corresponding moisture content increase and a decreasing A^* value. When the moisture content equaled and exceeded 6.5%, the octane vapor concentration generally increased, along with the corresponding A^* value increase. This occurred until moisture content equaled 8.5%

58

corresponding A^* value increase. This occurred until moisture content equaled 8.5% gravimetrically, at which time vapor concentrations appear to drops with the increased moisture content and increasing A^* value. It is postulated that vapor concentrations went down because the available porosity became progressively occluded so that there were progressively fewer pathways for vapor propagation. The A* value for 10% moisture content warrants further investigation.

Tortuosity factors decreased with increasing moisture contents up to 5% for octane vapor analytical models based on physical datasets. After 5% moisture content, tortuosity increased slightly up to 8.5% moisture content. At 9.25% moisture content, gravity drainage likely affected the results observed in the physical model in a manner that was carried over to the analytical model.

Tortuosity factors decreased with increasing moisture content for diesel fuel vapor experiments, for the moisture content range analyzed in this thesis.

Chaganti (1990), Johnson (1992), and Johnson and Kreamer (1994) discuss the implications of vapor propagation in porous media to soil-gas monitoring around underground storage tanks. These investigators modeled dry soil in their respective analytical models. When considering moisture content, the placement of soil-gas monitors relative to an underground storage tank location may be more critical than previously thought. Because soil moisture content by mass of 2% to 5% decreased diesel fuel vapor propagation rate, it is possible that infiltration of water from storms or facility washdowns could adversely affect the detection performance of soil-gas monitoring systems.

Recommendations

Results from this thesis indicate that additional experimental work and modeling analysis. Specifically, the moisture contents by mass should be narrowed to include additional datapoints for graphically representing the relationship between D_e to A^* as moisture content increases in smaller incremental steps between 2% to 7.5% moisture content for octane experiments. Similar experiments and modeling should be conducted for gasoline and diesel fuel vapors between the moisture content by mass range of 2% to 7.5% by mass. Higher moisture contents should be investigated for hydrocarbon vapor propagation effects, however, methods to increase moisture contents while not inducing gravity drainage will need to be addressed.

The physical model was small relative to physical models used by previous investigators. The result of physical-model size manifests itself in the graphs presented in Appendix C. The graphs illustrate that with close-by, symmetric, observation points, reproducible results of the various symmetries can be readily observed which can be used as a tool to detect possible malfunctioning syringes or heterogeneity of the sand placement. Despite this potential advantage, observation points that are more distant from the source and perhaps non-symmetrical may yield a better picture of the relationship between soil moisture D_e , and A^*. It is recommended that larger scale sandtank experiments be conducted in the future to assess the effects of greater distance from the vapor source. Additionally, soil types and physical barriers should also be varied in future physical models that may represent possible field conditions.

Appendix A

FORTRAN PROGRAM for Analytical Model

After Chaganti (1990)

61

```
C    MODEL TO ESTIMATE THE DIFFUSION PARAMETERS De AND q/A FROM
C    OBSERVED EXPERIMENTAL DATA
C
C    Program language is bolded here only for clarification
C
C
C    Data is input by referencing a file with extension .TXT which can be created in
C    Microsoft's Excel software, output file can be created with the extension .OUT, these
C    can be accessed with Microsoft's Excel software
C
C    Includes Images Values
C    Designed to take input as minutes, cm, and ug/cm3
C    Multiplies Concentration Input by 100
C
C    Estimate the parameters using RNLIN and E1 (from IMSL subroutines)
C    and find observed and estimated concentrations.
C
C    You must reference the IMSL FORTRAN Subroutines in the OPTIONS MENU,
C    click PROJECT, click on LINKER, then enter "maths_s.lib stats_s.lib"
C    in the OPTIONS STRING box at the end of the existing statement, click
C    on the OK button to exit the LINKER
C

     INTEGER LDR,NOBS,NPARM,MXOBS
     PARAMETER (MXOBS=200, NPARM=2, LDR=NPARM)
C
C    NOBS IS THE NUMBER OF OBSERVATIONS YOU HAVE.  NPARM IS THE
C    NUMBER OF PARAMETERS YOU WANT TO ESTIMATE.  IN THIS CASE I
C    WANT TO ESTIMATE  (Q/A)

C    AND THE EFFECTIVE DIFFUSIVE COEFFICIENT (D).
C
C    The "C" starting the third line below is a continue statement for the previous line
C
     INTEGER IDERIV,IRANK,NOUT
     REAL DFE,THC,R(LDR,NPARM),SSE,C(NPARM),T(MXOBS),
    CR1(MXOBS),R2(MXOBS),R3(MXOBS),R4(MXOBS),R5(MXOBS),Y(MXOBS)
     COMMON T,R1,R2,R3,R4,R5,Y,NOBS
     COMMON /UNITS/ LUIN,LUOUT,LUTTO,LUTTI,LOUT, CHARACTER
     INPFIL*12, OUTFIL*12, OUTFIL1*12,OUTFIL2*12,TITLE*80
     CHARACTER ANS,YES,SYES,NO,SNO
```

```
      EXTERNAL THC,RNLIN,UMACH,WRRRN,E1
C
      DATA YES,SYES,NO,SNO /'Y','y','N','n'/
C
C     READ TITLE
C
      WRITE(6,1)
   1  FORMAT(/1X,'GIVE TITLE AND DESCRIPTION (MAX 80
     CCHARACTERS)')
      READ (5,2)TITLE
   2  FORMAT(A80)
C
C     READ NOBS
C
      WRITE(6,*) 'TYPE NUMBER OF OBSERVATIONS'
      READ(5,*) NOBS
C
C     READ INPUT FILE NAMES
C
      WRITE(6,3)
   3  FORMAT(/,1X,'TYPE INPUT FILE NAME: ',$)
      READ(5,4)INPFIL
   4  FORMAT (A12)
C
      OPEN(UNIT=LUIN,FILE=INPFIL,STATUS='OLD')
C
C     READ R AND CONCENTRATION VALUES
C
      DO 5 I=1,NOBS
C
C     READS JUST TIME, DISTANCE, AND OBSERVED CONCENTRATION
C     VALUES.  SO INPUT FILE SHOULD HAVE THREE COLUMNS AND 'NOBS'
C     ROWS.  NOBS IS THE NUMBER OF OBSERVATIONS YOU HAVE. IN
C
      READ(LUIN,*)T(I),R1(I),R2(I),R3(I),R4(I),R5(I),Y(I)
C
C     ADJUSTS T TO SEC AND CONCENTRATION TO MG/ML S
C
      T(I)=T(I)*60
      Y(I)=Y(I)*1E2
C
   5  CONTINUE
C
      WRITE(6,7)
   7  FORMAT(/1X,'TYPEOUTPUT FILE NAME: ',$)
```

```
      READ(5,8) OUTFIL
  8   FORMAT(A12)

C     OUTFIL='out.out'
  9   OPEN(UNIT=LUOUT,FILE=OUTFIL,STATUS='NEW')
      WRITE(LUOUT,90) INPFIL,OUTFIL
 90   FORMAT(/,1X,'INPUT FILE: ',A12,//1X,'OUTPUT FILE: ',A12)
C
C
C     READ INTIAL GUESSES FOR PARAMETERS
C
C
 13   WRITE(6,18)
 18   FORMAT(1X,'GIVE INITIAL GUESSES FOR PARAMETERS')
      WRITE(6,*)'Q/A      D'
      READ(5,*)C
      WRITE(6,*)C
C
C     WRITE INITAL GUESSES IN OUTPUT FILE
C     The "C" starting the third line below is a continue statement for the previous line
C

      WRITE (LUOUT,19)C
 19   FORMAT(/,1X,'INITIAL GUESSES FOR THE PARAMETERS ARE:',
     C      /,1X, 'Q/A=',F15.6, 2X, 'D=',F15.6)
C
C     CALL THE SUBROUTINE TO ESTIMATE THE PARAMETERS AND WRITE
C     THE  RESULTS  TO THE OUTPUT FILE
C
      IDERIV=0
      CALL RNLIN(THC,NPARM,IDERIV,C,R,LDR,IRANK,DFE,SSE)
C
      WRITE(6,*) '========================================='
      WRITE(6,*) 'Q/A=', C(1), 'De=', C(2)
      WRITE(6,*) 'SSE=',SSE
C
C     The "C" starting the third line to the sixth line  below are continue statements for the
C     previous line

      WRITE(LOUT,999) C,IRANK,DFE,SSE
 999  FORMAT( /,1X, 'THE SOLUTION IS ',
     C      /,1X, 'Q (RATE OF DIFFUSION/SOR. COR. POR.)=',E15.9,
     C      /,1X, 'D (EFFECTIVE DIFFUSION COEFFICIENT)='E15.9,
     C      /,1X, 'THE RANK IS ', 10X,I3,
     C      /,1X, 'DFE=',F10.5,3X,'SSE',F19.3)
```

```
C
C    CALL WRRRN(TITLE,NPARM,PARM,R,LDR,0)
C    The "C" starting the third line to the sixth line  below are continue statements for the
C    previous line
C
     WRITE(LUOUT,20)
20   FORMAT( 1X,'  OBSERVED   ',' ESTIMATED  ',' RESIDUAL   '
     C    1X,'  % ERROR   '/
     C    1X,'_____','_____','_____'
     C    1X,'_____')
C
C    CALCULATE THE ESTIATED CONCENTRATIONS FROM THE ESTIMATED
C    PARAMETERS
C
     SSQ=0
     DO 30 I=1,NOBS
     R11=R1(I)**2/(4*C(2)*T(I))
     R12=R2(I)**2/(4*C(2)*T(I))
     R13=R3(I)**2/(4*C(2)*T(I))
     R14=R4(I)**2/(4*C(2)*T(I))
     R15=R5(I)**2/(4*C(2)*T(I))
C
C    R11 IS THE U IN THE WELL FUNCTION W(U); U=R**2/4DT
C    ESTIM ESTIMATES THE CONCENTRATION BASED ON THE ESTIMATED
C    PARAMETERS-C(1) WHICH IS Q/A AND C(2) WHICH IS D (DIFFUSION
C    COEFF.) I.E. ESTIM=(Q/(4*PI*A*D))*W(U).  IN THIS SUBROUTINE,
C    E1 CALCULATES C THE WELL FUNCTION.  E1 IS ALSO AN IMSL
C    FUNCTION SUBROUTINE.
C    Use a "+" sign for image sources and a "-" sign for image sinks, to calculate only
C    A* of q/A*, then isert the value X before C(1) as (X/(C(1)........this must also be
C    done below The "C" in the second line below is a continue statements for the
C    previous line
C
     ESTIM=(C(1)/(4*3.14159*C(2)))*((E1(R11))+E1(R12)+E1(R13)
     C    +E1(R14)-E1(R15))
     ERR=ABS(ESTIM-Y(I))
     SSQ=SSQ+ERR**2
     PERCERR=ERR*100/(Y(I))
     WRITE(LUOUT,*)Y(I),ESTIM,ERR,PERCERR
C
     IF (IND.EQ.1) THEN
     RRR1=R1(I)**2/(T(I))
          WRITE(8,*)RRR1,Y(I),ESTIM
          ENDIF
30   CONTINUE
```

```
C
      WRITE(LUOUT,21)
21    FORMAT (1X,'_____','_____','_____'
      C     1X,'_____')
      WRITE(LUOUT,22)SSQ
22    FORMAT(1X, 'SUM OF SQUARES OF RESIDUALS= ',E15.9)
C
      END
***********************************************************************
C       SUBROUTINE     WHICH     DEFINES     THE     PROBLEM
***********************************************************************
      SUBROUTINE THC(NPARM,C,IOPT,IOBS,FRQ,WT,E,DE,IEND)
      COMMON /UNITS/ LUIN,LUOUT,LUTTO,LUTTI,LOUT
      INTEGER NPARM,IOPT,IOBS,IEND,NOBS
      REAL C(NPARM),FRQ,WT,E,DE(1)
      EXTERNAL E1
C     E1 above is a reference to the IMSL Subroutines.  E1 is the Well Function.
      PARAMETER (MXOBS=200)
C     The "C" in the second line below is a continue statements for the previous line
      REAL EXP,T(MXOBS),R1(MXOBS),R2(MXOBS),R3(MXOBS),R4(MXOBS),
      C R5(MXOBS),Y(MXOBS)
      COMMON T,R1,R2,R3,R4,R5,Y,NOBS
      INTRINSIC EXP
      IF (IOBS.LE.NOBS) THEN
      WT=1.0E0
      FRQ=1.0E0
      IEND=0
      R11=R1(IOBS)**2/(4*C(2)*T(IOBS))
      R12=R2(IOBS)**2/(4*C(2)*T(IOBS))
      R13=R3(IOBS)**2/(4*C(2)*T(IOBS))
      R14=R4(IOBS)**2/(4*C(2)*T(IOBS))
      R15=R5(IOBS)**2/(4*C(2)*T(IOBS))
C     to calculate only A* of q/A*, then isert the value X before C(1) as (X/(C(1)........this
C     must also be done above
      WRITE (LUOUT,66) T(IOBS),R11, C(2)
 66   FORMAT(1X, F8.1, 1X, F15.8, 1X, F15.4)
      E=Y(IOBS)-(C(1)/(4*3.14159*C(2)))*(E1(R11)+E1(R12)+E1(R13)
      C +E1(R14)-E1(R15))
      WRITE (LUOUT,67) T(IOBS), R11, C(1)
 67   FORMAT (F8.1,1X, F15.8, 1X, F15.8)
      ELSE
      IEND=1
      ENDIF
      RETURN
      END
```

Appendix B

Analytical Modeling Input Data

67

Octane Vapor
Analytical Model Input from 0% Moisture Content By Mass Physical Experiment Data

	Observation Port		Image Sources			Image Sink	Vapor
	Label	r1	r2	r3	r4	r5	Concentration
Minutes		cm	cm	cm	cm	cm	ppmv
20	1a	12.3	21.5	40.5	40.1	25.9	0.1453
20	1b	8.3	26.6	34.3	39.1	24.1	0.0891
20	1c	8.3	34.3	26.6	39.1	24.1	0.1915
20	1d	12.3	40.5	21.5	40.1	25.9	0.1289
20	2a	9.8	20.8	39.8	33	33	0.1594
20	2b	3.5	26.5	26.5	31.6	31.6	0.2998
20	2c	3.5	33.5	26.5	31.6	31.6	0.3229
20	2d	9.8	39.8	20.8	33	33	0.1409
20	3a	12.3	21.5	40.5	25.9	40.1	0.1312
20	3b	8.3	26.6	34.3	24.1	39.1	0.2041
20	3c	8.3	34.3	26.6	24.1	39.1	0.1926
20	3d	12.3	40.5	21.5	25.9	40.1	0.1815
40	1a	12.3	21.5	40.5	40.1	25.9	0.2142
40	1b	8.3	26.6	34.3	39.1	24.1	0.2584
40	1c	8.3	34.3	26.6	39.1	24.1	0.2593
40	1d	12.3	40.5	21.5	40.1	25.9	0.2301
40	2a	9.8	20.8	39.8	33	33	0.2403
40	2b	3.5	26.5	26.5	31.6	31.6	0.384
40	2c	3.5	33.5	26.5	31.6	31.6	0.3743
40	2d	9.8	39.8	20.8	33	33	0.2644
40	3a	12.3	21.5	40.5	25.9	40.1	0.2072
40	3b	8.3	26.6	34.3	24.1	39.1	0.2532
40	3c	8.3	34.3	26.6	24.1	39.1	0.2563
40	3d	12.3	40.5	21.5	25.9	40.1	0.2364
60	1a	12.3	21.5	40.5	40.1	25.9	0.3061
60	1b	8.3	26.6	34.3	39.1	24.1	0.3349
60	1c	8.3	34.3	26.6	39.1	24.1	0.3284
60	1d	12.3	40.5	21.5	40.1	25.9	0.291
60	2a	9.8	20.8	39.8	33	33	0.364
60	2b	3.5	26.5	26.5	31.6	31.6	0.3898
60	2c	3.5	33.5	26.5	31.6	31.6	0.4297
60	2d	9.8	39.8	20.8	33	33	0.3207
60	3a	12.3	21.5	40.5	25.9	40.1	0.2744
60	3b	8.3	26.6	34.3	24.1	39.1	0.3615
60	3c	8.3	34.3	26.6	24.1	39.1	0.352
60	3d	12.3	40.5	21.5	25.9	40.1	0.2836
90	1a	12.3	21.5	40.5	40.1	25.9	0.3351
90	1b	8.3	26.6	34.3	39.1	24.1	0.3799
90	1c	8.3	34.3	26.6	39.1	24.1	0.4059
90	1d	12.3	40.5	21.5	40.1	25.9	0.3951

Octane Vapor
Analytical Model Input from 0% Moisture Content By Mass Physical Experiment Data

| Minutes | Observation Port | | Image Sources | | | Image Sink | Vapor |
| | Label | r1 | r2 | r3 | r4 | r5 | Concentration |
		cm	cm	cm	cm	cm	ppmv
90	2a	9.8	20.8	39.8	33	33	0.3739
90	2b	3.5	26.5	26.5	31.6	31.6	0.521
90	2c	3.5	33.5	26.5	31.6	31.6	0.5199
90	2d	9.8	39.8	20.8	33	33	0.3913
90	3a	12.3	21.5	40.5	25.9	40.1	0.3567
90	3b	8.3	26.6	34.3	24.1	39.1	0.4443
90	3c	8.3	34.3	26.6	24.1	39.1	0.4392
90	3d	12.3	40.5	21.5	25.9	40.1	0.4462
120	1a	12.3	21.5	40.5	40.1	25.9	0.4862
120	1b	8.3	26.6	34.3	39.1	24.1	0.5417
120	1c	8.3	34.3	26.6	39.1	24.1	0.5821
120	1d	12.3	40.5	21.5	40.1	25.9	0.4812
120	2a	9.8	20.8	39.8	33	33	0.5928
120	2b	3.5	26.5	26.5	31.6	31.6	0.635
120	2c	3.5	33.5	26.5	31.6	31.6	0.6064
120	2d	9.8	39.8	20.8	33	33	0.4509
120	3a	12.3	21.5	40.5	25.9	40.1	0.4506
120	3b	8.3	26.6	34.3	24.1	39.1	0.5772
120	3c	8.3	34.3	26.6	24.1	39.1	0.5296
120	3d	12.3	40.5	21.5	25.9	40.1	0.5948

Octane Vapor
Analytical Model Input from 1% Moisture Content By Mass Physical Experiment Data

	Observation Port		Image Sources			Image Sink	Vapor
	Label	r1	r2	r3	r4	r5	Concentration
Minutes		cm	cm	cm	cm	cm	ppmv
20	1a	12.3	21.5	40.5	40.1	25.9	0.17405
20	1b	8.3	26.6	34.3	39.1	24.1	0.2029
20	1c	8.3	34.3	26.6	39.1	24.1	0.20264
20	1d	12.3	40.5	21.5	40.1	25.9	0.18157
20	2a	9.8	20.8	39.8	33	33	0.14023
20	2b	3.5	26.5	26.5	31.6	31.6	0.24233
20	2c	3.5	33.5	26.5	31.6	31.6	0.25742
20	2d	9.8	39.8	20.8	33	33	0.14269
20	3a	12.3	21.5	40.5	25.9	40.1	0.13965
20	3b	8.3	26.6	34.3	24.1	39.1	0.20879
20	3c	8.3	34.3	26.6	24.1	39.1	0.21092
20	3d	12.3	40.5	21.5	25.9	40.1	0.13087
40	1a	12.3	21.5	40.5	40.1	25.9	0.28587
40	1b	8.3	26.6	34.3	39.1	24.1	0.28355
40	1c	8.3	34.3	26.6	39.1	24.1	0.28885
40	1d	12.3	40.5	21.5	40.1	25.9	0.25923
40	2a	9.8	20.8	39.8	33	33	0.24465
40	2b	3.5	26.5	26.5	31.6	31.6	0.37896
40	2c	3.5	33.5	26.5	31.6	31.6	0.33736
40	2d	9.8	39.8	20.8	33	33	0.24521
40	3a	12.3	21.5	40.5	25.9	40.1	0.2766
40	3b	8.3	26.6	34.3	24.1	39.1	0.37839
40	3c	8.3	34.3	26.6	24.1	39.1	0.28695
40	3d	12.3	40.5	21.5	25.9	40.1	0.26789
60	1a	12.3	21.5	40.5	40.1	25.9	0.33754
60	1b	8.3	26.6	34.3	39.1	24.1	0.37989
60	1c	8.3	34.3	26.6	39.1	24.1	0.37928
60	1d	12.3	40.5	21.5	40.1	25.9	0.40249
60	2a	9.8	20.8	39.8	33	33	0.29324
60	2b	3.5	26.5	26.5	31.6	31.6	0.46461
60	2c	3.5	33.5	26.5	31.6	31.6	0.50313
60	2d	9.8	39.8	20.8	33	33	0.34846
60	3a	12.3	21.5	40.5	25.9	40.1	0.32694
60	3b	8.3	26.6	34.3	24.1	39.1	0.39518
60	3c	8.3	34.3	26.6	24.1	39.1	0.4069
60	3d	12.3	40.5	21.5	25.9	40.1	0.35532
90	1a	12.3	21.5	40.5	40.1	25.9	0.40024
90	1b	8.3	26.6	34.3	39.1	24.1	0.42683
90	1c	8.3	34.3	26.6	39.1	24.1	0.45082
90	1d	12.3	40.5	21.5	40.1	25.9	0.38154

Octane Vapor
Analytical Model Input from 1% Moisture Content By Mass Physical Experiment Data

Minutes	Observation Port		Image Sources			Image Sink	Vapor
	Label	r1	r2	r3	r4	r5	Concentration
		cm	cm	cm	cm	cm	ppmv
90	2a	9.8	20.8	39.8	33	33	0.41278
90	2b	3.5	26.5	26.5	31.6	31.6	0.57412
90	2c	3.5	33.5	26.5	31.6	31.6	0.65063
90	2d	9.8	39.8	20.8	33	33	0.43766
90	3a	12.3	21.5	40.5	25.9	40.1	0.38417
90	3b	8.3	26.6	34.3	24.1	39.1	0.56261
90	3c	8.3	34.3	26.6	24.1	39.1	0.511
90	3d	12.3	40.5	21.5	25.9	40.1	0.47576
120	1a	12.3	21.5	40.5	40.1	25.9	0.47256
120	1b	8.3	26.6	34.3	39.1	24.1	0.47858
120	1c	8.3	34.3	26.6	39.1	24.1	0.48738
120	1d	12.3	40.5	21.5	40.1	25.9	0.44829
120	2a	9.8	20.8	39.8	33	33	0.4408
120	2b	3.5	26.5	26.5	31.6	31.6	0.60233
120	2c	3.5	33.5	26.5	31.6	31.6	0.66361
120	2d	9.8	39.8	20.8	33	33	0.51584
120	3a	12.3	21.5	40.5	25.9	40.1	0.60876
120	3b	8.3	26.6	34.3	24.1	39.1	0.64412
120	3c	8.3	34.3	26.6	24.1	39.1	0.58166
120	3d	12.3	40.5	21.5	25.9	40.1	0.57957

Octane Vapor
Analytical Model Input from 2% Moisture Content By Mass Physical Experiment Data

	Observation Port		Image Sources			Image Sink	Vapor
	Label	r1	r2	r3	r4	r5	Concentration
Minutes		cm	cm	cm	cm	cm	ppmv
20	1a	12.3	21.5	40.5	40.1	25.9	0.301087
20	1b	8.3	26.6	34.3	39.1	24.1	0.388225
20	1c	8.3	34.3	26.6	39.1	24.1	0.388225
20	1d	12.3	40.5	21.5	40.1	25.9	0.301087
20	2a	9.8	20.8	39.8	33	33	0.382538
20	2b	3.5	26.5	26.5	31.6	31.6	0.760652
20	2c	3.5	33.5	26.5	31.6	31.6	0.735095
20	2d	9.8	39.8	20.8	33	33	0.382538
20	3a	12.3	21.5	40.5	25.9	40.1	0.392393
20	3b	8.3	26.6	34.3	24.1	39.1	0.541719
20	3c	8.3	34.3	26.6	24.1	39.1	0.541719
20	3d	12.3	40.5	21.5	25.9	40.1	0.392393
40	1a	12.3	21.5	40.5	40.1	25.9	0.419422
40	1b	8.3	26.6	34.3	39.1	24.1	0.508263
40	1c	8.3	34.3	26.6	39.1	24.1	0.508263
40	1d	12.3	40.5	21.5	40.1	25.9	0.419422
40	2a	9.8	20.8	39.8	33	33	0.50854
40	2b	3.5	26.5	26.5	31.6	31.6	0.891467
40	2c	3.5	33.5	26.5	31.6	31.6	0.862826
40	2d	9.8	39.8	20.8	33	33	0.50854
40	3a	12.3	21.5	40.5	25.9	40.1	0.523923
40	3b	8.3	26.6	34.3	24.1	39.1	0.67532
40	3c	8.3	34.3	26.6	24.1	39.1	0.67532
40	3d	12.3	40.5	21.5	25.9	40.1	0.523923
60	1a	12.3	21.5	40.5	40.1	25.9	0.49417
60	1b	8.3	26.6	34.3	39.1	24.1	0.58369
60	1c	8.3	34.3	26.6	39.1	24.1	0.58369
60	1d	12.3	40.5	21.5	40.1	25.9	0.49417
60	2a	9.8	20.8	39.8	33	33	0.586086
60	2b	3.5	26.5	26.5	31.6	31.6	0.970791
60	2c	3.5	33.5	26.5	31.6	31.6	0.94104
60	2d	9.8	39.8	20.8	33	33	0.586086
60	3a	12.3	21.5	40.5	25.9	40.1	0.603508
60	3b	8.3	26.6	34.3	24.1	39.1	0.755684
60	3c	8.3	34.3	26.6	24.1	39.1	0.755684
60	3d	12.3	40.5	21.5	25.9	40.1	0.603508
90	1a	12.3	21.5	40.5	40.1	25.9	0.571611
90	1b	8.3	26.6	34.3	39.1	24.1	0.661618
90	1c	8.3	34.3	26.6	39.1	24.1	0.661618
90	1d	12.3	40.5	21.5	40.1	25.9	0.571611

Octane Vapor
Analytical Model Input from 2% Moisture Content By Mass Physical Experiment Data

	Observation Port		Image Sources			Image Sink	Vapor
	Label	r1	r2	r3	r4	r5	Concentration
Minutes		cm	cm	cm	cm	cm	ppmv
90	2a	9.8	20.8	39.8	33	33	0.665464
90	2b	3.5	26.5	26.5	31.6	31.6	1.051408
90	2c	3.5	33.5	26.5	31.6	31.6	1.020893
90	2d	9.8	39.8	20.8	33	33	0.665464
90	3a	12.3	21.5	40.5	25.9	40.1	0.684306
90	3b	8.3	26.6	34.3	24.1	39.1	0.837028
90	3c	8.3	34.3	26.6	24.1	39.1	0.837028
90	3d	12.3	40.5	21.5	25.9	40.1	0.684306
120	1a	12.3	21.5	40.5	40.1	25.9	0.627735
120	1b	8.3	26.6	34.3	39.1	24.1	0.717996
120	1c	8.3	34.3	26.6	39.1	24.1	0.717996
120	1d	12.3	40.5	21.5	40.1	25.9	0.627735
120	2a	9.8	20.8	39.8	33	33	0.72258
120	2b	3.5	26.5	26.5	31.6	31.6	1.109158
120	2c	3.5	33.5	26.5	31.6	31.6	1.078254
120	2d	9.8	39.8	20.8	33	33	0.72258
120	3a	12.3	21.5	40.5	25.9	40.1	0.742149
120	3b	8.3	26.6	34.3	24.1	39.1	0.895153
120	3c	8.3	34.3	26.6	24.1	39.1	0.895153
120	3d	12.3	40.5	21.5	25.9	40.1	0.742149

Octane Vapor
Analytical Model Input from 5% Moisture Content By Mass Physical Experiment Data

	Observation Port		Image Sources			Image Sink	Vapor
	Label	r1	r2	r3	r4	r5	Concentration
Minutes		cm	cm	cm	cm	cm	ppmv
20	1a	12.3	21.5	40.5	40.1	25.9	1.37396
20	1b	8.3	26.6	34.3	39.1	24.1	2.30453
20	1c	8.3	34.3	26.6	39.1	24.1	2.47509
20	1d	12.3	40.5	21.5	40.1	25.9	1.38774
20	2a	9.8	20.8	39.8	33	33	1.87925
20	2b	3.5	26.5	26.5	31.6	31.6	3.15585
20	2c	3.5	33.5	26.5	31.6	31.6	3.28453
20	2d	9.8	39.8	20.8	33	33	1.84283
20	3a	12.3	21.5	40.5	25.9	40.1	1.30415
20	3b	8.3	26.6	34.3	24.1	39.1	2.3483
20	3c	8.3	34.3	26.6	24.1	39.1	2.22038
20	3d	12.3	40.5	21.5	25.9	40.1	0.39045
40	1a	12.3	21.5	40.5	40.1	25.9	2.38151
40	1b	8.3	26.6	34.3	39.1	24.1	3.36906
40	1c	8.3	34.3	26.6	39.1	24.1	3.47472
40	1d	12.3	40.5	21.5	40.1	25.9	2.23509
40	2a	9.8	20.8	39.8	33	33	3.09094
40	2b	3.5	26.5	26.5	31.6	31.6	4.31547
40	2c	3.5	33.5	26.5	31.6	31.6	4.40302
40	2d	9.8	39.8	20.8	33	33	3.39094
40	3a	12.3	21.5	40.5	25.9	40.1	2.39849
40	3b	8.3	26.6	34.3	24.1	39.1	3.17245
40	3c	8.3	34.3	26.6	24.1	39.1	3.59434
40	3d	12.3	40.5	21.5	25.9	40.1	2.28377
60	1a	12.3	21.5	40.5	40.1	25.9	3.2166
60	1b	8.3	26.6	34.3	39.1	24.1	3.5966
60	1c	8.3	34.3	26.6	39.1	24.1	4.67849
60	1d	12.3	40.5	21.5	40.1	25.9	3.19208
60	2a	9.8	20.8	39.8	33	33	4.11887
60	2b	3.5	26.5	26.5	31.6	31.6	5.15057
60	2c	3.5	33.5	26.5	31.6	31.6	5.24038
60	2d	9.8	39.8	20.8	33	33	3.47736
60	3a	12.3	21.5	40.5	25.9	40.1	3.67736
60	3b	8.3	26.6	34.3	24.1	39.1	4.31019
60	3c	8.3	34.3	26.6	24.1	39.1	3.71434
60	3d	12.3	40.5	21.5	25.9	40.1	3.63057
120	1a	12.3	21.5	40.5	40.1	25.9	4.48264
120	1b	8.3	26.6	34.3	39.1	24.1	5.65509
120	1c	8.3	34.3	26.6	39.1	24.1	5.32717
120	1d	12.3	40.5	21.5	40.1	25.9	4.51472

Octane Vapor
Analytical Model Input from 5% Moisture Content By Mass Physical Experiment Data

	Observation Port		Image Sources			Image Sink	Vapor
	Label	r1	r2	r3	r4	r5	Concentration
Minutes		cm	cm	cm	cm	cm	ppmv
120	2a	9.8	20.8	39.8	33	33	4.38868
120	2b	3.5	26.5	26.5	31.6	31.6	6.22528
120	2c	3.5	33.5	26.5	31.6	31.6	6.62717
120	2d	9.8	39.8	20.8	33	33	5.49811
120	3a	12.3	21.5	40.5	25.9	40.1	5.97736
120	3b	8.3	26.6	34.3	24.1	39.1	4.84491
120	3c	8.3	34.3	26.6	24.1	39.1	5.35849
120	3d	12.3	40.5	21.5	25.9	40.1	4.49736
150	1a	12.3	21.5	40.5	40.1	25.9	6.83132
150	1b	8.3	26.6	34.3	39.1	24.1	6.92792
150	1c	8.3	34.3	26.6	39.1	24.1	6.06377
150	1d	12.3	40.5	21.5	40.1	25.9	6.39774
150	2a	9.8	20.8	39.8	33	33	6.11547
150	2b	3.5	26.5	26.5	31.6	31.6	7.80075
150	2c	3.5	33.5	26.5	31.6	31.6	8.09094
150	2d	9.8	39.8	20.8	33	33	6.05245
150	3a	12.3	21.5	40.5	25.9	40.1	6.12415
150	3b	8.3	26.6	34.3	24.1	39.1	7.07717
150	3c	8.3	34.3	26.6	24.1	39.1	7.21226
150	3d	12.3	40.5	21.5	25.9	40.1	7.61819

Octane Vapor
Analytical Model Input from 5% Moisture Content By Mass Physical Experiment Data

	Observation Port		Image Sources			Image Sink	Vapor
	Label	r1	r2	r3	r4	r5	Concentration
Minutes		cm	cm	cm	cm	cm	ppmv
20	1a	12.3	21.5	40.5	40.1	25.9	1.37396
20	1b	8.3	26.6	34.3	39.1	24.1	2.30453
20	1c	8.3	34.3	26.6	39.1	24.1	2.47509
20	1d	12.3	40.5	21.5	40.1	25.9	1.38774
20	2a	9.8	20.8	39.8	33	33	1.87925
20	2b	3.5	26.5	26.5	31.6	31.6	3.15585
20	2c	3.5	33.5	26.5	31.6	31.6	3.28453
20	2d	9.8	39.8	20.8	33	33	1.84283
20	3a	12.3	21.5	40.5	25.9	40.1	1.30415
20	3b	8.3	26.6	34.3	24.1	39.1	2.3483
20	3c	8.3	34.3	26.6	24.1	39.1	2.22038
20	3d	12.3	40.5	21.5	25.9	40.1	0.39045
40	1a	12.3	21.5	40.5	40.1	25.9	2.38151
40	1b	8.3	26.6	34.3	39.1	24.1	3.36906
40	1c	8.3	34.3	26.6	39.1	24.1	3.47472
40	1d	12.3	40.5	21.5	40.1	25.9	2.23509
40	2a	9.8	20.8	39.8	33	33	3.09094
40	2b	3.5	26.5	26.5	31.6	31.6	4.31547
40	2c	3.5	33.5	26.5	31.6	31.6	4.40302
40	2d	9.8	39.8	20.8	33	33	3.39094
40	3a	12.3	21.5	40.5	25.9	40.1	2.39849
40	3b	8.3	26.6	34.3	24.1	39.1	3.17245
40	3c	8.3	34.3	26.6	24.1	39.1	3.59434
40	3d	12.3	40.5	21.5	25.9	40.1	2.28377
60	1a	12.3	21.5	40.5	40.1	25.9	3.2166
60	1b	8.3	26.6	34.3	39.1	24.1	3.5966
60	1c	8.3	34.3	26.6	39.1	24.1	4.67849
60	1d	12.3	40.5	21.5	40.1	25.9	3.19208
60	2a	9.8	20.8	39.8	33	33	4.11887
60	2b	3.5	26.5	26.5	31.6	31.6	5.15057
60	2c	3.5	33.5	26.5	31.6	31.6	5.24038
60	2d	9.8	39.8	20.8	33	33	3.47736
60	3a	12.3	21.5	40.5	25.9	40.1	3.67736
60	3b	8.3	26.6	34.3	24.1	39.1	4.31019
60	3c	8.3	34.3	26.6	24.1	39.1	3.71434
60	3d	12.3	40.5	21.5	25.9	40.1	3.63057
120	1a	12.3	21.5	40.5	40.1	25.9	4.48264
120	1b	8.3	26.6	34.3	39.1	24.1	5.65509
120	1c	8.3	34.3	26.6	39.1	24.1	5.32717
120	1d	12.3	40.5	21.5	40.1	25.9	4.51472

Octane Vapor
Analytical Model Input from 5% Moisture Content By Mass Physical Experiment Data

	Observation Port		Image Sources			Image Sink	Vapor
	Label	r1	r2	r3	r4	r5	Concentration
Minutes		cm	cm	cm	cm	cm	ppmv
120	2a	9.8	20.8	39.8	33	33	4.38868
120	2b	3.5	26.5	26.5	31.6	31.6	6.22528
120	2c	3.5	33.5	26.5	31.6	31.6	6.62717
120	2d	9.8	39.8	20.8	33	33	5.49811
120	3a	12.3	21.5	40.5	25.9	40.1	5.97736
120	3b	8.3	26.6	34.3	24.1	39.1	4.84491
120	3c	8.3	34.3	26.6	24.1	39.1	5.35849
120	3d	12.3	40.5	21.5	25.9	40.1	4.49736
150	1a	12.3	21.5	40.5	40.1	25.9	6.83132
150	1b	8.3	26.6	34.3	39.1	24.1	6.92792
150	1c	8.3	34.3	26.6	39.1	24.1	6.06377
150	1d	12.3	40.5	21.5	40.1	25.9	6.39774
150	2a	9.8	20.8	39.8	33	33	6.11547
150	2b	3.5	26.5	26.5	31.6	31.6	7.80075
150	2c	3.5	33.5	26.5	31.6	31.6	8.09094
150	2d	9.8	39.8	20.8	33	33	6.05245
150	3a	12.3	21.5	40.5	25.9	40.1	6.12415
150	3b	8.3	26.6	34.3	24.1	39.1	7.07717
150	3c	8.3	34.3	26.6	24.1	39.1	7.21226
150	3d	12.3	40.5	21.5	25.9	40.1	7.61819

Octane Vapor
Analytical Model Input from 7.5% Moisture Content By Mass Physical Experiment Data

Minutes	Observation Port		Image Sources			Image Sink	Vapor
	Label	r1	r2	r3	r4	r5	Concentration
Minutes		cm	cm	cm	cm	cm	ppmv
20	1a	12.3	21.5	40.5	40.1	25.9	0.14456
20	1b	8.3	26.6	34.3	39.1	24.1	0.29925
20	1c	8.3	34.3	26.6	39.1	24.1	0.36554
20	1d	12.3	40.5	21.5	40.1	25.9	0.17098
20	2a	9.8	20.8	39.8	33	33	0.30689
20	2b	3.5	26.5	26.5	31.6	31.6	1.07724
20	2c	3.5	33.5	26.5	31.6	31.6	1.88651
20	2d	9.8	39.8	20.8	33	33	0.36276
20	3a	12.3	21.5	40.5	25.9	40.1	0.2
20	3b	8.3	26.6	34.3	24.1	39.1	0.5713
20	3c	8.3	34.3	26.6	24.1	39.1	0.568
20	3d	12.3	40.5	21.5	25.9	40.1	0.19307
40	1a	12.3	21.5	40.5	40.1	25.9	0.58842
40	1b	8.3	26.6	34.3	39.1	24.1	0.89022
40	1c	8.3	34.3	26.6	39.1	24.1	1.06202
40	1d	12.3	40.5	21.5	40.1	25.9	0.76036
40	2a	9.8	20.8	39.8	33	33	0.82785
40	2b	3.5	26.5	26.5	31.6	31.6	1.97609
40	2c	3.5	33.5	26.5	31.6	31.6	2.71843
40	2d	9.8	39.8	20.8	33	33	0.88464
40	3a	12.3	21.5	40.5	25.9	40.1	0.66135
40	3b	8.3	26.6	34.3	24.1	39.1	1.06309
40	3c	8.3	34.3	26.6	24.1	39.1	1.09207
40	3d	12.3	40.5	21.5	25.9	40.1	0.5751
60	1a	12.3	21.5	40.5	40.1	25.9	0.90607
60	1b	8.3	26.6	34.3	39.1	24.1	1.22477
60	1c	8.3	34.3	26.6	39.1	24.1	1.33609
60	1d	12.3	40.5	21.5	40.1	25.9	0.89852
60	2a	9.8	20.8	39.8	33	33	1.27391
60	2b	3.5	26.5	26.5	31.6	31.6	3.38714
60	2c	3.5	33.5	26.5	31.6	31.6	3.02934
60	2d	9.8	39.8	20.8	33	33	1.44544
60	3a	12.3	21.5	40.5	25.9	40.1	1.25155
60	3b	8.3	26.6	34.3	24.1	39.1	1.66958
60	3c	8.3	34.3	26.6	24.1	39.1	1.48792
60	3d	12.3	40.5	21.5	25.9	40.1	1.03874
120	1a	12.3	21.5	40.5	40.1	25.9	1.28338
120	1b	8.3	26.6	34.3	39.1	24.1	1.42039
120	1c	8.3	34.3	26.6	39.1	24.1	1.58732
120	1d	12.3	40.5	21.5	40.1	25.9	1.22202

Octane Vapor
Analytical Model Input from 7.5% Moisture Content By Mass Physical Experiment Data

		Observation Port	Image Sources			Image Sink	Vapor
	Label	r1	r2	r3	r4	r5	Concentration
Minutes		cm	cm	cm	cm	cm	ppmv
120	2a	9.8	20.8	39.8	33	33	1.71257
120	2b	3.5	26.5	26.5	31.6	31.6	3.04105
120	2c	3.5	33.5	26.5	31.6	31.6	3.08506
120	2d	9.8	39.8	20.8	33	33	1.76405
120	3a	12.3	21.5	40.5	25.9	40.1	1.83813
120	3b	8.3	26.6	34.3	24.1	39.1	1.97017
120	3c	8.3	34.3	26.6	24.1	39.1	2.01052
120	3d	12.3	40.5	21.5	25.9	40.1	1.94292
180	1a	12.3	21.5	40.5	40.1	25.9	1.30434
180	1b	8.3	26.6	34.3	39.1	24.1	1.38687
180	1c	8.3	34.3	26.6	39.1	24.1	1.69659
180	1d	12.3	40.5	21.5	40.1	25.9	1.39128
180	2a	9.8	20.8	39.8	33	33	1.77442
180	2b	3.5	26.5	26.5	31.6	31.6	2.66366
180	2c	3.5	33.5	26.5	31.6	31.6	2.96369
180	2d	9.8	39.8	20.8	33	33	1.7701
180	3a	12.3	21.5	40.5	25.9	40.1	2.83329
180	3b	8.3	26.6	34.3	24.1	39.1	2.1369
180	3c	8.3	34.3	26.6	24.1	39.1	2.12603
180	3d	12.3	40.5	21.5	25.9	40.1	2.64162

Octane Vapor
Analytical Model Input from 8.5% Moisture Content By Mass Physical Experiment Data

	Observation Port		Image Sources			Image Sink	Vapor
	Label	r1	r2	r3	r4	r5	Concentration
Minutes		cm	cm	cm	cm	cm	ppmv
20	1a	12.3	21.5	40.5	40.1	25.9	0.28495
20	1b	8.3	26.6	34.3	39.1	24.1	0.28075
20	1c	8.3	34.3	26.6	39.1	24.1	0.3136
20	1d	12.3	40.5	21.5	40.1	25.9	0.32828
20	2a	9.8	20.8	39.8	33	33	0.56839
20	2b	3.5	26.5	26.5	31.6	31.6	0.69964
20	2c	3.5	33.5	26.5	31.6	31.6	1.48882
20	2d	9.8	39.8	20.8	33	33	0.44593
20	3a	12.3	21.5	40.5	25.9	40.1	1.14887
20	3b	8.3	26.6	34.3	24.1	39.1	1.08211
20	3c	8.3	34.3	26.6	24.1	39.1	0.48952
20	3d	12.3	40.5	21.5	25.9	40.1	0.77277
40	1a	12.3	21.5	40.5	40.1	25.9	0.66422
40	1b	8.3	26.6	34.3	39.1	24.1	0.82052
40	1c	8.3	34.3	26.6	39.1	24.1	0.97475
40	1d	12.3	40.5	21.5	40.1	25.9	0.61645
40	2a	9.8	20.8	39.8	33	33	0.76677
40	2b	3.5	26.5	26.5	31.6	31.6	1.98117
40	2c	3.5	33.5	26.5	31.6	31.6	1.64372
40	2d	9.8	39.8	20.8	33	33	1.14898
40	3a	12.3	21.5	40.5	25.9	40.1	0.94984
40	3b	8.3	26.6	34.3	24.1	39.1	1.5862
40	3c	8.3	34.3	26.6	24.1	39.1	1.62769
40	3d	12.3	40.5	21.5	25.9	40.1	1.0324
60	1a	12.3	21.5	40.5	40.1	25.9	0.91769
60	1b	8.3	26.6	34.3	39.1	24.1	1.06691
60	1c	8.3	34.3	26.6	39.1	24.1	0.83357
60	1d	12.3	40.5	21.5	40.1	25.9	0.84119
60	2a	9.8	20.8	39.8	33	33	1.59105
60	2b	3.5	26.5	26.5	31.6	31.6	2.20298
60	2c	3.5	33.5	26.5	31.6	31.6	2.63581
60	2d	9.8	39.8	20.8	33	33	1.38873
60	3a	12.3	21.5	40.5	25.9	40.1	1.43427
60	3b	8.3	26.6	34.3	24.1	39.1	1.81016
60	3c	8.3	34.3	26.6	24.1	39.1	1.7917
60	3d	12.3	40.5	21.5	25.9	40.1	1.46376
120	1a	12.3	21.5	40.5	40.1	25.9	1.17902
120	1b	8.3	26.6	34.3	39.1	24.1	1.42785
120	1c	8.3	34.3	26.6	39.1	24.1	1.42784
120	1d	12.3	40.5	21.5	40.1	25.9	1.07663

Octane Vapor
Analytical Model Input from 8.5% Moisture Content By Mass Physical Experiment Data

	Observation Port		Image Sources			Image Sink	Vapor
	Label	r1	r2	r3	r4	r5	Concentration
Minutes		cm	cm	cm	cm	cm	ppmv
120	2a	9.8	20.8	39.8	33	33	1.67674
120	2b	3.5	26.5	26.5	31.6	31.6	2.75872
120	2c	3.5	33.5	26.5	31.6	31.6	2.27891
120	2d	9.8	39.8	20.8	33	33	1.9094
120	3a	12.3	21.5	40.5	25.9	40.1	2.04545
120	3b	8.3	26.6	34.3	24.1	39.1	1.80368
120	3c	8.3	34.3	26.6	24.1	39.1	1.46782
120	3d	12.3	40.5	21.5	25.9	40.1	2.01301
150	1a	12.3	21.5	40.5	40.1	25.9	1.22016
150	1b	8.3	26.6	34.3	39.1	24.1	1.39205
150	1c	8.3	34.3	26.6	39.1	24.1	1.49475
150	1d	12.3	40.5	21.5	40.1	25.9	1.25035
150	2a	9.8	20.8	39.8	33	33	1.74133
150	2b	3.5	26.5	26.5	31.6	31.6	2.71845
150	2c	3.5	33.5	26.5	31.6	31.6	2.20547
150	2d	9.8	39.8	20.8	33	33	1.7502
150	3a	12.3	21.5	40.5	25.9	40.1	2.09328
150	3b	8.3	26.6	34.3	24.1	39.1	1.62827
150	3c	8.3	34.3	26.6	24.1	39.1	2.17731
150	3d	12.3	40.5	21.5	25.9	40.1	2.19167

Octane Vapor

Analytical Model Input from 9.25% Moisture Content By Mass Physical Experiment Data

	Observation Port		Image Sources			Image Sink	Vapor
	Label	r1	r2	r3	r4	r5	Concentration
Minutes		cm	cm	cm	cm	cm	ppmv
20	1a	12.3	21.5	40.5	40.1	25.9	0.0315
20	1b	8.3	26.6	34.3	39.1	24.1	0.03766
20	1c	8.3	34.3	26.6	39.1	24.1	0.03901
20	1d	12.3	40.5	21.5	40.1	25.9	0.02376
20	2a	9.8	20.8	39.8	33	33	0.02723
20	2b	3.5	26.5	26.5	31.6	31.6	0.11234
20	2c	3.5	33.5	26.5	31.6	31.6	0.10968
20	2d	9.8	39.8	20.8	33	33	0.03327
20	3a	12.3	21.5	40.5	25.9	40.1	0.01519
20	3b	8.3	26.6	34.3	24.1	39.1	0.03434
20	3c	8.3	34.3	26.6	24.1	39.1	0.03574
20	3d	12.3	40.5	21.5	25.9	40.1	0.02073
40	1a	12.3	21.5	40.5	40.1	25.9	0.05566
40	1b	8.3	26.6	34.3	39.1	24.1	0.09625
40	1c	8.3	34.3	26.6	39.1	24.1	0.10097
40	1d	12.3	40.5	21.5	40.1	25.9	0.05397
40	2a	9.8	20.8	39.8	33	33	0.06052
40	2b	3.5	26.5	26.5	31.6	31.6	0.21857
40	2c	3.5	33.5	26.5	31.6	31.6	0.22138
40	2d	9.8	39.8	20.8	33	33	0.08098
40	3a	12.3	21.5	40.5	25.9	40.1	0.05087
40	3b	8.3	26.6	34.3	24.1	39.1	0.08191
40	3c	8.3	34.3	26.6	24.1	39.1	0.09375
40	3d	12.3	40.5	21.5	25.9	40.1	0.05658
60	1a	12.3	21.5	40.5	40.1	25.9	0.13344
60	1b	8.3	26.6	34.3	39.1	24.1	0.14871
60	1c	8.3	34.3	26.6	39.1	24.1	0.14946
60	1d	12.3	40.5	21.5	40.1	25.9	0.09837
60	2a	9.8	20.8	39.8	33	33	0.26527
60	2b	3.5	26.5	26.5	31.6	31.6	0.42023
60	2c	3.5	33.5	26.5	31.6	31.6	0.43437
60	2d	9.8	39.8	20.8	33	33	0.19007
60	3a	12.3	21.5	40.5	25.9	40.1	0.18659
60	3b	8.3	26.6	34.3	24.1	39.1	0.22743
60	3c	8.3	34.3	26.6	24.1	39.1	0.1341
60	3d	12.3	40.5	21.5	25.9	40.1	0.14278
90	1a	12.3	21.5	40.5	40.1	25.9	0.22497
90	1b	8.3	26.6	34.3	39.1	24.1	0.18253
90	1c	8.3	34.3	26.6	39.1	24.1	0.1952
90	1d	12.3	40.5	21.5	40.1	25.9	0.22446

Octane Vapor
Analytical Model Input from 9.25% Moisture Content By Mass Physical Experiment
Data

Minutes	Observation Port		Image Sources			Image Sink	Vapor
	Label	r1	r2	r3	r4	r5	Concentration
		cm	cm	cm	cm	cm	ppmv
90	2a	9.8	20.8	39.8	33	33	0.27646
90	2b	3.5	26.5	26.5	31.6	31.6	0.50939
90	2c	3.5	33.5	26.5	31.6	31.6	0.34956
90	2d	9.8	39.8	20.8	33	33	0.29016
90	3a	12.3	21.5	40.5	25.9	40.1	0.15627
90	3b	8.3	26.6	34.3	24.1	39.1	0.26557
90	3c	8.3	34.3	26.6	24.1	39.1	0.35912
90	3d	12.3	40.5	21.5	25.9	40.1	0.26393
120	1a	12.3	21.5	40.5	40.1	25.9	0.25523
120	1b	8.3	26.6	34.3	39.1	24.1	0.19543
120	1c	8.3	34.3	26.6	39.1	24.1	0.26143
120	1d	12.3	40.5	21.5	40.1	25.9	0.18501
120	2a	9.8	20.8	39.8	33	33	0.38529
120	2b	3.5	26.5	26.5	31.6	31.6	0.37302
120	2c	3.5	33.5	26.5	31.6	31.6	0.56952
120	2d	9.8	39.8	20.8	33	33	0.38611
120	3a	12.3	21.5	40.5	25.9	40.1	0.22689
120	3b	8.3	26.6	34.3	24.1	39.1	0.56222
120	3c	8.3	34.3	26.6	24.1	39.1	0.25575
120	3d	12.3	40.5	21.5	25.9	40.1	0.34152

Octane Vapor
Analytical Model Input from 10% Moisture Content By Mass Physical Experiment Data

	Observation Port		Image Sources			Image Sink	Vapor
	Label	r1	r2	r3	r4	r5	Concentration
Minutes		cm	cm	cm	cm	cm	ppmv
20	1a	12.3	21.5	40.5	40.1	25.9	0.08641
20	1b	8.3	26.6	34.3	39.1	24.1	0.136148
20	1c	8.3	34.3	26.6	39.1	24.1	0.148126
20	1d	12.3	40.5	21.5	40.1	25.9	0.078928
20	2a	9.8	20.8	39.8	33	33	0.093776
20	2b	3.5	26.5	26.5	31.6	31.6	0.482632
20	2c	3.5	33.5	26.5	31.6	31.6	0.599749
20	2d	9.8	39.8	20.8	33	33	0.104912
20	3a	12.3	21.5	40.5	25.9	40.1	0.097754
20	3b	8.3	26.6	34.3	24.1	39.1	0.222365
20	3c	8.3	34.3	26.6	24.1	39.1	0.196225
20	3d	12.3	40.5	21.5	25.9	40.1	0.099905
40	1a	12.3	21.5	40.5	40.1	25.9	0.189123
40	1b	8.3	26.6	34.3	39.1	24.1	0.264503
40	1c	8.3	34.3	26.6	39.1	24.1	0.27047
40	1d	12.3	40.5	21.5	40.1	25.9	0.150857
40	2a	9.8	20.8	39.8	33	33	0.266258
40	2b	3.5	26.5	26.5	31.6	31.6	0.587936
40	2c	3.5	33.5	26.5	31.6	31.6	0.710915
40	2d	9.8	39.8	20.8	33	33	0.294339
40	3a	12.3	21.5	40.5	25.9	40.1	0.217253
40	3b	8.3	26.6	34.3	24.1	39.1	0.432785
40	3c	8.3	34.3	26.6	24.1	39.1	0.360534
40	3d	12.3	40.5	21.5	25.9	40.1	0.298515
60	1a	12.3	21.5	40.5	40.1	25.9	0.356636
60	1b	8.3	26.6	34.3	39.1	24.1	0.303575
60	1c	8.3	34.3	26.6	39.1	24.1	0.41592
60	1d	12.3	40.5	21.5	40.1	25.9	0.209464
60	2a	9.8	20.8	39.8	33	33	0.468851
60	2b	3.5	26.5	26.5	31.6	31.6	1.043519
60	2c	3.5	33.5	26.5	31.6	31.6	0.869872
60	2d	9.8	39.8	20.8	33	33	0.463494
60	3a	12.3	21.5	40.5	25.9	40.1	0.577451
60	3b	8.3	26.6	34.3	24.1	39.1	0.724841
60	3c	8.3	34.3	26.6	24.1	39.1	0.726045
60	3d	12.3	40.5	21.5	25.9	40.1	0.636329
90	1a	12.3	21.5	40.5	40.1	25.9	0.415309
90	1b	8.3	26.6	34.3	39.1	24.1	0.422535
90	1c	8.3	34.3	26.6	39.1	24.1	0.459839
90	1d	12.3	40.5	21.5	40.1	25.9	0.311381

Octane Vapor

Analytical Model Input from 10% Moisture Content By Mass Physical Experiment Data

Minutes	Observation Port		Image Sources			Image Sink	Vapor
	Label	r1	r2	r3	r4	r5	Concentration
		cm	cm	cm	cm	cm	ppmv
90	2a	9.8	20.8	39.8	33	33	0.578457
90	2b	3.5	26.5	26.5	31.6	31.6	0.831836
90	2c	3.5	33.5	26.5	31.6	31.6	0.392982
90	2d	9.8	39.8	20.8	33	33	0.622256
90	3a	12.3	21.5	40.5	25.9	40.1	0.457134
90	3b	8.3	26.6	34.3	24.1	39.1	0.31179
90	3c	8.3	34.3	26.6	24.1	39.1	0.739798
90	3d	12.3	40.5	21.5	25.9	40.1	0.36698
120	1a	12.3	21.5	40.5	40.1	25.9	0.409135
120	1b	8.3	26.6	34.3	39.1	24.1	0.415753
120	1c	8.3	34.3	26.6	39.1	24.1	0.479537
120	1d	12.3	40.5	21.5	40.1	25.9	0.367624
120	2a	9.8	20.8	39.8	33	33	0.414563
120	2b	3.5	26.5	26.5	31.6	31.6	0.738448
120	2c	3.5	33.5	26.5	31.6	31.6	0.432924
120	2d	9.8	39.8	20.8	33	33	0.514149
120	3a	12.3	21.5	40.5	25.9	40.1	0.410943
120	3b	8.3	26.6	34.3	24.1	39.1	0.639341
120	3c	8.3	34.3	26.6	24.1	39.1	0.424182
120	3d	12.3	40.5	21.5	25.9	40.1	0.418919

Octane Vapor by Port

Analytical Model Input from 0% Moisture Content By Mass Physical Experiment Data

	Observation Port		Image Sources			Image Sink	Vapor
	Label	r1	r2	r3	r4	r5	Concentration
Minutes		cm	cm	cm	cm	cm	ppmv
20	1a	12.3	21.5	40.5	40.1	25.9	0.1453
20	1d	8.3	26.6	34.3	39.1	24.1	0.1289
20	2a	8.3	34.3	26.6	39.1	24.1	0.1594
20	2d	12.3	40.5	21.5	40.1	25.9	0.1409
40	1a	9.8	20.8	39.8	33	33	0.2142
40	1d	3.5	26.5	26.5	31.6	31.6	0.2301
40	2a	3.5	33.5	26.5	31.6	31.6	0.2403
40	2d	9.8	39.8	20.8	33	33	0.2644
60	1a	12.3	21.5	40.5	25.9	40.1	0.3061
60	1d	8.3	26.6	34.3	24.1	39.1	0.291
60	2a	8.3	34.3	26.6	24.1	39.1	0.364
60	2d	12.3	40.5	21.5	25.9	40.1	0.3207
90	1a	12.3	21.5	40.5	40.1	25.9	0.3351
90	1d	8.3	26.6	34.3	39.1	24.1	0.3951
90	2a	8.3	34.3	26.6	39.1	24.1	0.3739
90	2d	12.3	40.5	21.5	40.1	25.9	0.3913
120	2a	9.8	20.8	39.8	33	33	0.4862
120	2b	3.5	26.5	26.5	31.6	31.6	0.4812
120	2c	3.5	33.5	26.5	31.6	31.6	0.5928
120	2d	9.8	39.8	20.8	33	33	0.4509

Octane Vapor by Port
Analytical Model Input from 1% Moisture Content By Mass Physical Experiment Data

	Observation Port		Image Sources			Image Sink	Vapor
	Label	r1	r2	r3	r4	r5	Concentration
Minutes		cm	cm	cm	cm	cm	ppmv
20	1a	12.3	21.5	40.5	40.1	25.9	0.17405
20	1d	8.3	26.6	34.3	39.1	24.1	0.18157
20	2a	8.3	34.3	26.6	39.1	24.1	0.14023
20	2d	12.3	40.5	21.5	40.1	25.9	0.14269
40	1a	9.8	20.8	39.8	33	33	0.28587
40	1d	3.5	26.5	26.5	31.6	31.6	0.25923
40	2a	3.5	33.5	26.5	31.6	31.6	0.24465
40	2d	9.8	39.8	20.8	33	33	0.24521
60	1a	12.3	21.5	40.5	25.9	40.1	0.33754
60	1d	8.3	26.6	34.3	24.1	39.1	0.40249
60	2a	8.3	34.3	26.6	24.1	39.1	0.29324
60	2d	12.3	40.5	21.5	25.9	40.1	0.34846
90	1a	12.3	21.5	40.5	40.1	25.9	0.40024
90	1d	8.3	26.6	34.3	39.1	24.1	0.38154
90	2a	8.3	34.3	26.6	39.1	24.1	0.41278
90	2d	12.3	40.5	21.5	40.1	25.9	0.43766
120	2a	9.8	20.8	39.8	33	33	0.47256
120	2b	3.5	26.5	26.5	31.6	31.6	0.44829
120	2c	3.5	33.5	26.5	31.6	31.6	0.4408
120	2d	9.8	39.8	20.8	33	33	0.51584

Octane Vapor by Port

Analytical Model Input from 2% Moisture Content By Mass Physical Experiment Data

	Observation Port		Image Sources			Image Sink	Vapor
	Label	r1	r2	r3	r4	r5	Concentration
Minutes		cm	cm	cm	cm	cm	ppmv
20	1a	12.3	21.5	40.5	40.1	25.9	0.301087
20	1d	8.3	26.6	34.3	39.1	24.1	0.301087
20	2a	8.3	34.3	26.6	39.1	24.1	0.382538
20	2d	12.3	40.5	21.5	40.1	25.9	0.382538
40	1a	9.8	20.8	39.8	33	33	0.419422
40	1d	3.5	26.5	26.5	31.6	31.6	0.419422
40	2a	3.5	33.5	26.5	31.6	31.6	0.50854
40	2d	9.8	39.8	20.8	33	33	0.50854
60	1a	12.3	21.5	40.5	25.9	40.1	0.49417
60	1d	8.3	26.6	34.3	24.1	39.1	0.49417
60	2a	8.3	34.3	26.6	24.1	39.1	0.586086
60	2d	12.3	40.5	21.5	25.9	40.1	0.586086
90	1a	12.3	21.5	40.5	40.1	25.9	0.571611
90	1d	8.3	26.6	34.3	39.1	24.1	0.571611
90	2a	8.3	34.3	26.6	39.1	24.1	0.665464
90	2d	12.3	40.5	21.5	40.1	25.9	0.665464
120	2a	9.8	20.8	39.8	33	33	0.627735
120	2b	3.5	26.5	26.5	31.6	31.6	0.627735
120	2c	3.5	33.5	26.5	31.6	31.6	0.72258
120	2d	9.8	39.8	20.8	33	33	0.72258

Octane Vapor by Port
Analytical Model Input from 5% Moisture Content By Mass Physical Experiment Data

	Observation Port		Image Sources			Image Sink	Vapor
	Label	r1	r2	r3	r4	r5	Concentration
Minutes		cm	cm	cm	cm	cm	ppmv
20	1a	12.3	21.5	40.5	40.1	25.9	1.37396
20	1d	8.3	26.6	34.3	39.1	24.1	1.38774
20	2a	8.3	34.3	26.6	39.1	24.1	1.87925
20	2d	12.3	40.5	21.5	40.1	25.9	1.84283
40	1a	9.8	20.8	39.8	33	33	2.38151
40	1d	3.5	26.5	26.5	31.6	31.6	2.23509
40	2a	3.5	33.5	26.5	31.6	31.6	3.09094
40	2d	9.8	39.8	20.8	33	33	3.39094
60	1a	12.3	21.5	40.5	25.9	40.1	3.2166
60	1d	8.3	26.6	34.3	24.1	39.1	3.19208
60	2a	8.3	34.3	26.6	24.1	39.1	4.11887
60	2d	12.3	40.5	21.5	25.9	40.1	3.47736
120	1a	12.3	21.5	40.5	40.1	25.9	4.48264
120	1d	8.3	26.6	34.3	39.1	24.1	4.51472
120	2a	8.3	34.3	26.6	39.1	24.1	4.38868
120	2d	12.3	40.5	21.5	40.1	25.9	5.49811
150	2a	9.8	20.8	39.8	33	33	6.83132
150	2b	3.5	26.5	26.5	31.6	31.6	6.39774
150	2c	3.5	33.5	26.5	31.6	31.6	6.11547
150	2d	9.8	39.8	20.8	33	33	6.05245

Octane Vapor by Port
Analytical Model Input from 6.5% Moisture Content By Mass Physical Experiment Data

Minutes	Observation Port		Image Sources			Image Sink	Vapor
	Label	r1	r2	r3	r4	r5	Concentration
		cm	cm	cm	cm	cm	ppmv
20	1a	12.3	21.5	40.5	40.1	25.9	0.71523
20	1d	8.3	26.6	34.3	39.1	24.1	0.35654
20	2a	8.3	34.3	26.6	39.1	24.1	0.86084
20	2d	12.3	40.5	21.5	40.1	25.9	1.03741
40	1a	9.8	20.8	39.8	33	33	1.25046
40	1d	3.5	26.5	26.5	31.6	31.6	0.72776
40	2a	3.5	33.5	26.5	31.6	31.6	1.81472
40	2d	9.8	39.8	20.8	33	33	2.00685
60	1a	12.3	21.5	40.5	25.9	40.1	1.88922
60	1d	8.3	26.6	34.3	24.1	39.1	1.40601
60	2a	8.3	34.3	26.6	24.1	39.1	2.24335
60	2d	12.3	40.5	21.5	25.9	40.1	2.51967
120	1a	12.3	21.5	40.5	40.1	25.9	2.37515
120	1d	8.3	26.6	34.3	39.1	24.1	2.39311
120	2a	8.3	34.3	26.6	39.1	24.1	2.80397
120	2d	12.3	40.5	21.5	40.1	25.9	2.39949
150	2a	9.8	20.8	39.8	33	33	2.70987
150	2b	3.5	26.5	26.5	31.6	31.6	2.63071
150	2c	3.5	33.5	26.5	31.6	31.6	2.88656
150	2d	9.8	39.8	20.8	33	33	2.68674

Octane Vapor by Port
Analytical Model Input from 7.5% Moisture Content By Mass Physical Experiment Data

Minutes	Observation Port		Image Sources			Image Sink	Vapor
	Label	r1	r2	r3	r4	r5	Concentration
Minutes		cm	cm	cm	cm	cm	ppmv
20	1a	12.3	21.5	40.5	40.1	25.9	0.71523
20	1d	8.3	26.6	34.3	39.1	24.1	0.35654
20	2a	8.3	34.3	26.6	39.1	24.1	0.86084
20	2d	12.3	40.5	21.5	40.1	25.9	1.03741
40	1a	9.8	20.8	39.8	33	33	1.25046
40	1d	3.5	26.5	26.5	31.6	31.6	0.72776
40	2a	3.5	33.5	26.5	31.6	31.6	1.81472
40	2d	9.8	39.8	20.8	33	33	2.00685
60	1a	12.3	21.5	40.5	25.9	40.1	1.88922
60	1d	8.3	26.6	34.3	24.1	39.1	1.40601
60	2a	8.3	34.3	26.6	24.1	39.1	2.24335
60	2d	12.3	40.5	21.5	25.9	40.1	2.51967
120	1a	12.3	21.5	40.5	40.1	25.9	2.37515
120	1d	8.3	26.6	34.3	39.1	24.1	2.39311
120	2a	8.3	34.3	26.6	39.1	24.1	2.80397
120	2d	12.3	40.5	21.5	40.1	25.9	2.39949
150	2a	9.8	20.8	39.8	33	33	2.70987
150	2b	3.5	26.5	26.5	31.6	31.6	2.63071
150	2c	3.5	33.5	26.5	31.6	31.6	2.88656
150	2d	9.8	39.8	20.8	33	33	2.68674

Octane Vapor by Port
Analytical Model Input from 8.5% Moisture Content By Mass Physical Experiment Data

Minutes	Observation Port Label	r1 cm	Image Sources r2 cm	r3 cm	r4 cm	Image Sink r5 cm	Vapor Concentration ppmv
20	1a	12.3	21.5	40.5	40.1	25.9	0.14456
20	1d	8.3	26.6	34.3	39.1	24.1	0.17098
20	2a	8.3	34.3	26.6	39.1	24.1	0.30689
20	2d	12.3	40.5	21.5	40.1	25.9	0.36276
40	1a	9.8	20.8	39.8	33	33	0.58842
40	1d	3.5	26.5	26.5	31.6	31.6	0.76036
40	2a	3.5	33.5	26.5	31.6	31.6	0.82785
40	2d	9.8	39.8	20.8	33	33	0.88464
60	1a	12.3	21.5	40.5	25.9	40.1	0.90607
60	1d	8.3	26.6	34.3	24.1	39.1	0.89852
60	2a	8.3	34.3	26.6	24.1	39.1	1.27391
60	2d	12.3	40.5	21.5	25.9	40.1	1.44544
120	1a	12.3	21.5	40.5	40.1	25.9	1.28338
120	1d	8.3	26.6	34.3	39.1	24.1	1.22202
120	2a	8.3	34.3	26.6	39.1	24.1	1.71257
120	2d	12.3	40.5	21.5	40.1	25.9	1.76405
180	2a	9.8	20.8	39.8	33	33	1.30434
180	2b	3.5	26.5	26.5	31.6	31.6	1.39128
180	2c	3.5	33.5	26.5	31.6	31.6	1.77442
180	2d	9.8	39.8	20.8	33	33	1.7701

Octane Vapor by Port
Analytical Model Input from 9.25% Moisture Content By Mass Physical Experiment Data

	Observation Port		Image Sources			Image Sink	Vapor
	Label	r1	r2	r3	r4	r5	Concentration
Minutes		cm	cm	cm	cm	cm	ppmv
20	1a	12.3	21.5	40.5	40.1	25.9	0.0315
20	1d	8.3	26.6	34.3	39.1	24.1	0.02376
20	2a	8.3	34.3	26.6	39.1	24.1	0.02723
20	2d	12.3	40.5	21.5	40.1	25.9	0.03327
40	1a	9.8	20.8	39.8	33	33	0.05566
40	1d	3.5	26.5	26.5	31.6	31.6	0.05397
40	2a	3.5	33.5	26.5	31.6	31.6	0.06052
40	2d	9.8	39.8	20.8	33	33	0.08098
60	1a	12.3	21.5	40.5	25.9	40.1	0.13344
60	1d	8.3	26.6	34.3	24.1	39.1	0.09837
60	2a	8.3	34.3	26.6	24.1	39.1	0.26527
60	2d	12.3	40.5	21.5	25.9	40.1	0.19007
90	1a	12.3	21.5	40.5	40.1	25.9	0.22497
90	1d	8.3	26.6	34.3	39.1	24.1	0.22446
90	2a	8.3	34.3	26.6	39.1	24.1	0.27646
90	2d	12.3	40.5	21.5	40.1	25.9	0.29016
120	2a	9.8	20.8	39.8	33	33	0.25523
120	2b	3.5	26.5	26.5	31.6	31.6	0.18501
120	2c	3.5	33.5	26.5	31.6	31.6	0.38529
120	2d	9.8	39.8	20.8	33	33	0.38611

Octane Vapor by Port

Analytical Model Input from 10% Moisture Content By Mass Physical Experiment Data

	Observation Port		Image Sources			Image Sink	Vapor
	Label	r1	r2	r3	r4	r5	Concentration
Minutes		cm	cm	cm	cm	cm	ppmv
20	1a	12.3	21.5	40.5	40.1	25.9	0.08641
20	1d	8.3	26.6	34.3	39.1	24.1	0.078928
20	2a	8.3	34.3	26.6	39.1	24.1	0.093776
20	2d	12.3	40.5	21.5	40.1	25.9	0.104912
40	1a	9.8	20.8	39.8	33	33	0.189123
40	1d	3.5	26.5	26.5	31.6	31.6	0.150857
40	2a	3.5	33.5	26.5	31.6	31.6	0.266258
40	2d	9.8	39.8	20.8	33	33	0.294339
60	1a	12.3	21.5	40.5	25.9	40.1	0.356636
60	1d	8.3	26.6	34.3	24.1	39.1	0.209464
60	2a	8.3	34.3	26.6	24.1	39.1	0.468851
60	2d	12.3	40.5	21.5	25.9	40.1	0.463494
90	1a	12.3	21.5	40.5	40.1	25.9	0.415309
90	1d	8.3	26.6	34.3	39.1	24.1	0.311381
90	2a	8.3	34.3	26.6	39.1	24.1	0.578457
90	2d	12.3	40.5	21.5	40.1	25.9	0.622256
120	2a	9.8	20.8	39.8	33	33	0.409135
120	2b	3.5	26.5	26.5	31.6	31.6	0.367624
120	2c	3.5	33.5	26.5	31.6	31.6	0.414563
120	2d	9.8	39.8	20.8	33	33	0.514149

Diesel Fuel Vapor
Analytical Model Input from 0% Moisture Content By Mass Physical Experiment Data

|	Observation Port		Image Sources			Image Sink	Vapor
	Label	r1	r2	r3	r4	r5	Concentration
Minutes		cm	cm	cm	cm	cm	ppmv
40	1a	12.3	21.5	40.5	40.1	25.9	0.60922
40	1b	8.3	26.6	34.3	39.1	24.1	0.63432
40	2a	9.8	20.8	39.8	33	33	0.61099
40	2b	3.5	26.5	26.5	31.6	31.6	0.84793
40	3a	12.3	21.5	40.5	25.9	40.1	0.67648
40	3b	8.3	26.6	34.3	24.1	39.1	0.59566
60	1a	12.3	21.5	40.5	40.1	25.9	0.65263
60	1b	8.3	26.6	34.3	39.1	24.1	0.77653
60	2a	9.8	20.8	39.8	33	33	0.74977
60	2b	3.5	26.5	26.5	31.6	31.6	0.79345
60	3a	12.3	21.5	40.5	25.9	40.1	0.64362
60	3b	8.3	26.6	34.3	24.1	39.1	0.68214
100	1a	12.3	21.5	40.5	40.1	25.9	0.92649
100	1b	8.3	26.6	34.3	39.1	24.1	0.99935
100	2a	9.8	20.8	39.8	33	33	0.72695
100	2b	3.5	26.5	26.5	31.6	31.6	0.9223
100	3a	12.3	21.5	40.5	25.9	40.1	0.8928
100	3b	8.3	26.6	34.3	24.1	39.1	0.91567
150	1a	12.3	21.5	40.5	40.1	25.9	1.10845
150	1b	8.3	26.6	34.3	39.1	24.1	0.85379
150	2a	9.8	20.8	39.8	33	33	0.9956
150	2b	3.5	26.5	26.5	31.6	31.6	1.08189
150	3a	12.3	21.5	40.5	25.9	40.1	1.06127
150	3b	8.3	26.6	34.3	24.1	39.1	0.91883
210	1a	12.3	21.5	40.5	40.1	25.9	0.85568
210	1b	8.3	26.6	34.3	39.1	24.1	1.03595
210	2a	9.8	20.8	39.8	33	33	0.86076
210	2b	3.5	26.5	26.5	31.6	31.6	1.14258
210	3a	12.3	21.5	40.5	25.9	40.1	0.80641
210	3b	8.3	26.6	34.3	24.1	39.1	1.07667
270	1a	12.3	21.5	40.5	40.1	25.9	1.19518
270	1b	8.3	26.6	34.3	39.1	24.1	1.14153
270	2a	9.8	20.8	39.8	33	33	1.13414
270	2b	3.5	26.5	26.5	31.6	31.6	1.15396
270	3a	12.3	21.5	40.5	25.9	40.1	0.9296
270	3b	8.3	26.6	34.3	24.1	39.1	1.16776
330	1a	12.3	21.5	40.5	40.1	25.9	1.23119
330	1b	8.3	26.6	34.3	39.1	24.1	1.31869
330	2a	9.8	20.8	39.8	33	33	1.07798
330	2b	3.5	26.5	26.5	31.6	31.6	1.28559
330	3a	12.3	21.5	40.5	25.9	40.1	1.08772
330	3b	8.3	26.6	34.3	24.1	39.1	1.38538

Diesel Fuel Vapor
Analytical Model Input from 2% Moisture Content By Mass Physical Experiment Data

	Observation Port		Image Sources			Image Sink	Vapor
	Label	r1	r2	r3	r4	r5	Concentration
Minutes		cm	cm	cm	cm	cm	ppmv
40	1a	12.3	21.5	40.5	40.1	25.9	0.65709
40	1b	8.3	26.6	34.3	39.1	24.1	0.68355
40	2a	9.8	20.8	39.8	33	33	0.67677
40	2b	3.5	26.5	26.5	31.6	31.6	0.8441
40	3a	12.3	21.5	40.5	25.9	40.1	0.67072
40	3b	8.3	26.6	34.3	24.1	39.1	0.67422
60	1a	12.3	21.5	40.5	40.1	25.9	0.70675
60	1b	8.3	26.6	34.3	39.1	24.1	0.82355
60	2a	9.8	20.8	39.8	33	33	0.80931
60	2b	3.5	26.5	26.5	31.6	31.6	0.90165
60	3a	12.3	21.5	40.5	25.9	40.1	0.69224
60	3b	8.3	26.6	34.3	24.1	39.1	0.76555
100	1a	12.3	21.5	40.5	40.1	25.9	0.92473
100	1b	8.3	26.6	34.3	39.1	24.1	1.00003
100	2a	9.8	20.8	39.8	33	33	0.81181
100	2b	3.5	26.5	26.5	31.6	31.6	1.04581
100	3a	12.3	21.5	40.5	25.9	40.1	0.95189
100	3b	8.3	26.6	34.3	24.1	39.1	0.98749
150	1a	12.3	21.5	40.5	40.1	25.9	1.10038
150	1b	8.3	26.6	34.3	39.1	24.1	1.01728
150	2a	9.8	20.8	39.8	33	33	1.03929
150	2b	3.5	26.5	26.5	31.6	31.6	1.15663
150	3a	12.3	21.5	40.5	25.9	40.1	1.08679
150	3b	8.3	26.6	34.3	24.1	39.1	1.02985
210	1a	12.3	21.5	40.5	40.1	25.9	1.08583
210	1b	8.3	26.6	34.3	39.1	24.1	1.14183
210	2a	9.8	20.8	39.8	33	33	1.03534
210	2b	3.5	26.5	26.5	31.6	31.6	1.26101
210	3a	12.3	21.5	40.5	25.9	40.1	1.01019
210	3b	8.3	26.6	34.3	24.1	39.1	1.10459
270	1a	12.3	21.5	40.5	40.1	25.9	1.21176
270	1b	8.3	26.6	34.3	39.1	24.1	1.21522
270	2a	9.8	20.8	39.8	33	33	1.22809
270	2b	3.5	26.5	26.5	31.6	31.6	1.31122
270	3a	12.3	21.5	40.5	25.9	40.1	1.06697
270	3b	8.3	26.6	34.3	24.1	39.1	1.23333
330	1a	12.3	21.5	40.5	40.1	25.9	1.21135
330	1b	8.3	26.6	34.3	39.1	24.1	1.33494
330	2a	9.8	20.8	39.8	33	33	1.22049
330	2b	3.5	26.5	26.5	31.6	31.6	1.40847
330	3a	12.3	21.5	40.5	25.9	40.1	1.20962
330	3b	8.3	26.6	34.3	24.1	39.1	1.36274

Diesel Fuel Vapor
Analytical Model Input from 5% Moisture Content By Mass Physical Experiment Data

	Observation Port		Image Sources			Image Sink	Vapor
	Label	r1	r2	r3	r4	r5	Concentration
Minutes		cm	cm	cm	cm	cm	ppmv
40	1a	12.3	21.5	40.5	40.1	25.9	0.6099
40	1b	8.3	26.6	34.3	39.1	24.1	0.68224
40	2a	9.8	20.8	39.8	33	33	0.83631
40	2b	3.5	26.5	26.5	31.6	31.6	0.8183
40	3a	12.3	21.5	40.5	25.9	40.1	0.80056
40	3b	8.3	26.6	34.3	24.1	39.1	0.68576
60	1a	12.3	21.5	40.5	40.1	25.9	0.73312
60	1b	8.3	26.6	34.3	39.1	24.1	0.76109
60	2a	9.8	20.8	39.8	33	33	0.86014
60	2b	3.5	26.5	26.5	31.6	31.6	0.73334
60	3a	12.3	21.5	40.5	25.9	40.1	0.8233
60	3b	8.3	26.6	34.3	24.1	39.1	0.97684
100	1a	12.3	21.5	40.5	40.1	25.9	0.90455
100	1b	8.3	26.6	34.3	39.1	24.1	1.00673
100	2a	9.8	20.8	39.8	33	33	1.03913
100	2b	3.5	26.5	26.5	31.6	31.6	1.03354
100	3a	12.3	21.5	40.5	25.9	40.1	1.04478
100	3b	8.3	26.6	34.3	24.1	39.1	1.09712
150	1a	12.3	21.5	40.5	40.1	25.9	1.13902
150	1b	8.3	26.6	34.3	39.1	24.1	1.12176
150	2a	9.8	20.8	39.8	33	33	1.07804
150	2b	3.5	26.5	26.5	31.6	31.6	1.12159
150	3a	12.3	21.5	40.5	25.9	40.1	1.13043
150	3b	8.3	26.6	34.3	24.1	39.1	1.15429
210	1a	12.3	21.5	40.5	40.1	25.9	1.14131
210	1b	8.3	26.6	34.3	39.1	24.1	1.11326
210	2a	9.8	20.8	39.8	33	33	1.21626
210	2b	3.5	26.5	26.5	31.6	31.6	1.28241
210	3a	12.3	21.5	40.5	25.9	40.1	1.15989
210	3b	8.3	26.6	34.3	24.1	39.1	1.30727
270	1a	12.3	21.5	40.5	40.1	25.9	1.20784
270	1b	8.3	26.6	34.3	39.1	24.1	1.13231
270	2a	9.8	20.8	39.8	33	33	1.23989
270	2b	3.5	26.5	26.5	31.6	31.6	1.2125
270	3a	12.3	21.5	40.5	25.9	40.1	1.2078
270	3b	8.3	26.6	34.3	24.1	39.1	1.32722
330	1a	12.3	21.5	40.5	40.1	25.9	1.44039
330	1b	8.3	26.6	34.3	39.1	24.1	1.43544
330	2a	9.8	20.8	39.8	33	33	1.54881
330	2b	3.5	26.5	26.5	31.6	31.6	1.32593
330	3a	12.3	21.5	40.5	25.9	40.1	1.54685
330	3b	8.3	26.6	34.3	24.1	39.1	1.55323

Diesel Fuel Vapor
Analytical Model Input from 5% Moisture Content By Mass Physical Experiment Data

	Observation Port		Image Sources			Image Sink	Vapor
	Label	r1	r2	r3	r4	r5	Concentration
Minutes		cm	cm	cm	cm	cm	ppmv
390	1a	12.3	21.5	40.5	40.1	25.9	1.58042
390	1b	8.3	26.6	34.3	39.1	24.1	1.43894
390	2a	9.8	20.8	39.8	33	33	1.4572
390	2b	3.5	26.5	26.5	31.6	31.6	1.54719
390	3a	12.3	21.5	40.5	25.9	40.1	1.65152
390	3b	8.3	26.6	34.3	24.1	39.1	1.63166
450	1a	12.3	21.5	40.5	40.1	25.9	1.57455
450	1b	8.3	26.6	34.3	39.1	24.1	1.73639
450	2a	9.8	20.8	39.8	33	33	1.76106
450	2b	3.5	26.5	26.5	31.6	31.6	1.86459
450	3a	12.3	21.5	40.5	25.9	40.1	1.6433
450	3b	8.3	26.6	34.3	24.1	39.1	1.73625

Appendix C

Observed Concentrations versus Analytically Estimated Values

of Octane and Diesel Fuel Vapors for Various Moisture Contents by Mass

99

**Observed Concentrations versus Analytically Estimated Values of
Octane Vapor for
0% Moisture Content by Mass**
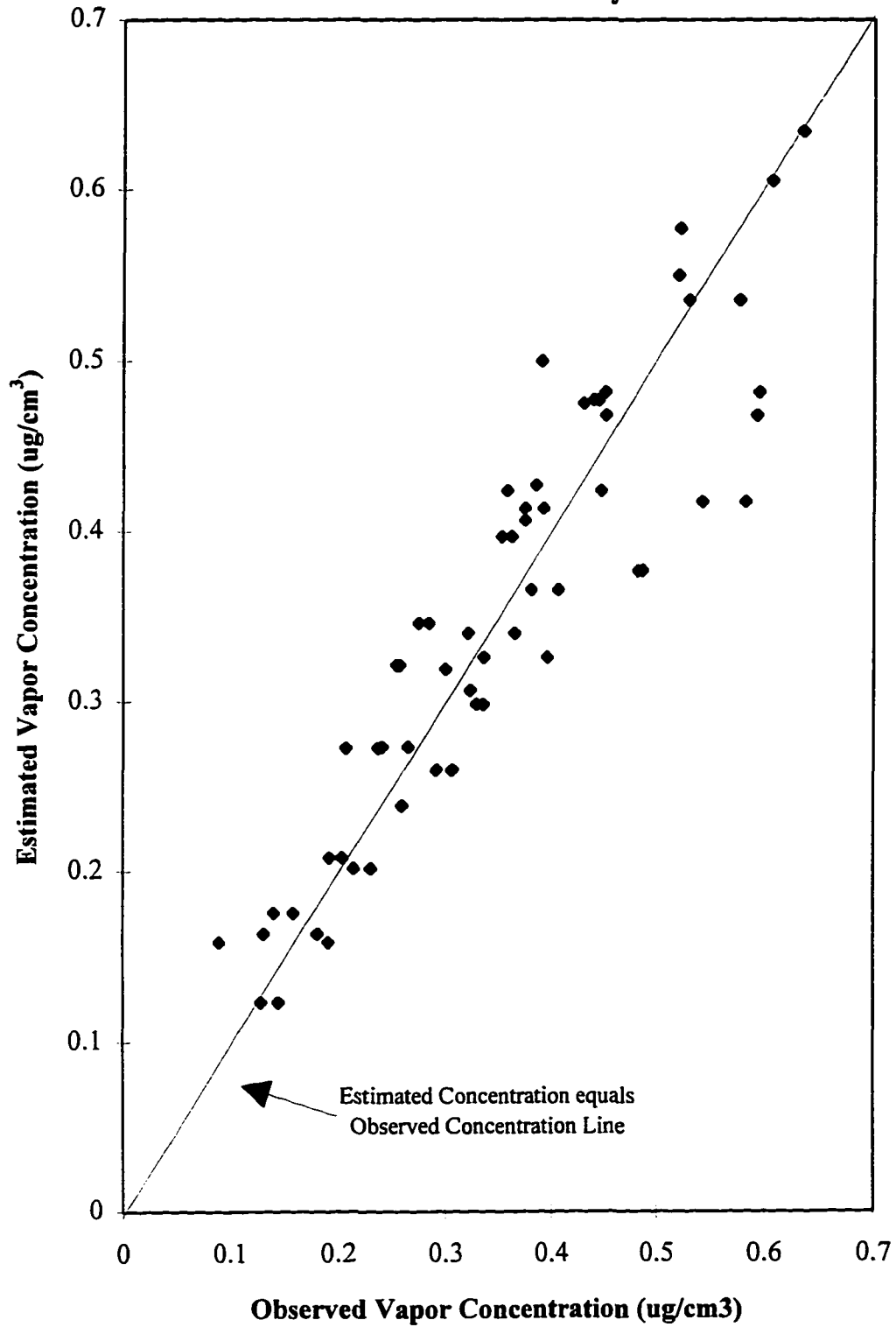
**Observed Concentrations versus Analytically Estimated Values of
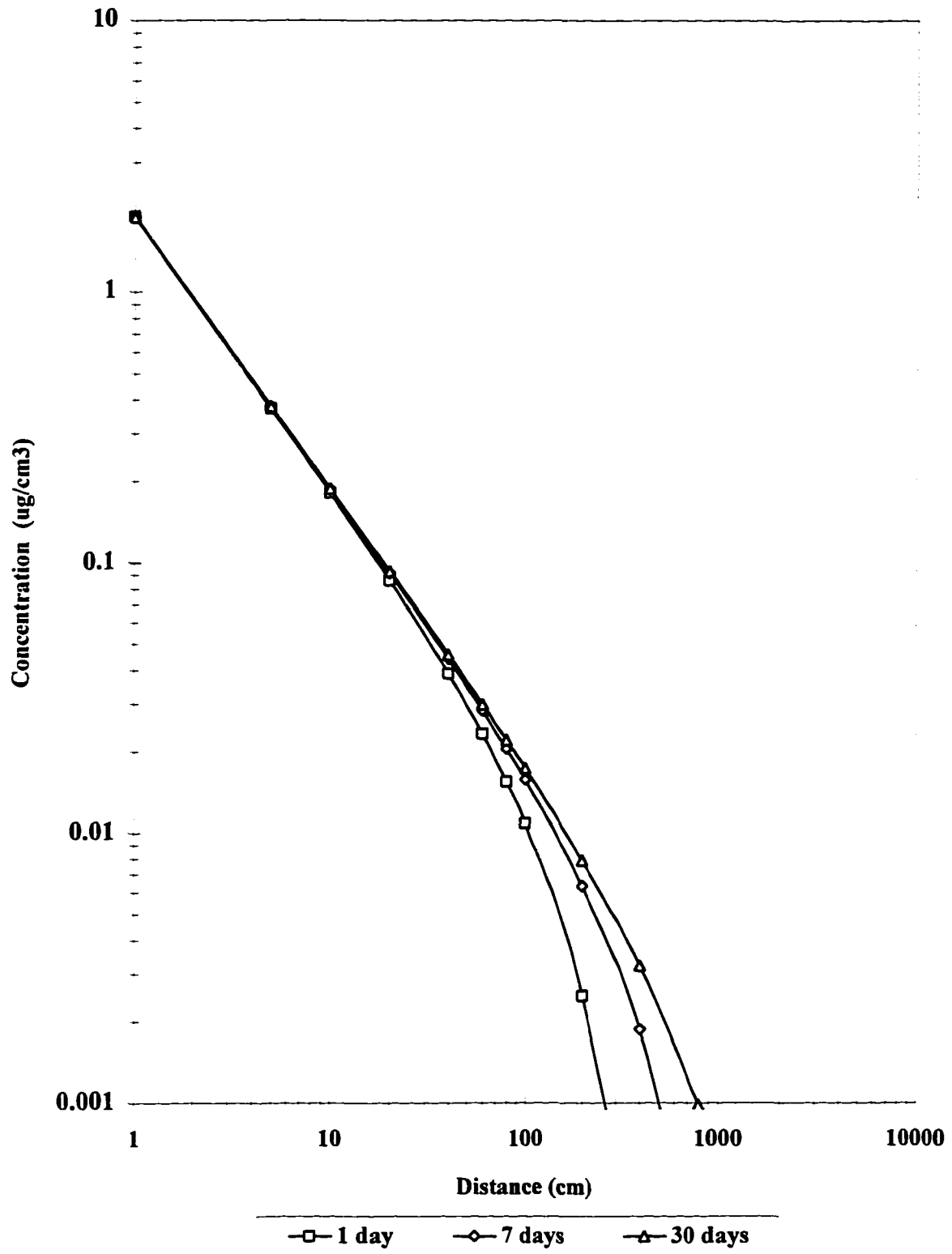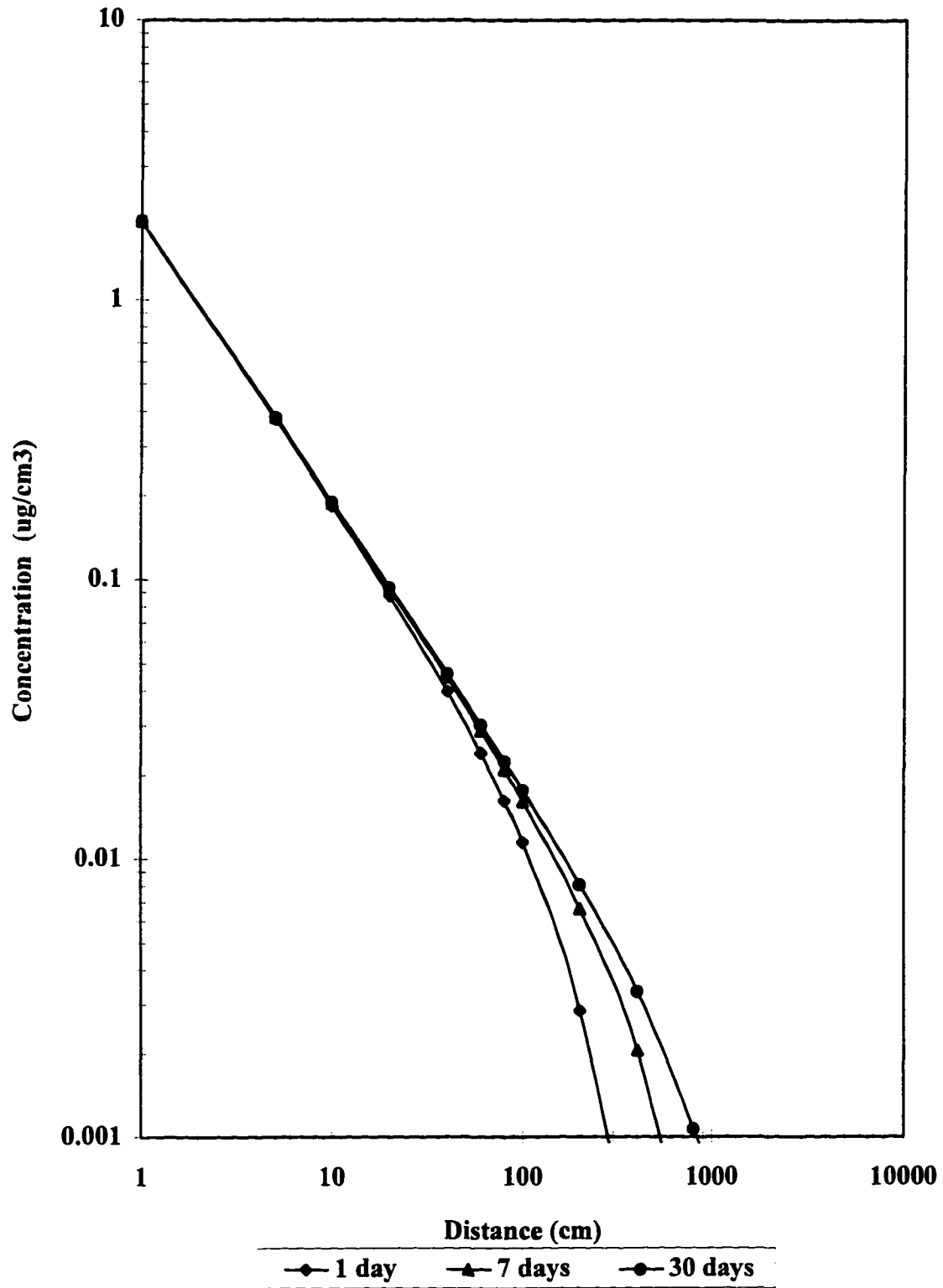Octane Vapor for
1% Moisture Content by Mass**
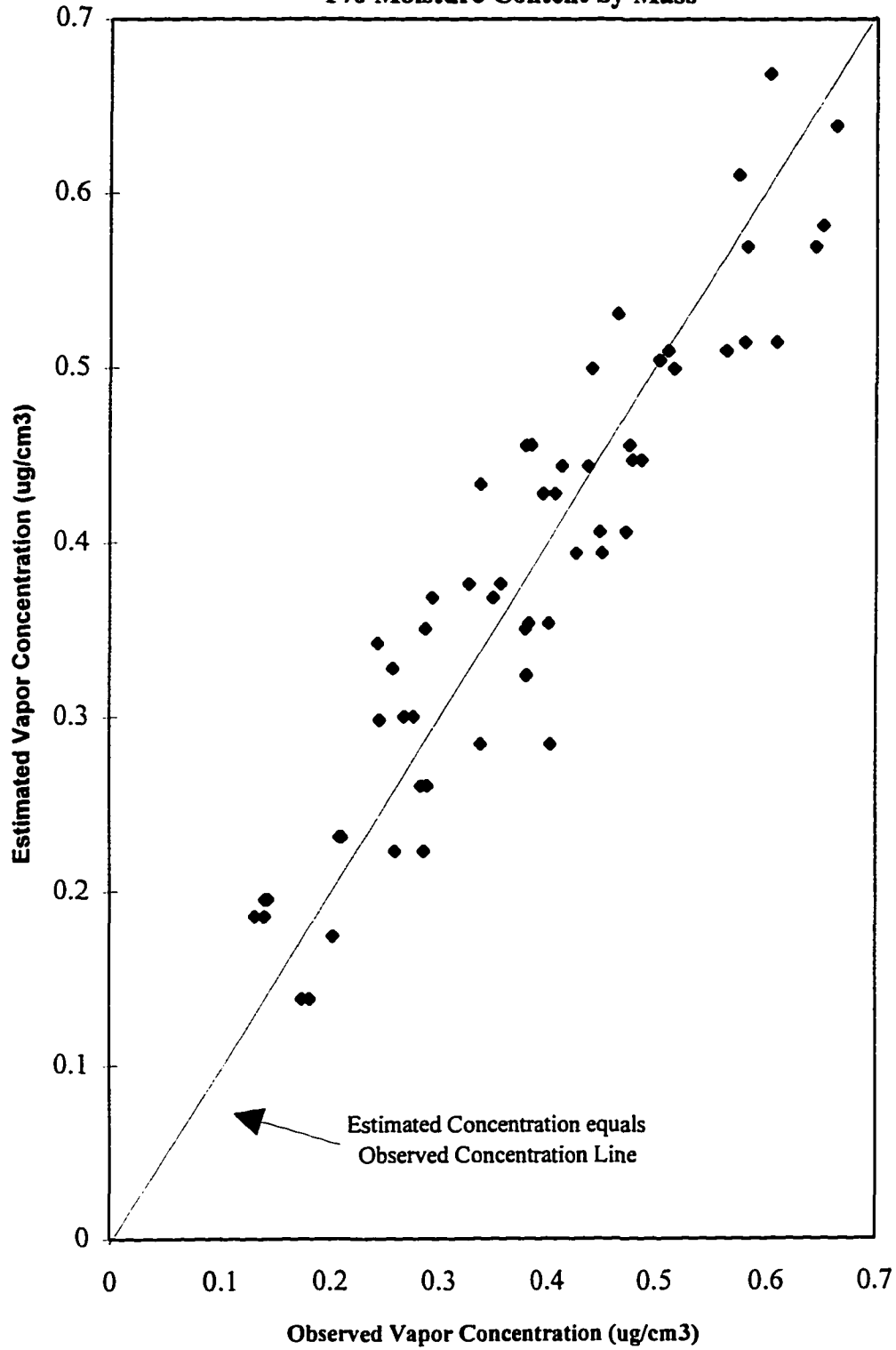
Observed Concentrations versus Analytically Estimated Values of Octane Vapor for 2% Moisture Content by Mass
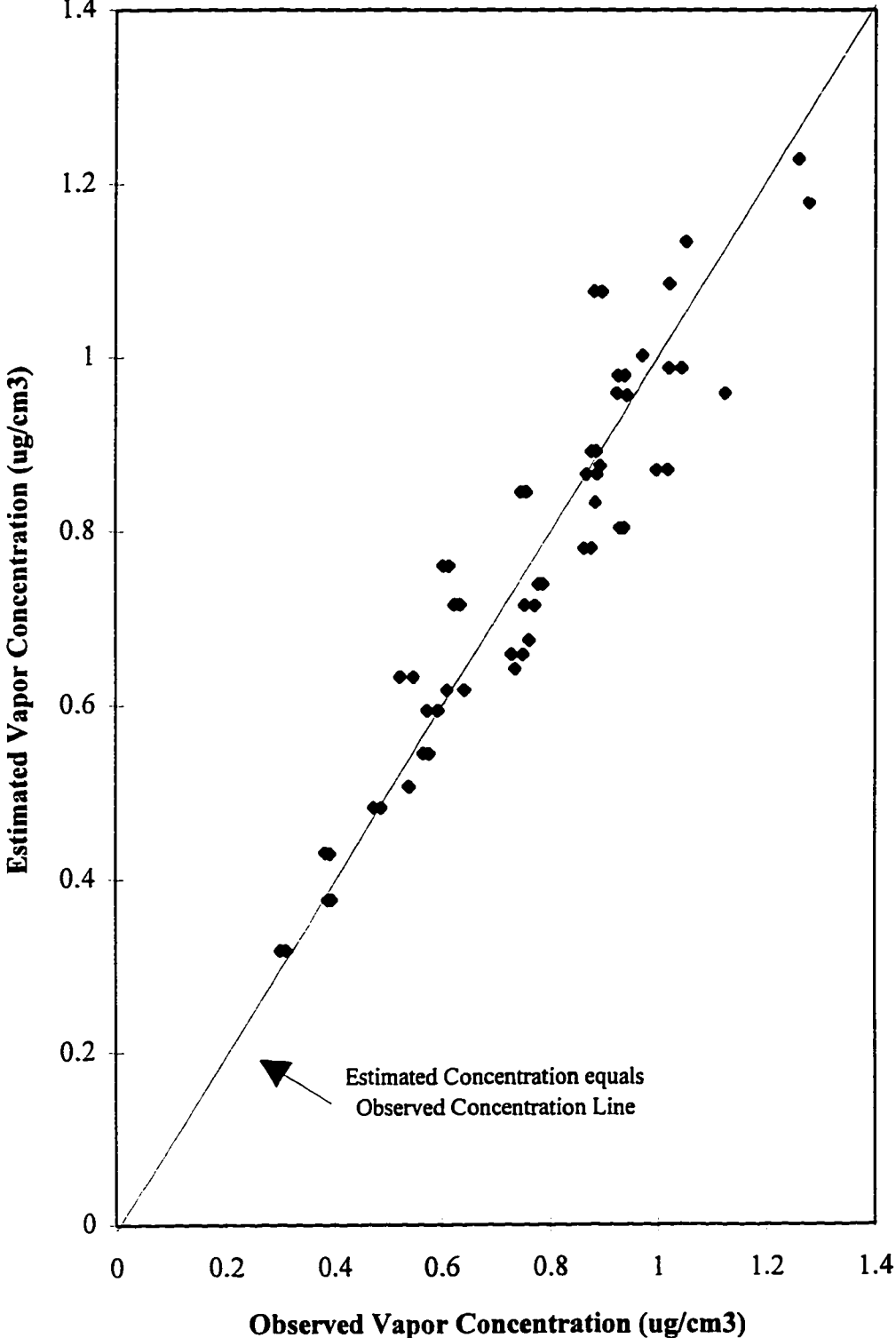
Observed Concentrations versus Analytically Estimated Values of Octane Vapor for 5% Moisture Content by Mass
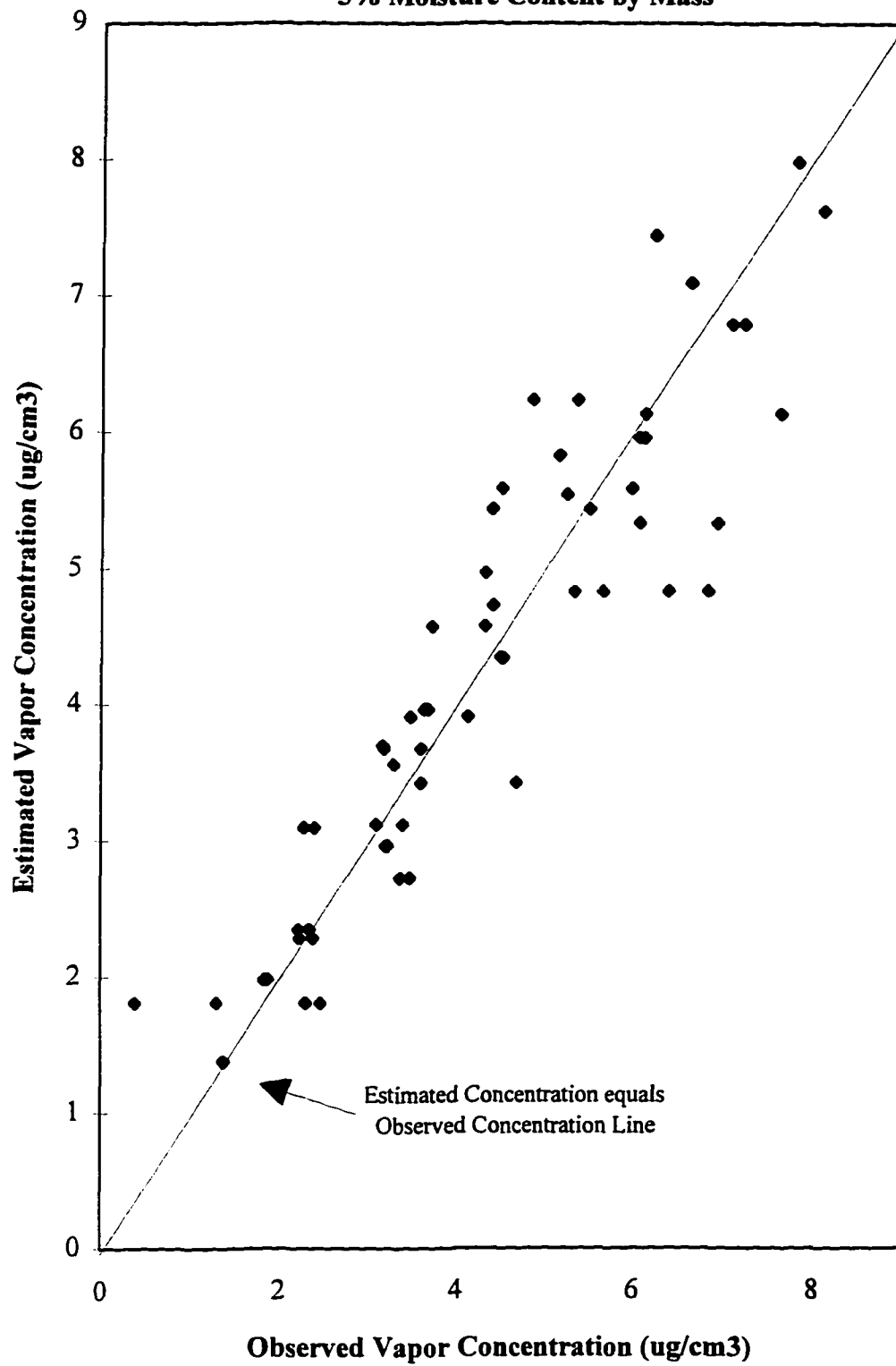
Observed Concentrations versus Analytically Estimated Values of Octane Vapor for 6.5% Moisture Content by Mass

Estimated Concentration equals
Observed Concentration Line

Estimated Vapor Concentration (ug/cm3)

Observed Vapor Concentration (ug/cm3)
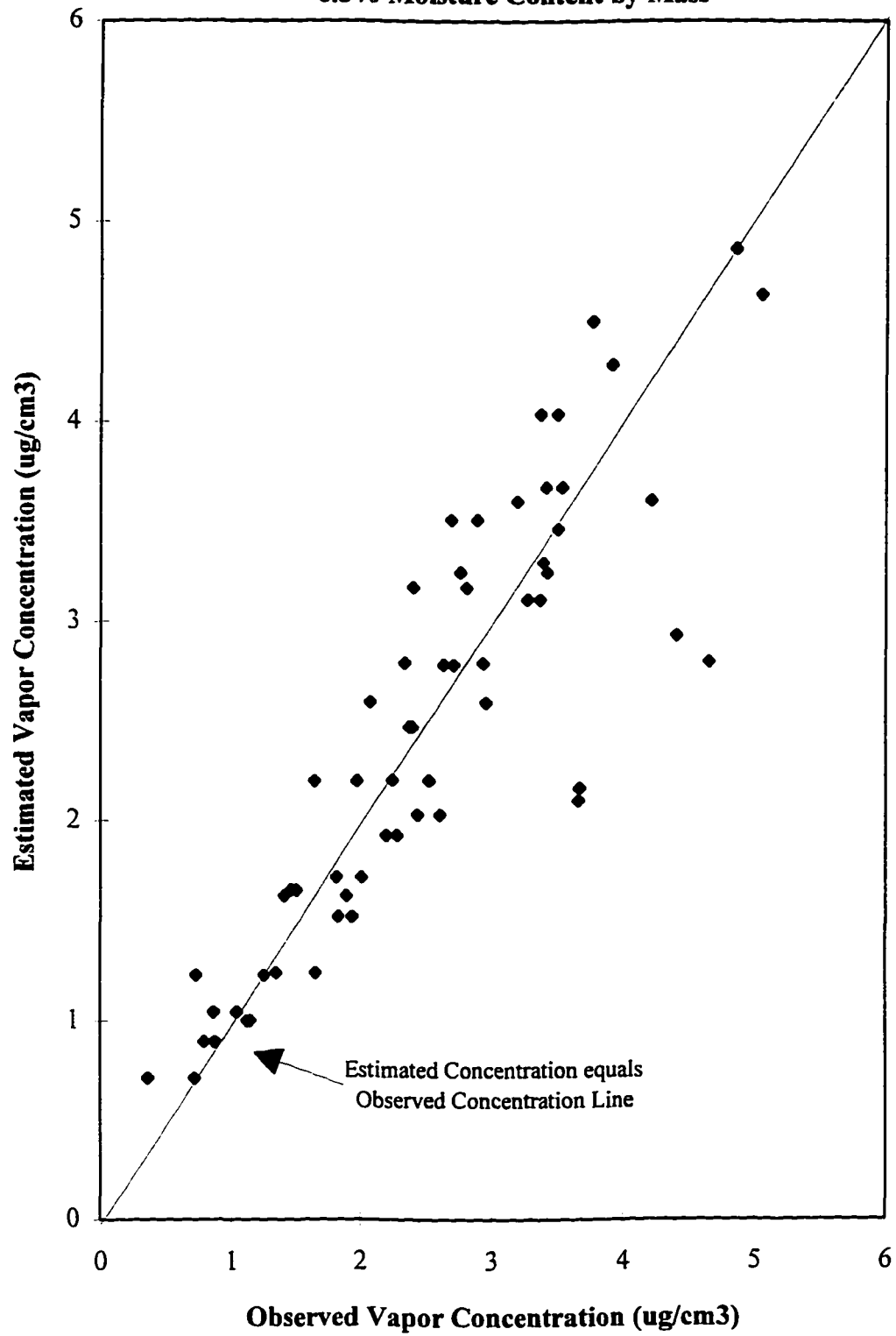
Observed Concentrations versus Analytically Estimated Values of Octane Vapor for 7.5% Moisture Content by Mass

Estimated Concentration equals Observed Concentration Line

Estimated Vapor Concentration (ng/cm3)

Observed Vapor Concentration (ug/cm3)
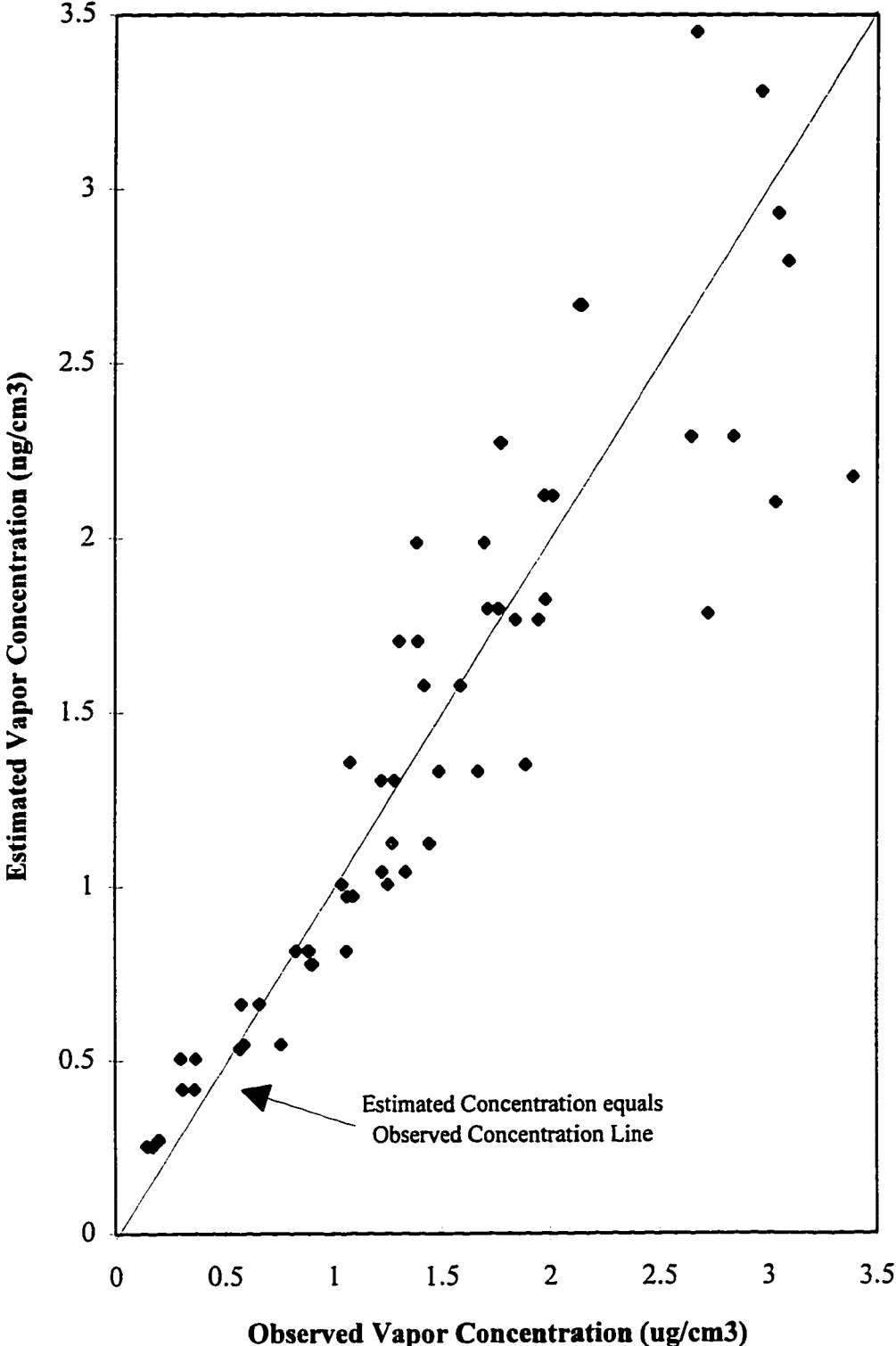
Observed Concentrations versus Analytically Estimated Values of Octane Vapor for 8.5% Moisture Content by Mass
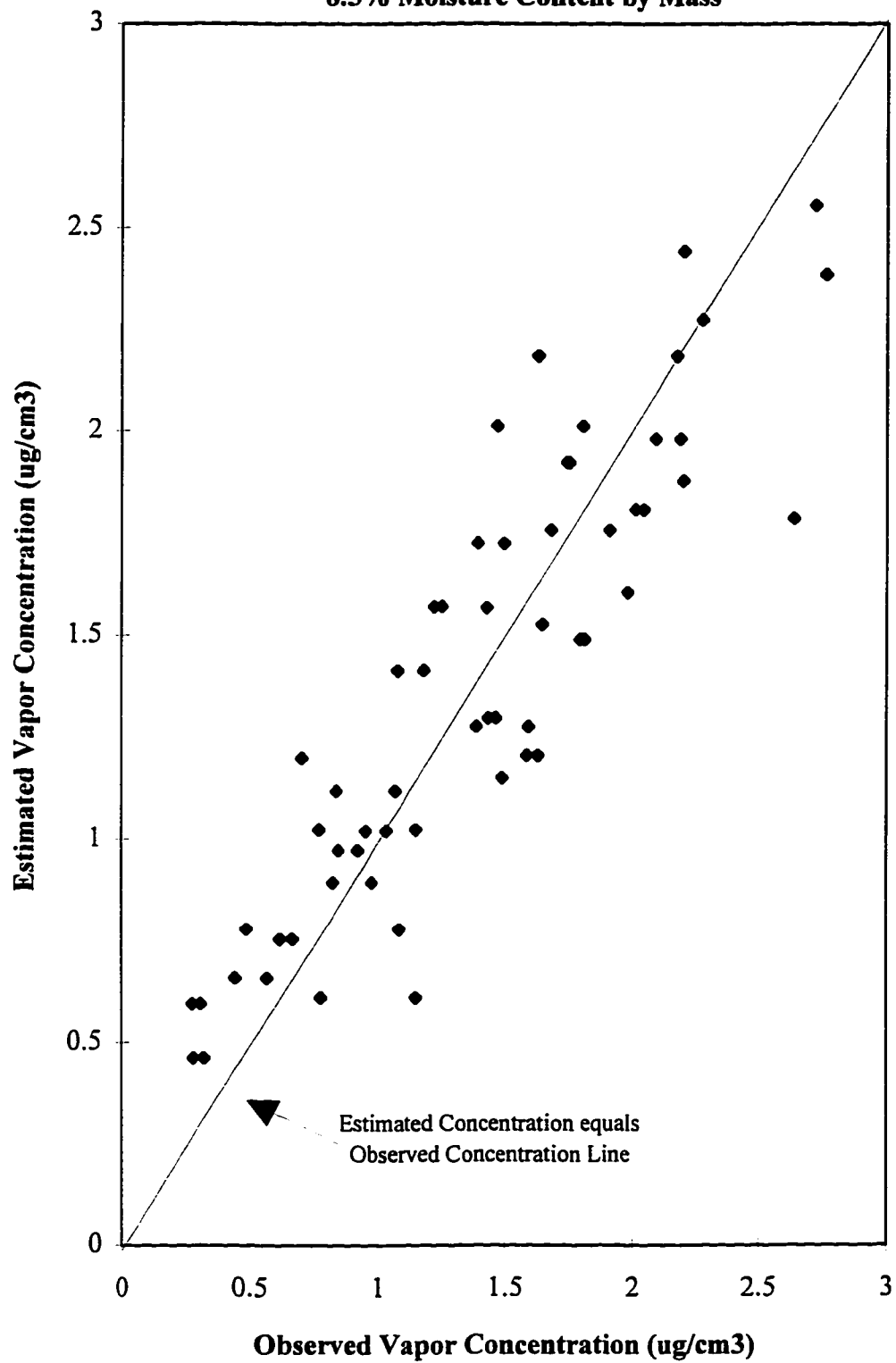
**Observed Concentrations versus Analytically Estimated Values of
Octane Vapor for
9.25% Moisture Content by Mass**

Estimated Concentration equals
Observed Concentration Line
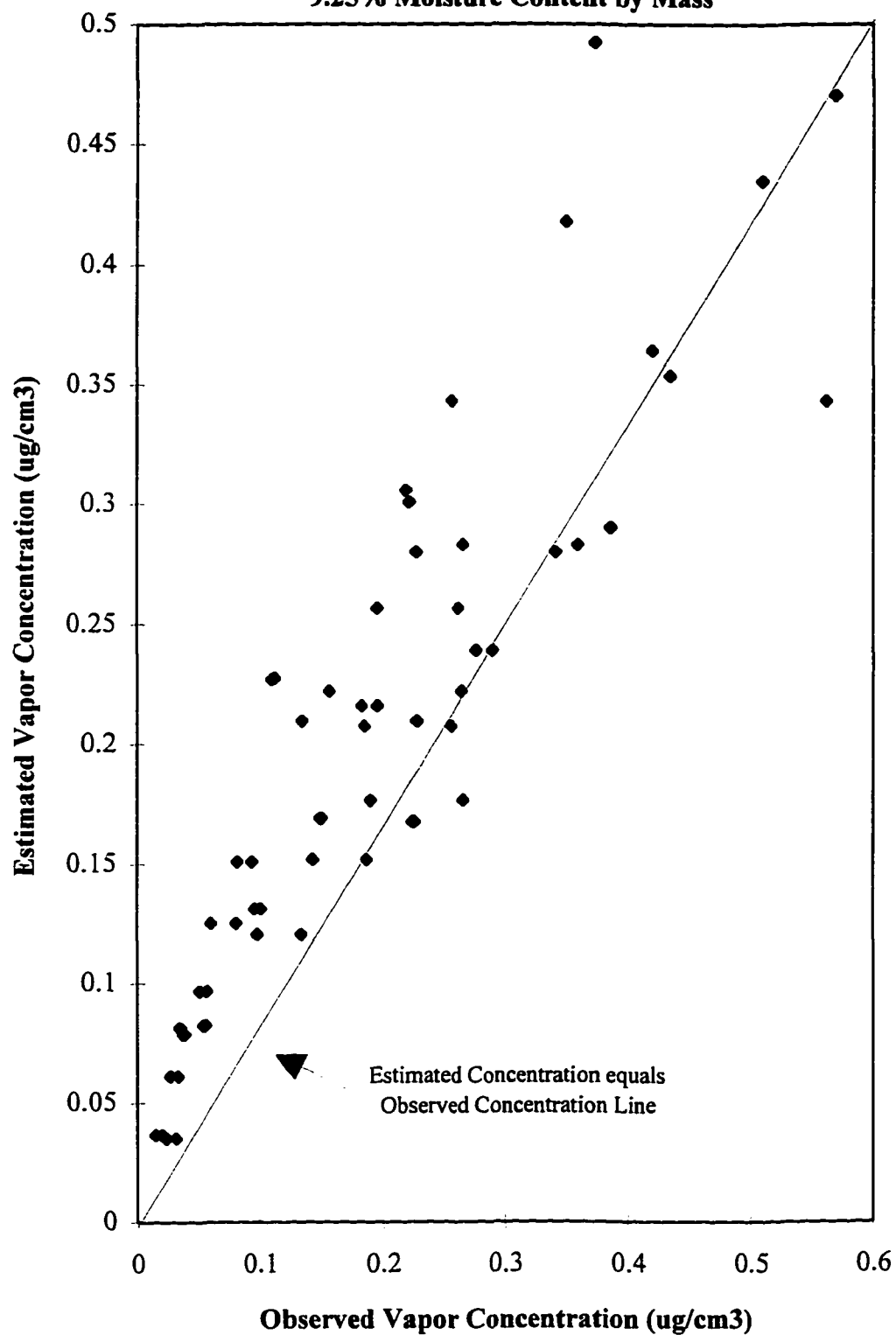
Observed Concentrations versus Analytically Estimated Values of Octane Vapor for 10% Moisture Content by Mass
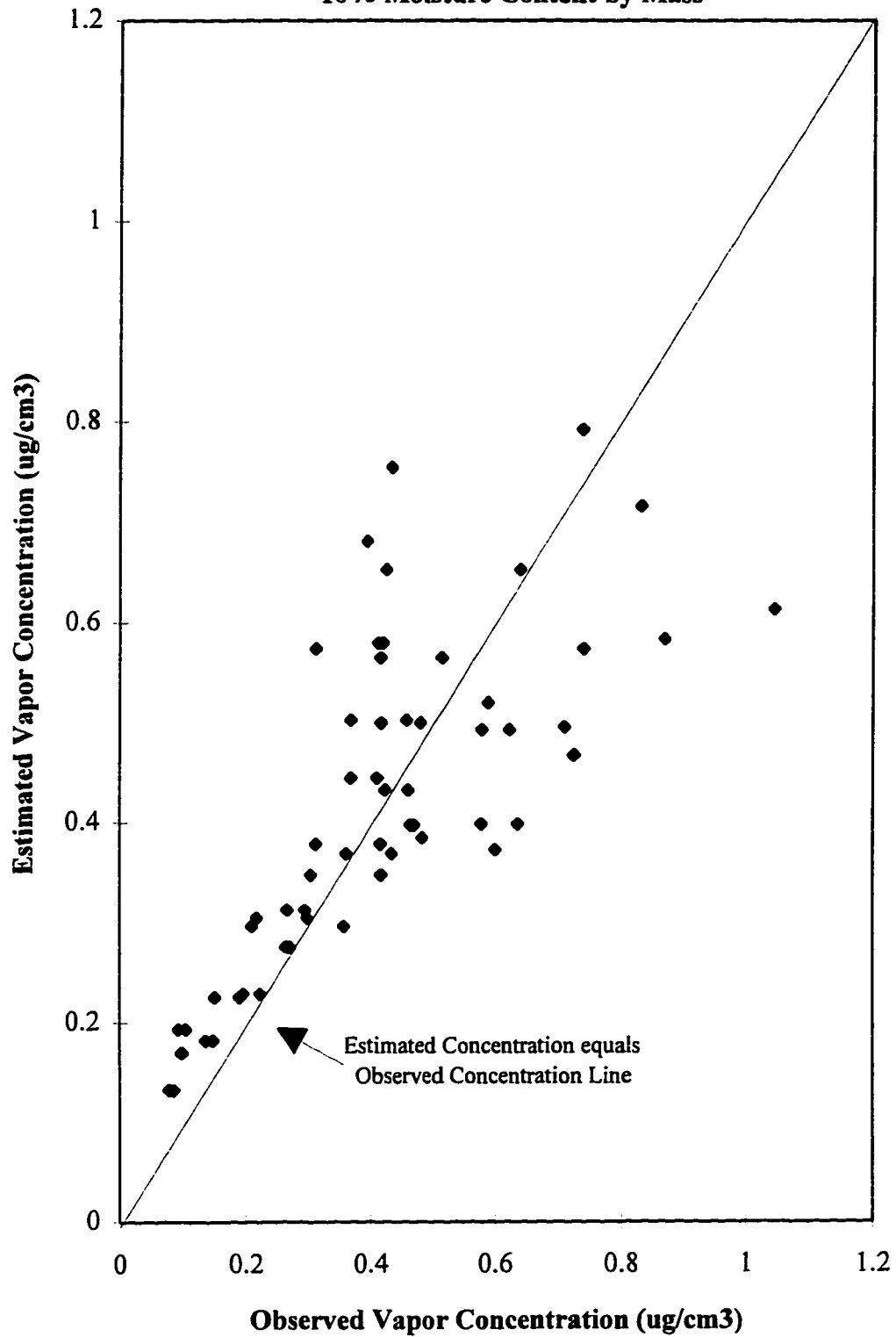
**Observed Concentrations versus Analytically Estimated Values of Diesel Fuel Vapor for
0% Moisture Content by Mass**
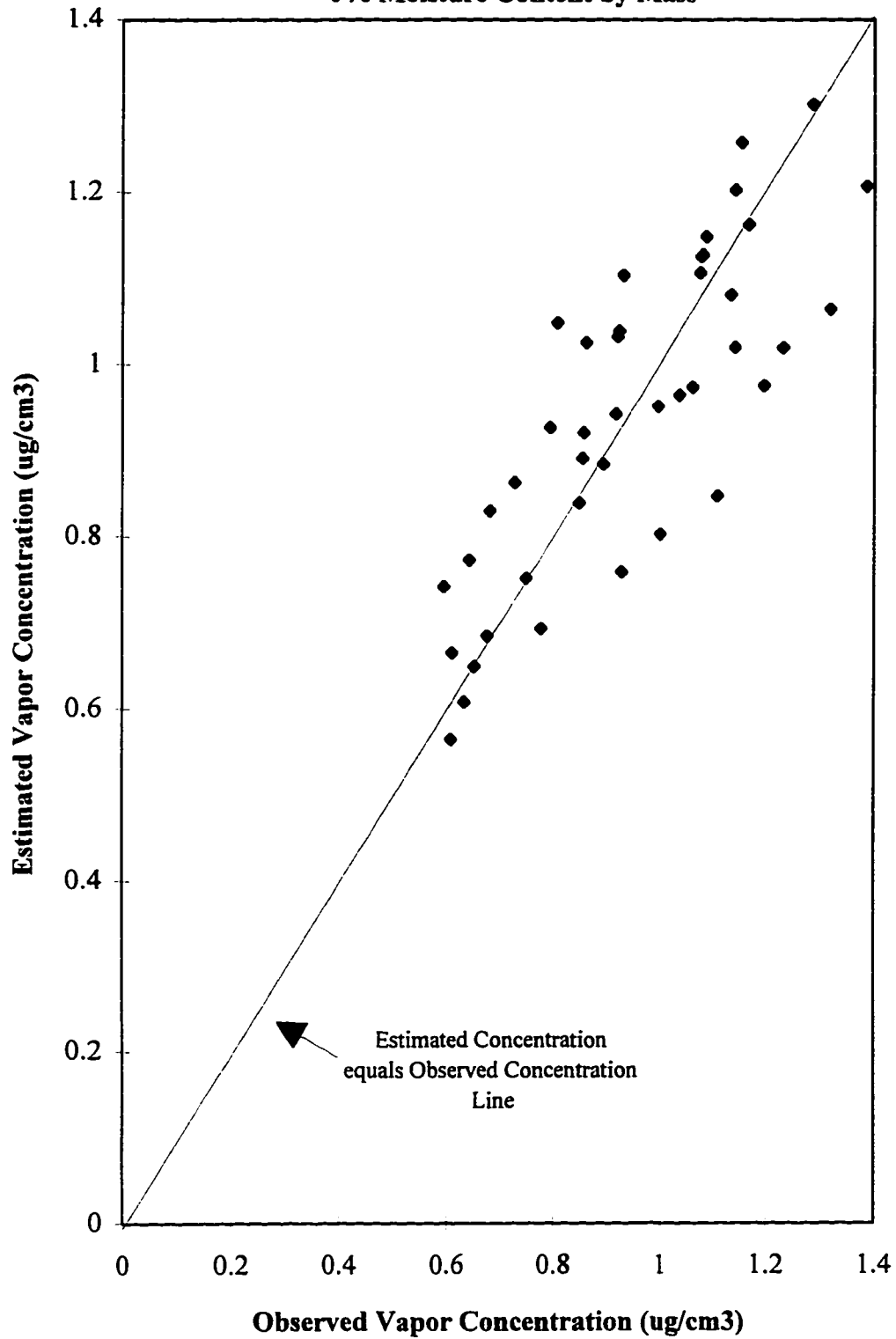
Observed Concentrations versus Analytically Estimated Values of Diesel Fuel Vapor for 2% Moisture Content by Mass
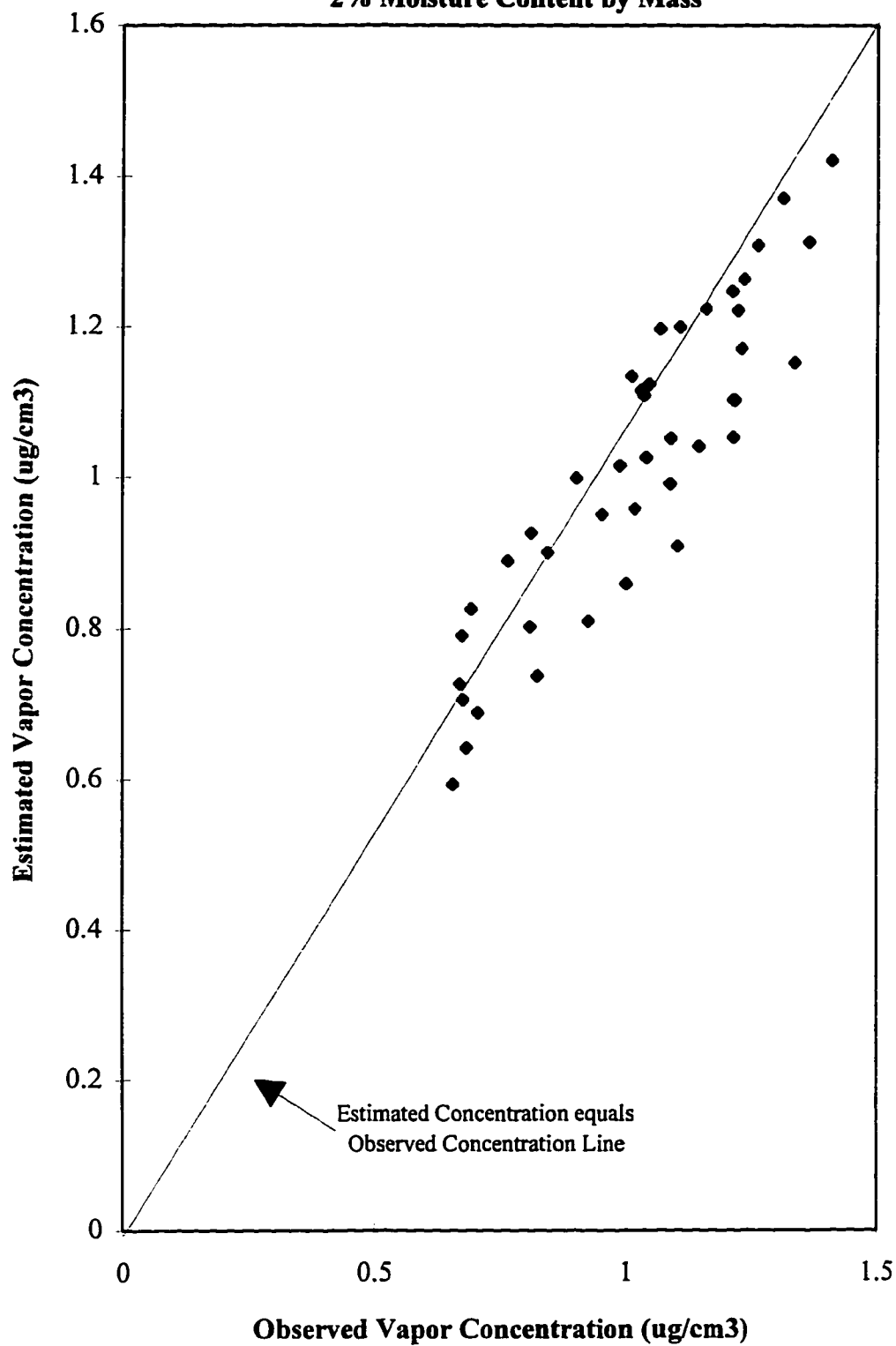
Observed Concentrations versus Analytically Estimated Values of Diesel Fuel Vapor for 5% Moisture Content by Mass
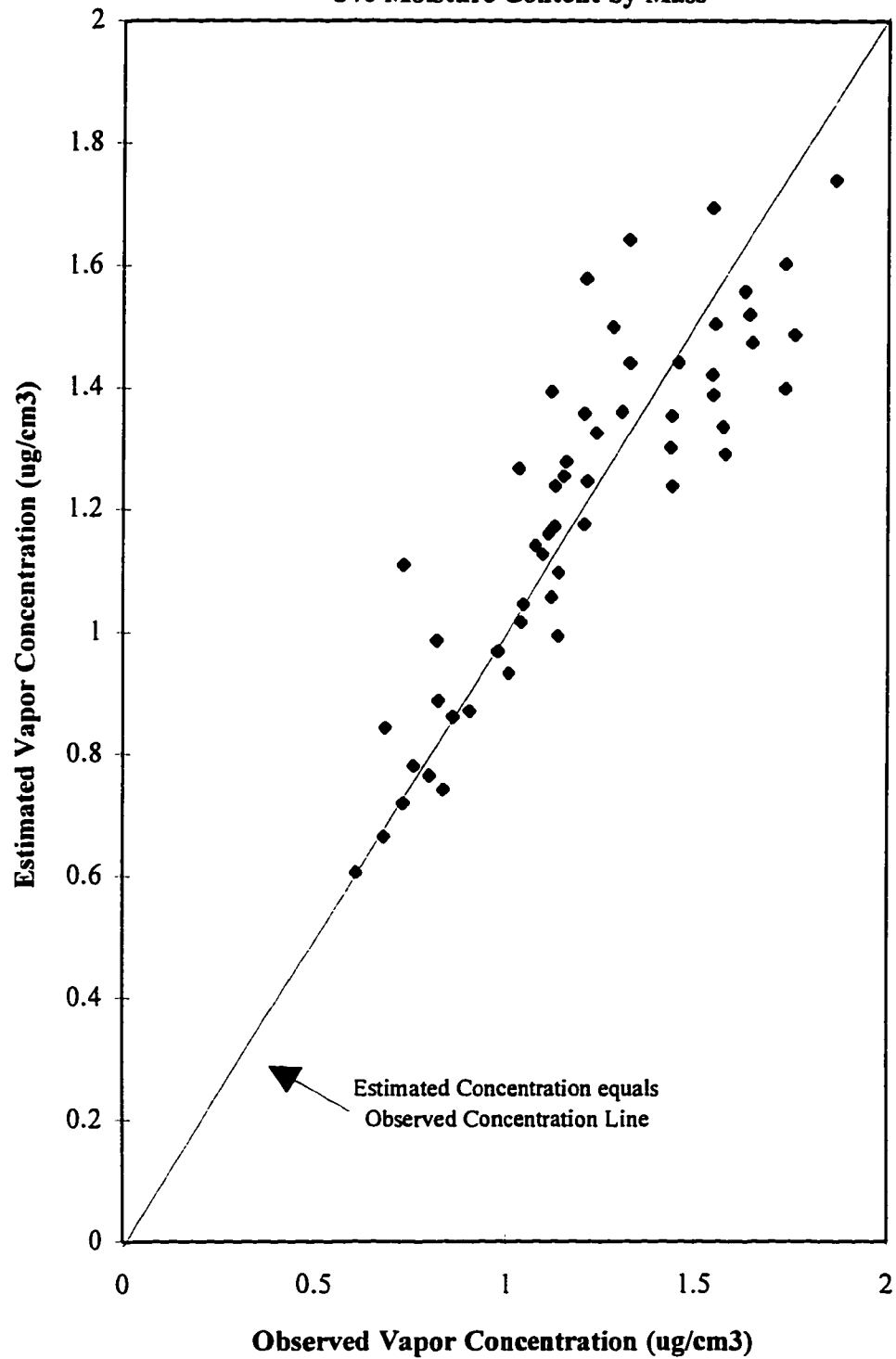
Appendix D

Octane and Diesel Fuel Vapor Analytical Modeled Concentration Curves for

1-day, 7-day, and 30-day Time Intervals and Various Moisture Contents by Mass

112

**Analytically Modeled Octane Vapor
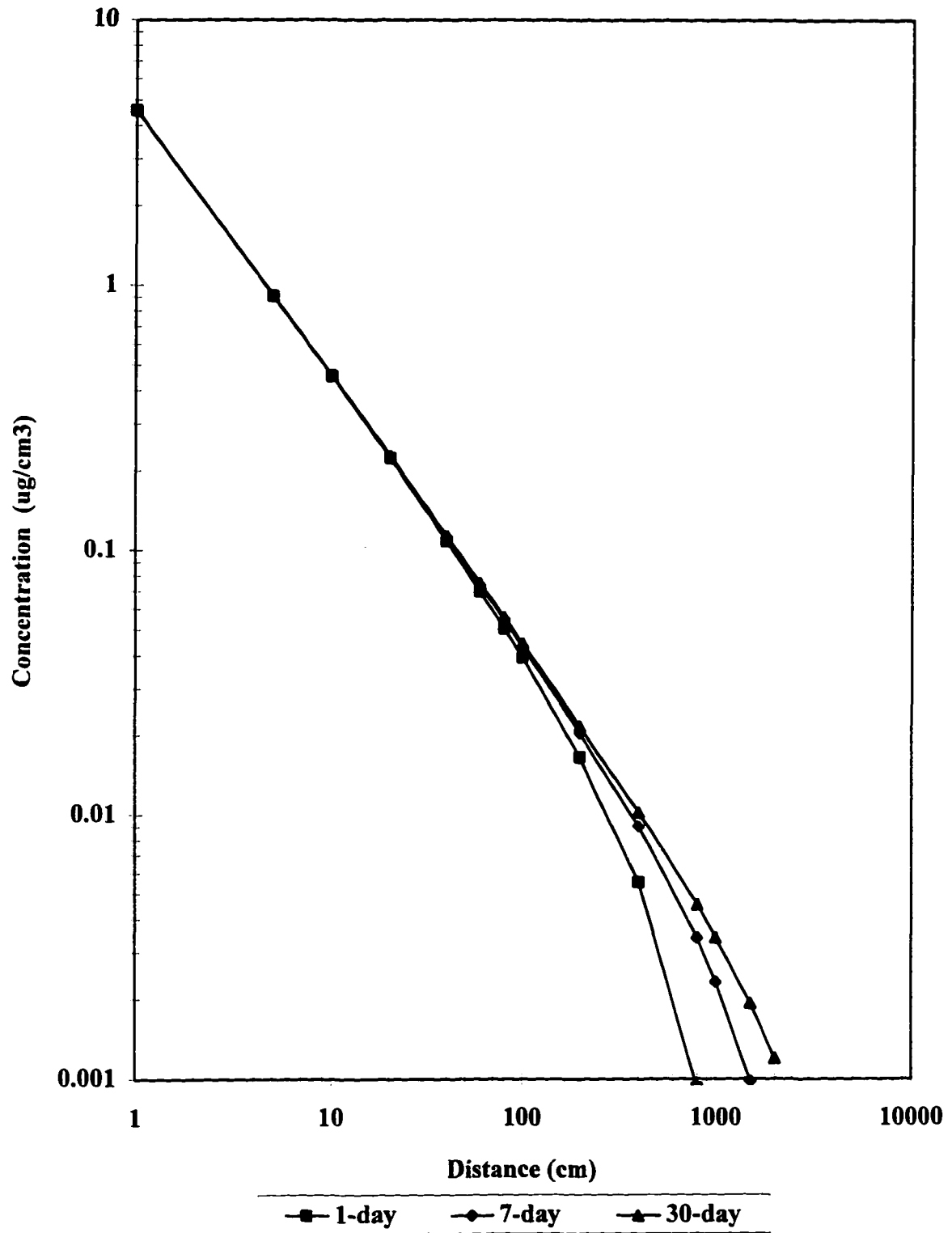Concentration for 0% Moisture Content by Mass**

Distance (cm)

Concentration (ug/cm3)

—□— 1 day   —◇— 7 days   —△— 30 days

**Analytically Modeled Octane Vapor
Concentration for 1% Moisture Content by Mass**

**Analytically Modeled Octane Vapor
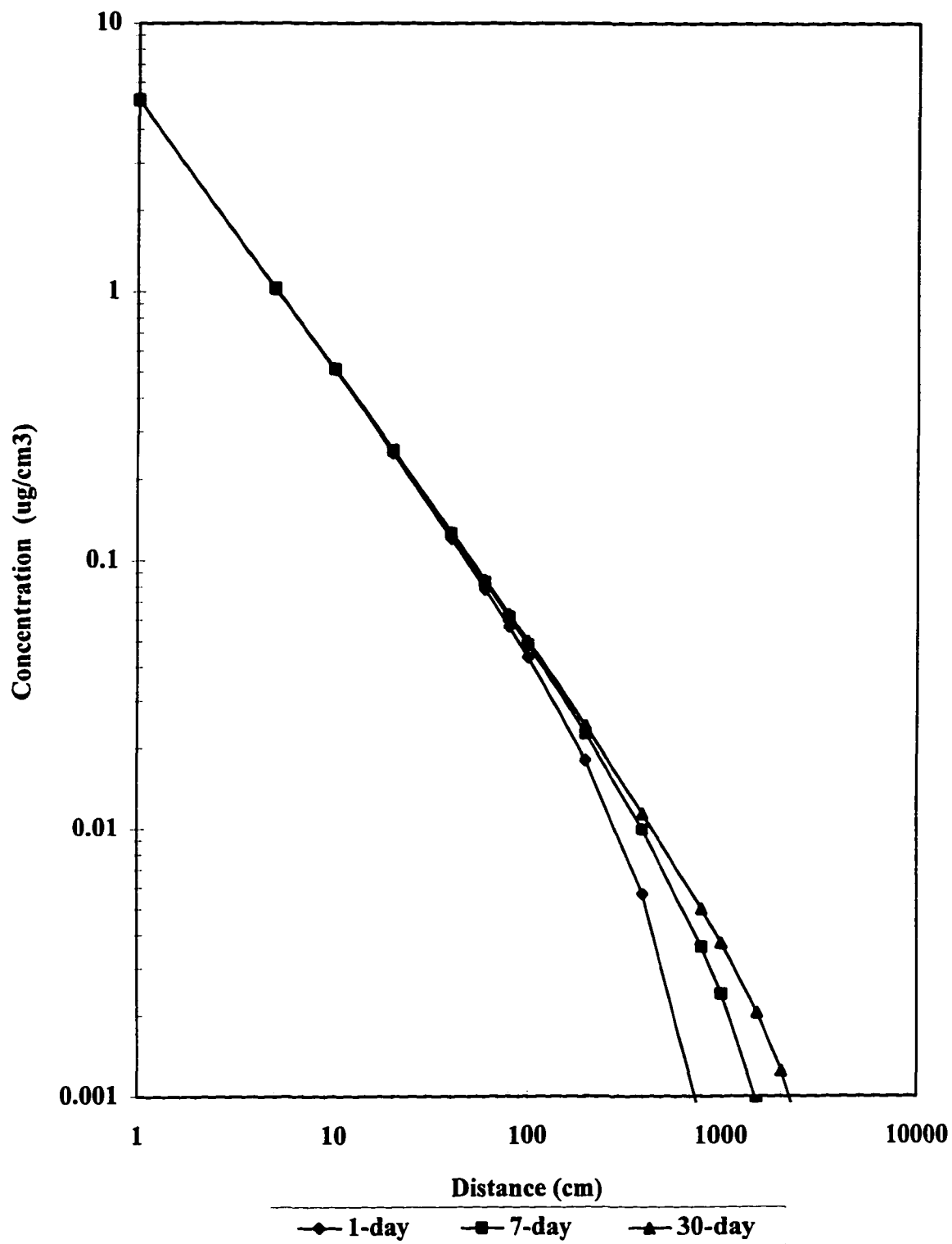Concentration for 2% Moisture Content by Mass**
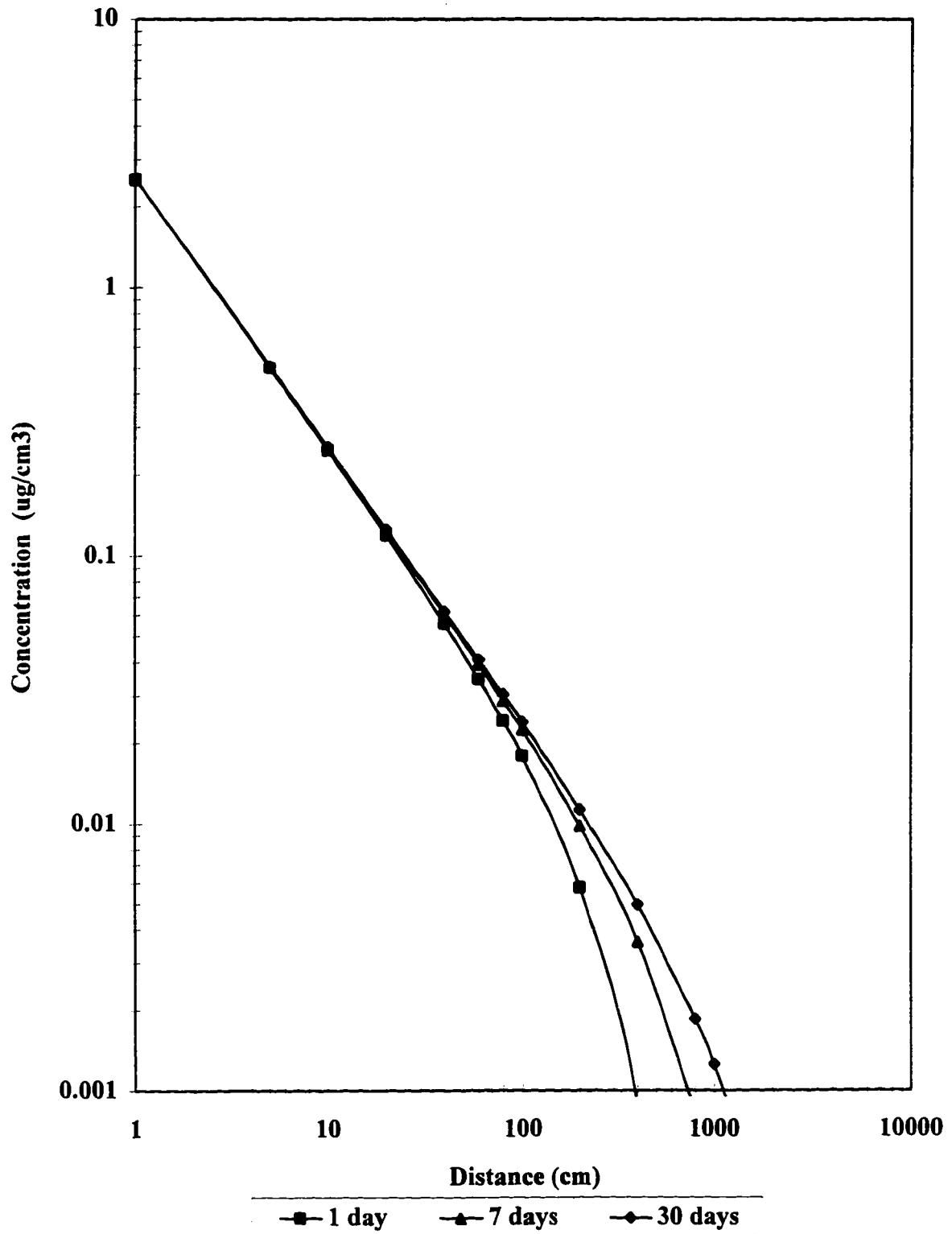
**Analytically Modeled Octane Vapor
Concentration for 5% Moisture Content by Mass**
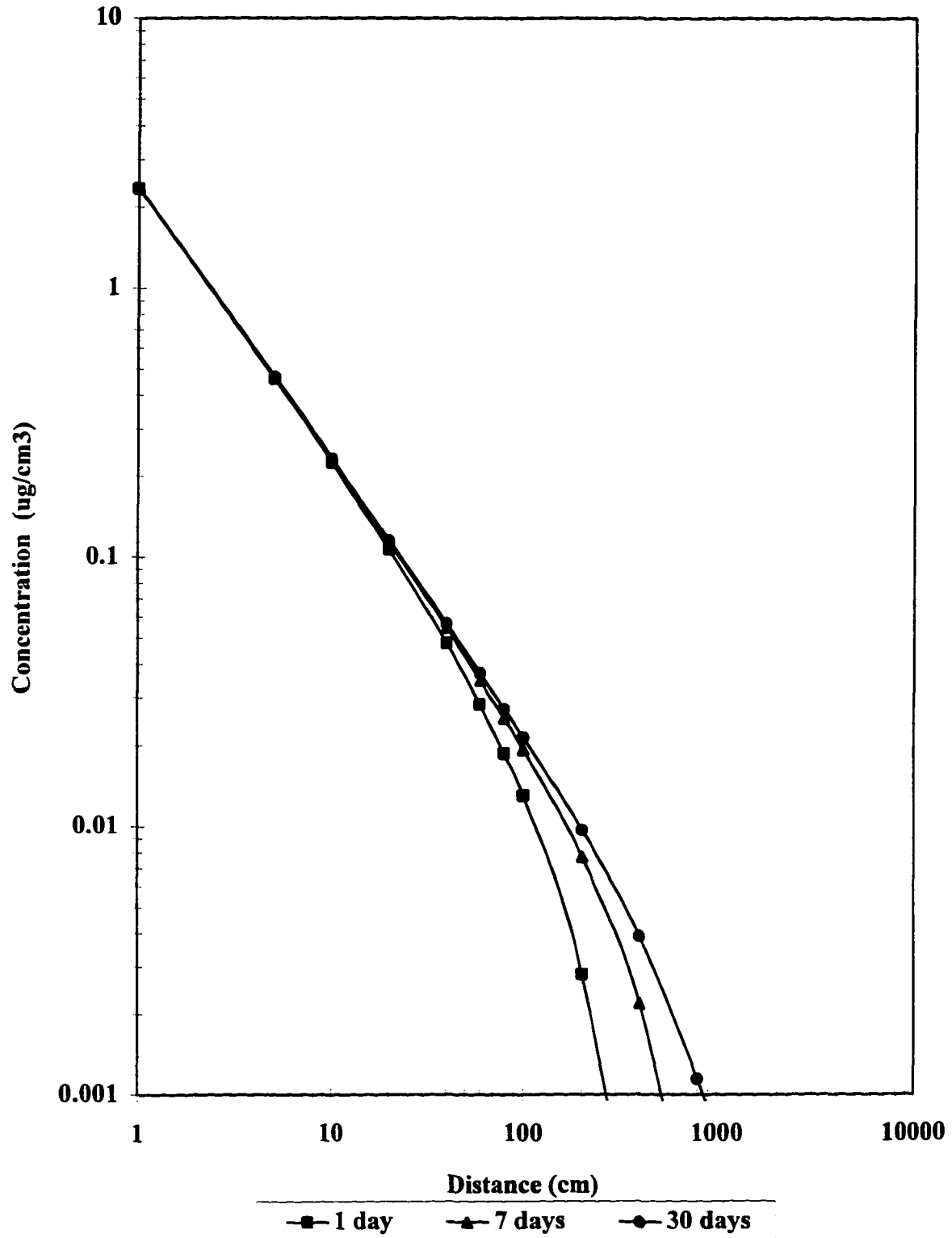
Analytically Modeled Octane Vapor
Concentration for 6.5% Moisture Content by Mass
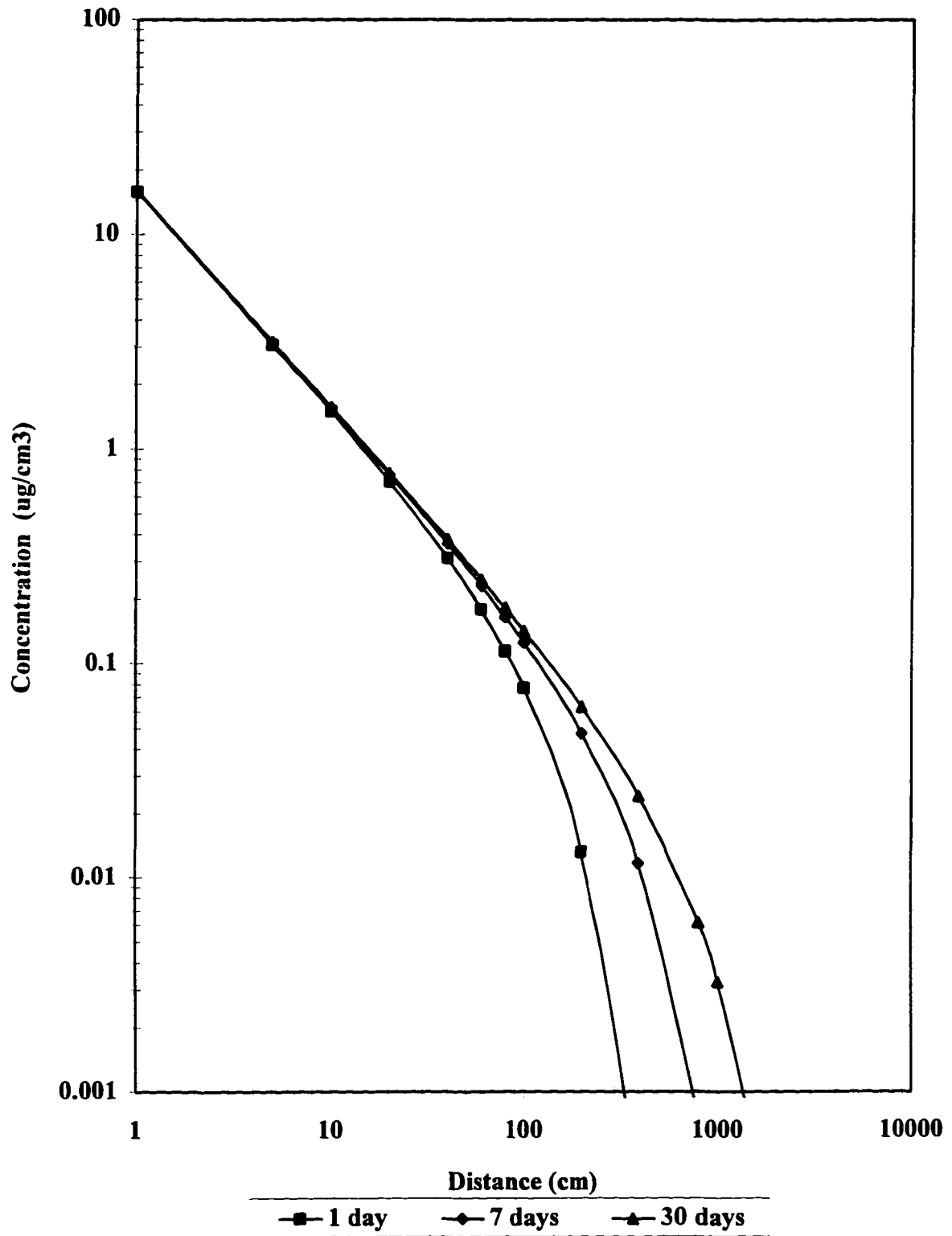
**Analytically Modeled Octane Vapor
Concentration for 7.5% Moisture Content by Mass**
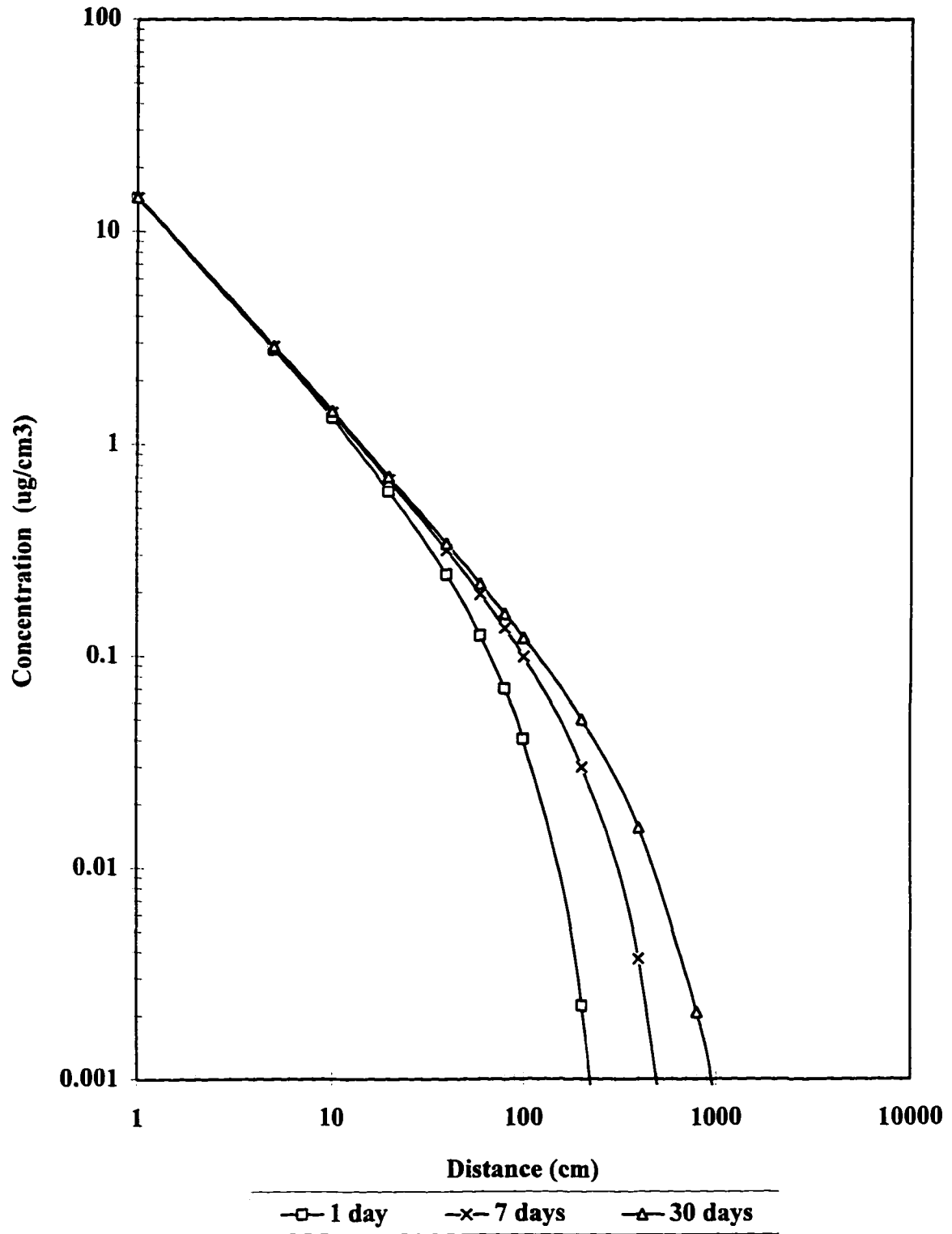
**Analytically Modeled Octane Vapor
Concentration for 8.5% Moisture Content by Mass**
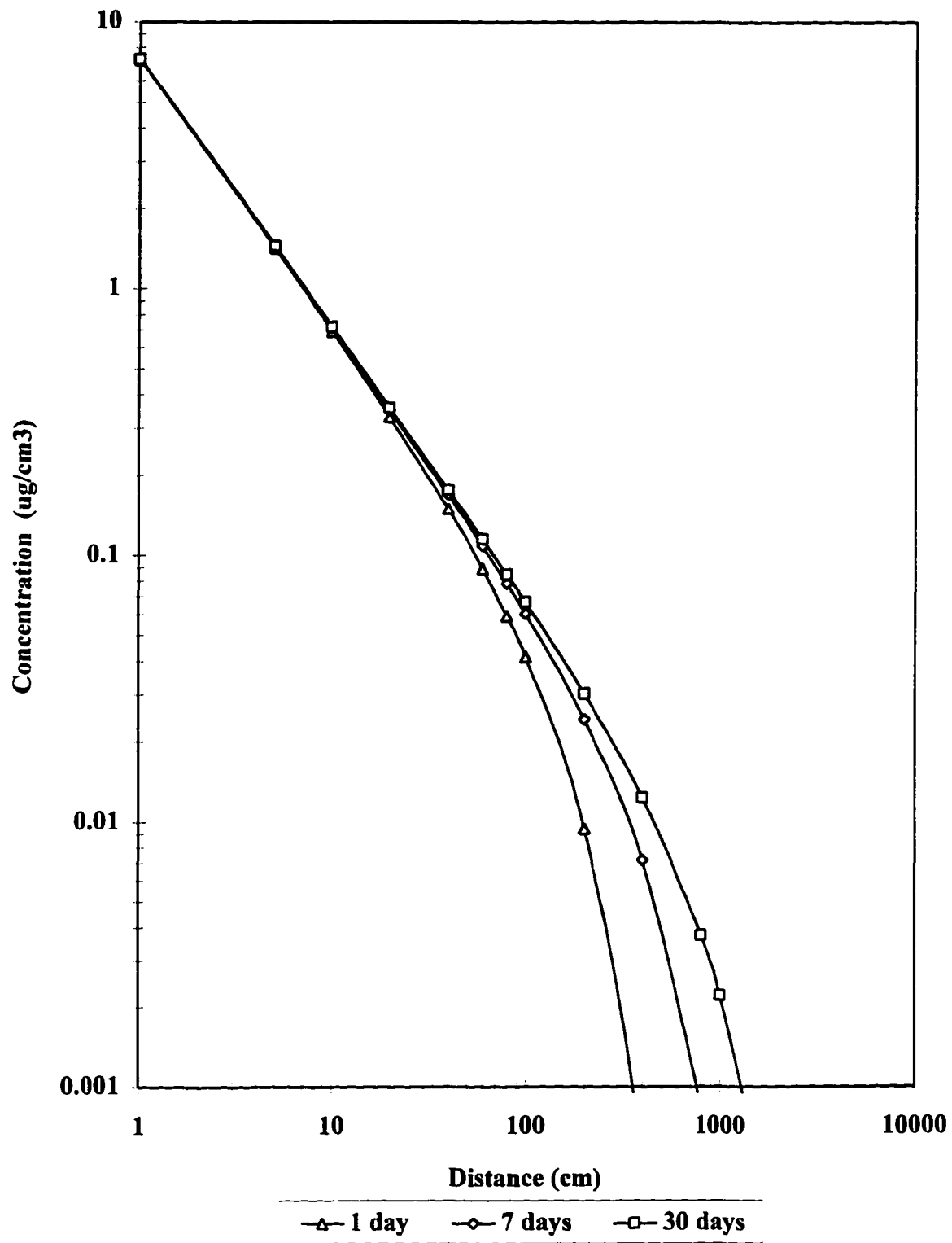
**Analytically Modeled Octane Vapor
Concentration for 9.25% Moisture Content by Mass**
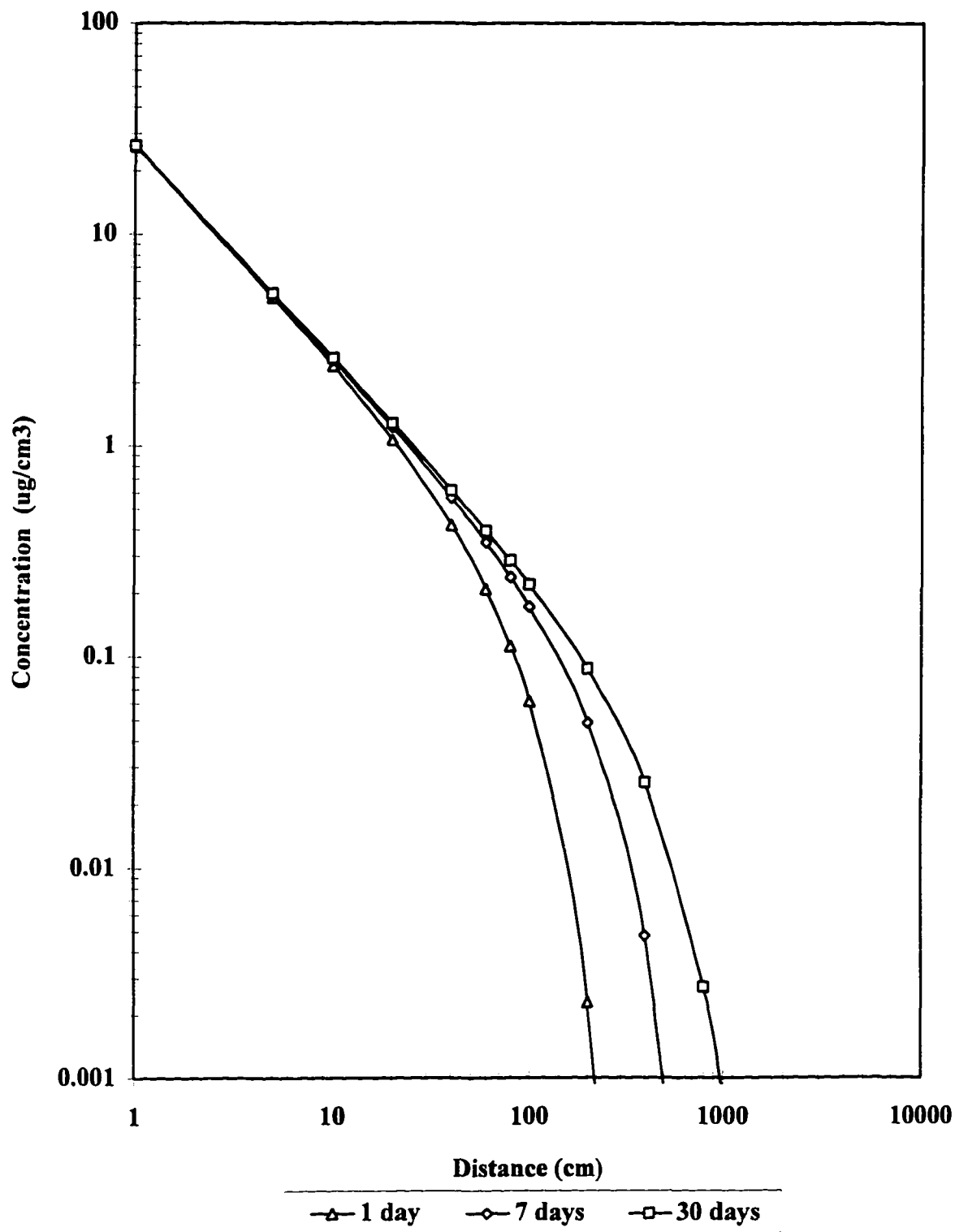
**Analytically Modeled Octane Vapor
Concentration for 10% Moisture Content by Mass**
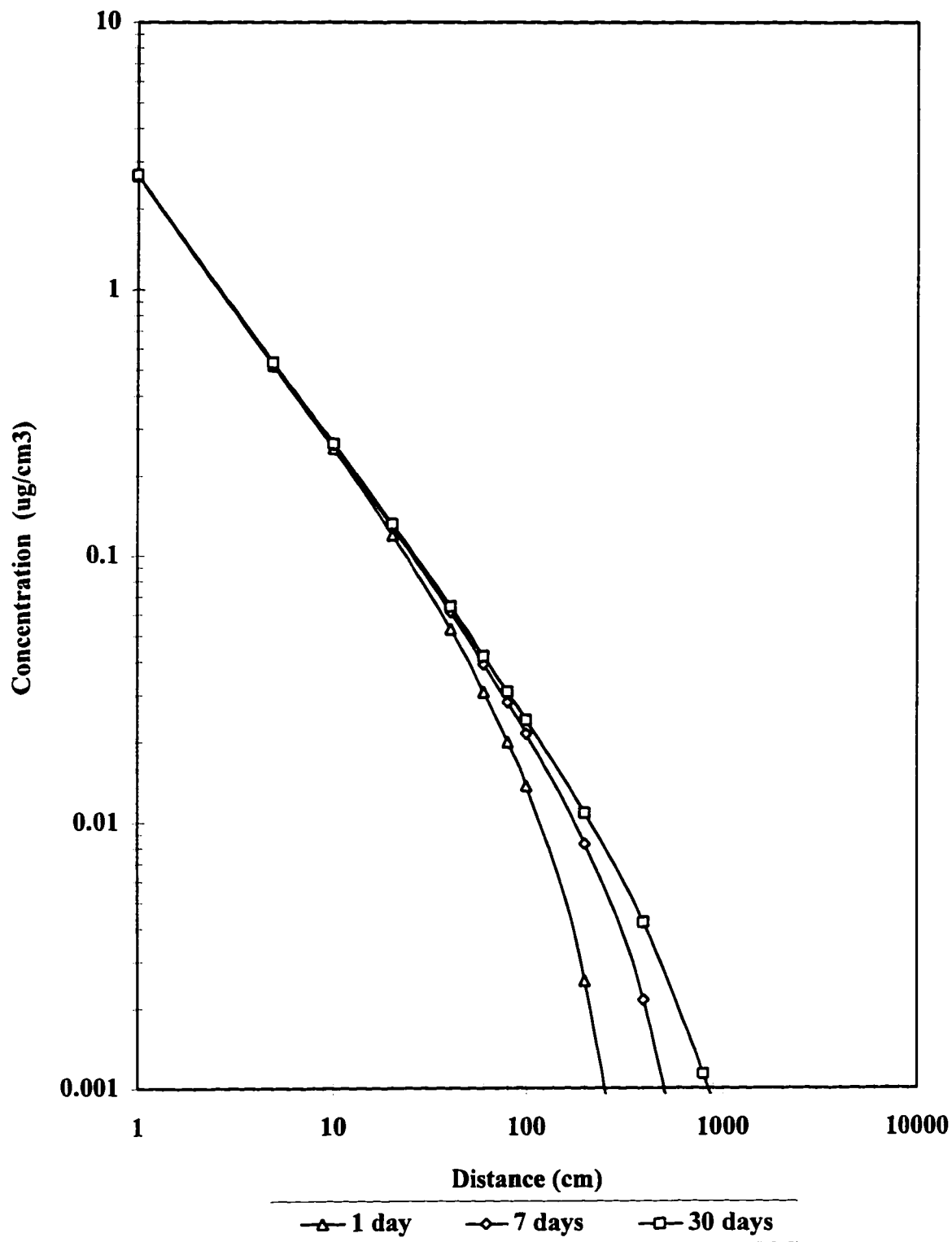
**Analytically Modeled Diesel Fuel Vapor
Concentration for 0% Moisture Content by Mass**

Analytically Modeled Diesel Fuel Vapor Concentration for 2% Moisture Content by Mass

**Analytically Modeled Diesel Fuel Vapor
Concentration for 5% Moisture Content by Mass**
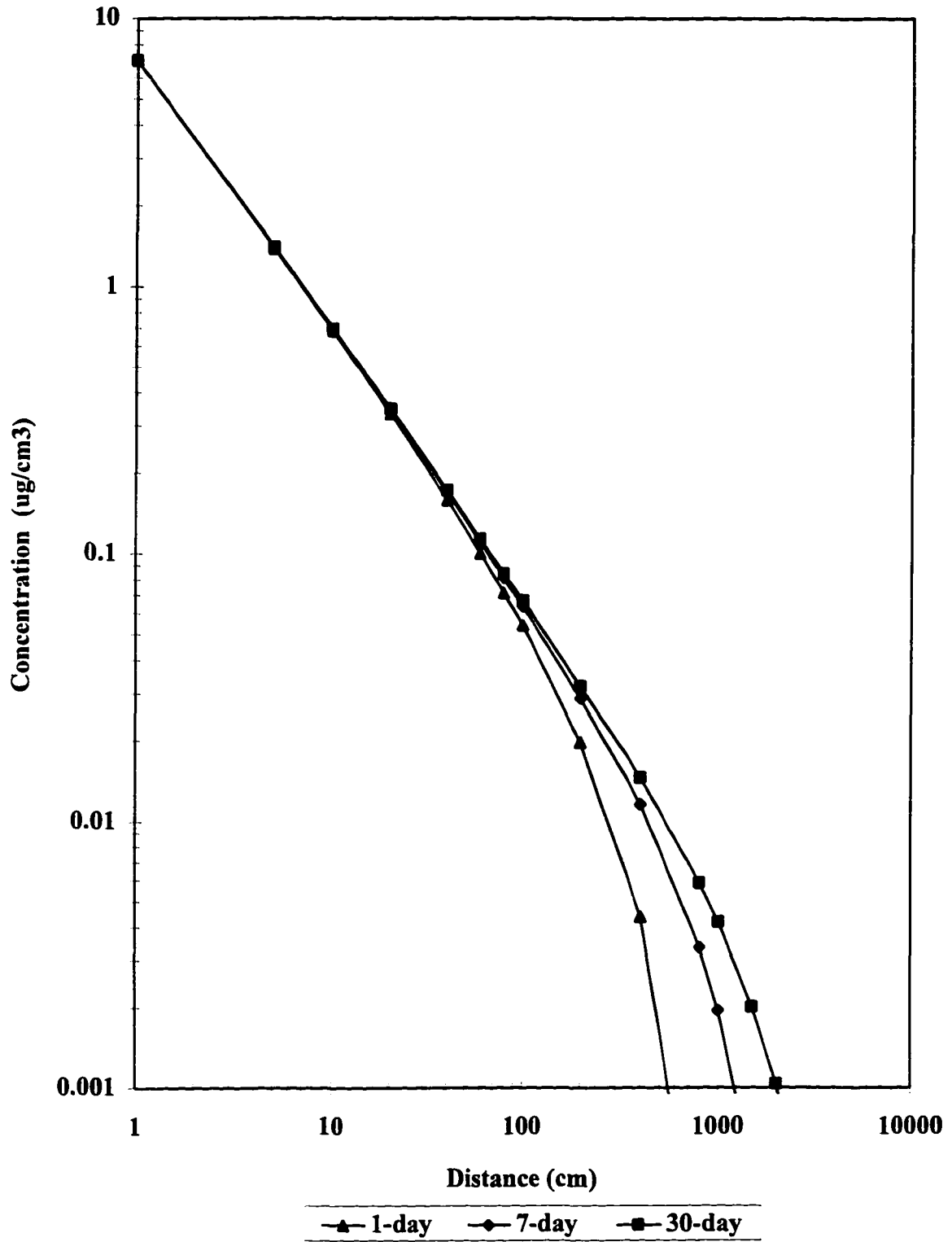
Bibliography

Ballestero, T., Herzog, B., Evans, O.D. and Thompson, G., 1991, *Monitoring and Sampling the Vadose Zone*, Practical Handbook of Ground-Water Monitoring, Lewis Pubs., Chelsea, MI, p. 97-141.

Batterman, S., Kulsherestha, and Cheng, H.Y. 1995, *Hydrocarbon Vapor Transport in Low Moisture Soils*, Environmental Science and Technology, vol. 29, no. 1, p. 171-179.

Beckett, G.D., and Huntley, D., 1994, Characterization of Flow Parameters Controlling Soil Vapor Extraction, Ground Water, vol. 32, no. 2, pp. 239-247.

Brooks, R.H., and Corey, A.T., 1964, *Hydraulic Properties of Porous Media*, Colorado State University, Fort Collins, CO, Hydrology Paper No. 3 pp. 27.

Block, R.N., and Bishop, M., 1990, *Assessment of Diesel Contamination in Soil*, Hydrocarbon Contaminated Soils Conference, September 24 - 27, 1990.

Carslaw, H.S., and Jaeger, J.C., 1959, *Conduction of Heat in Solids, Second Edition*, Oxford University Press, New York, p. 261

Chaganti, S., 1990, *Vapor Transport Modelling Around Simulated Leaky Underground Storage Tank Environments*, Masters Thesis, Arizona State University, pp. 75.

Chiou, C.T., and Shoup, T.D. 1985, *Soil Sorption of Organic Vapors and Effects of Humidity on Sorptive Mechanism and Capacity*, Environmental Science and Technology, vol. 19, no. 1, p. 1196-1200

Fick, A, 1855, Annln. Physics, Vol. 170, no. 59.

Flagan, R.C., and Seinfeld, J.H., 1988, *Fundamentals of Air Pollution Engineering*, Prentice-Hall Inc., Englewood Cliffs, NJ, pp. 542.

Freeze R.A., and Cherry J.A., 1979, *Groundwater*, Prentice-Hall Inc., Englewood Cliffs, NJ, pp. 604.

Hamaker, J.W., 1972, *Diffusion and Volatilization*, Chapter 5 in *Organic Chemicals in the Soil Environment*, vol. 1, ed. by Goring and Hamaker, Marcel Decker, New York.

125

Hantush, M.S., and Jacob, C.E., 1955, *Non-steady radial flow in an infinite leaky aquifer*, Trans. American Geophysical Union, v. 36, no. 1, pp. 95-112.

Jarvis, M.W., and Lugg, G.A., 1968, *The Calculation of Diffusion Coefficients of Vapors of Liquids into Air*, Report 318, Australian Defense Scientific Service, Alexandria, Virginia, p.33

Johnson, T.E., 1992, *Modeling Diesel Vapor Transport in a Simulated Underground Environment*, M.S. Thesis, Arizona State University, pp. 113.

Johnson, T.E., and Kreamer, D.E., 1994, *Physical and Mathematical Modeling of Diesel Fuel Liquid and Vapor Movement in Porous Media*, Ground Water, v. 32, n. 4, July-August 1994, p. 551-560.

Kerfoot, H.B., 1990, *Soil-gas surveys for the detection and delineation of groundwater contamination*, Trends in Analytical Chemistry, volume 9, number 5, p. 157-163.

Kreamer, D.K., 1982, *In-situ Measurement of Gas Diffusion Characteristics in Unsaturated Porous Media by Means of Tracer Experiments*, Doctorate Dissertation, University of Arizona, pp. 209.

Kreamer, D.K., Weeks, E.P., and Thompson, G.M., 1988, *A Field Technique to Measure the Tortuosity and Sorption-Affected Porosity for Gaseous Diffusion of Materials in the Unsaturated Zone with Experimental Results from Near Barnwell, South Carolina*, Water Resources Research, vol. 24, no. 3, March 1988, Pages 331-341

Lyman, W.J., Reehl, W.F., and Rosenblatt, D.H., 1990, *Handbook of Chemical Property Estimation Methods*, American Chemical Society, Washington D.C.

McNerney, R.T., 1989, *Continuous Vapor Monitoring of Leaks*, Pollution Engineering, September 1989, p. 96-102.

Mendoza, C.A., and McAlary, T.A., 1990, *Modeling of Ground-Water Contamination Caused by Organic Solvent Vapors*, Ground Water, vol. 28, no. 2, p.199-206.

Microsoft, Inc., 1994, *FORTRAN PowerStation*, Seattle, WA, 4 - 3.5 inch diskettes

Rajagopalan, V., 1994, *Influence of Grain Size on the Movement of Diesel Fuel in Porous Media due to Water table Fluctuations*, M.S. Thesis, University of Nevada, Las Vegas,

Robbins, G.A., Deyo, B.G., Temple, M.R., Stuart, J.D., and Lacy, M.J., 1990, *Soil-Gas Surveying for Subsurface Gasoline Contamination Using Total Organic Vapor Detection Instruments Part I. Theory and Laboratory Experimentation*, Ground Water Monitoring Review, vol. X, no. 3, p. 122-131.

Robbins, G.A., Deyo, B.G., Temple, M.R., Stuart, J.D., and Lacy, M.J., 1990, *Soil-Gas Surveying for Subsurface Gasoline Contamination Using Total Organic Vapor Detection Instruments Part II. Field Experimentation*, Ground Water Monitoring Review, vol. X, no. 4, p. 110-117.

Sabapathi, J., 1993, *Effect of Water table Fluctuations on Petroleum Contamination Distribution*, M.S. Thesis, University of Nevada, Las Vegas.

Schiegg, H.O., and McBride, J.F., 1987, *Laboratory setup to study two-dimensional multiphase flow in porous media.* Presentation at the Hydrocarbons and Organic Chemicals in Groundwater Conference, Houston, TX, November 17-19, 1987.

Sepher M. and Samani Z.A., 1993, *In Situ Remediation Using Vapor Extraction Wells, Development and Testing of a Three Dimensional Finite Difference Model*, Ground Water, vol. 31, no. 3, p. 425-436.

Silka, L.R., 1988, *Simulation of Vapor Transport Through the Unsaturated Zone - Interpretation of Soil-Gas Surveys*, Ground Water Monitoring Review, vol. VIII, no. 2, p. 115-123

Solley, W.B., Merk, C.F., and Pierce, R.R., 1988, *Estimated Water Use in the United States in 1985*, U.S. Geologic Survey Circular 1004.

Swallow, J.A., and Gschwend, P.M., 1983, *Volatilization of Organic Compounds from Unconfined Aquifers*, Proceedings from the Third National Symposium on Aquifer Restoration and Groundwater Monitoring, National Water Well Association, p327-333.

Theis, C.V., 1935, *The relation between the lowering of the piezometric surface and the rate and duration of a well using ground-water storage*, Trans. Am. Geophysical Union, v. 16, pp. 373-421.

Visual Numerics, Inc., 1994, *IMSL 32 - Bit Numerical Libraries - Mathematical & Statistical Functions Version 2.0*, FORTRAN Subroutines for Microsoft FORTRAN PowerStation, Houston, TX, 12 - 3.5 inch diskettes.

Weast, R.C., 1983, *Values of the Gas Constant, R*, CRC Handbook of Chemistry and Physics, 64th Edition, CRC Press, Inc., Boca Raton, FL, p. F-197